NTNU
Norwegian University of Science and Technology
Department of Marine Technology

M.Sc.THESIS

Title:	**Delivered:**
Estimation of ALS wave-column impact loads for a semi-submersible and a simplified assessment of the associated structural response	14.06.2011
	Availability: Open
Student: Eirik Dalane	**Number of pages:** 130

Abstract:

Breaking waves that impacts with a platform column will give large impact loads. These loads are some of the largest loads acting on a platform during its lifetime. During the summer 2010, MARINTEK performed model tests on a semi-submersible, called Midgard, where these impact loads were measured at one of the platform columns.

In this report, two methods have been used to predict the ALS impact loads from breaking waves. A numerical method based on DNV-RP-C205 and stochastic analysis of model test data. The uncertainty in each method has been assessed, and it was concluded that there is large uncertainties related to the problem of breaking wave impact.

The ALS impact load predicted using stochastic analysis of model test data became almost twice as large as what was predicted using the numerical method. The main reason for this difference was that the numerical method used an estimated value for the horizontal velocity between the wave and the platform that was too small compared with the model tests.

The different sensors measured impact force during the model tests has been compared. This showed that for a breaking wave that hit all the sensors, the sensor located highest on the column would experience largest impact while the lowest sensor would experience least impact force. The sensors horizontal location on the column was of less importance. Based on this information some load models was suggested.

A simplified structural model was made of the column. Static and dynamic analyses were performed using the suggested load models. The dynamic effects were found to be small because the duration of the impact load was so much higher than the natural period of the column.

The largest bending moment at the top of the column was compared with the column's elastic moment capacity. It was found to be of little importance. This indicates that ALS impact loads from breaking waves do not give a significant contribution to global structural response.

Keyword:

Semi-submersible
Breaking waves
Impact loads
Model test

Advisor:

Professor Sverre Haver

Address:
NTNU
Department of Marine Technology
N-7491 Trondheim

Location
Marinteknisk Senter
O. Nielsens vei 10

Tel. +47 73 595501
Fax +47 73 595697

M.Sc. thesis 2011

for

Stud.techn.

Eirik Dalane

Estimation of ALS wave-column impact loads for a semi-submersible and a simplified assessment of the associated structural response

(Estimering av ALS bølgeslag mot søyle på en halvt nedsenkbar plattform og en forenklet vurdering av dets betydning for respons.)

In most cases the aim of a design process is that the structure shall fulfil various limit states, SLS, FLS, ULS and ALS. Here we will focus on ALS (accidental limit state). In connection with ALS loads and responses corresponding to an annual exceedance probability and 10^{-4} represent the target quantities. The overall aim of this investigation is to estimate a proper ALS load event representing the impact loads from breaking waves against platform column. This can be done numerically using recommendations in available recommended practise, by CFD calculations or by model test results. The focus in this work will be to consider available model test data.

The impact pressures from breaking waves are expected to be of rather short duration. A simplified structural model is to be established. The structural model shall be exposed to the estimated ALS load history and it is to be investigated whether the impact load from breaking waves merely is a local structural problem or if it also can represent significant contribution to a more global response quantity.

The candidate may follow his own approach for solving the problem described. But a possible division into sub-tasks are given below:

- A brief interpretation of ALS for the problem under consideration including references to adequate paragraphs in governing regulations. Explain why you can use the provided model test data for obtaining a reasonable estimate for the impact load.

- Review the method found in DNV RP C-205 for estimating loads from breaking waves. Discuss uncertainties related to the quantities involved in this procedure.

- A crucial quantity is relative speed between fluid particles and the surface they are impacting. Use model test results for estimating the speed of the platform column as significant impacts are measured. Discuss correlations between selected measured impacts and simultaneous speed of instrumented column. Is platform speed important? (A comparison between measured speed and calculated speed from WADAM can be considered if found to be of interest.)

- Establish a proper probabilistic model for spatial and temporal variability of the measured impact values. Discuss spatial correlation between various impact sensors on the instrumented column. Propose if possible standard spatial shape for the major impacts characterized merely the areal maximum impact pressure. The variation with time of maximum force during impact shall also be assessed.

- Discuss various methods available for estimated maximum impact pressure corresponding to a 0.1 probability of being exceeded during the 3-hour storm event. Estimate target pressures by the various methods and discuss the associated uncertainties.

- Establish a simplified structural model for a platform column. Expose the model to the estimated ALS impact load history. Estimate end forces of the structural model and consider these force versus end forces when no breaking wave takes place. Assessment is meant to be simple and the results can only be taken as an indication.

- Consider if the importance can be estimated from model test data. The total load on the column with the force panels is available from the model test experiment. Can consequences of major impacts be seen in mooring line forces or accelerations?

The work may show to be more extensive than anticipated. Some topics may therefore be left out after discussion with the supervisor without any negative influence on the grading.

The candidate should in his report give a personal contribution to the solution of the problem formulated in this text. All assumptions and conclusions must be supported by mathematical models and/or references to physical effects in a logical manner. The candidate should apply all available sources to find relevant literature and information on the actual problem.

The report should be well organised and give a clear presentation of the work and all conclusions. It is important that the text is well written and that tables and figures are used to support the verbal presentation. The report should be complete, but still as short as possible.

The final report must contain this text, an acknowledgement, summary, main body, conclusions, suggestions for further work, symbol list, references and appendices. All figures, tables and equations must be identified by numbers. References should be given by author and year in the text,

and presented alphabetically in the reference list. The report must be submitted in two copies unless otherwise has been agreed with the supervisor.

The supervisor may require that the candidate should give a written plan that describes the progress of the work after having received this text. The plan may contain a table of content for the report and also assumed use of computer resources.

From the report it should be possible to identify the work carried out by the candidate and what has been found in the available literature. It is important to give references to the original source for theories and experimental results.

The report must be signed by the candidate, include this text, appear as a paperback, and - if needed - have a separate enclosure (binder, diskette or CD-ROM) with additional material.

Supervisor: Prof. II Sverre Haver, Statoil ASA.

Summary

Breaking waves that impacts with a platform column will give large impact loads. These loads are some of the largest loads acting on a platform during its lifetime. It is therefore important that the platform is designed to withstand these large loads.

During the summer 2010, MARINTEK performed model tests on a platform called Midgard. This platform is a semi-submersible that was suggested as a possible concept for the Midgard field in the Norwegian Sea. The model of Midgard was instrumented with 8 slamming sensors that measured the impact force from breaking wave impacts.

In this report, two methods have been used to predict the ALS impact loads from breaking waves. These loads will have a 10^{-4} annual probability of exceedence. The two methods used to predict these impact loads were a numerical method based on DNVs recommended practice, DNV-RP-C205 (2007), and stochastic analysis of model test data.

The ALS impact load from breaking waves became almost twice as large when using stochastic analysis of model test data compared to when the numerical method was used. The reason for the large difference in these two methods was discussed. The estimated values used in the numerical method were compared with values obtained from model test data. This showed that there is a large difference in the horizontal impact velocity. This is the combined velocity of the wave impact velocity and the platform surge velocity. Both of these velocities were discussed. It was found that the wave impact velocity for the largest slams in the model tests was almost twice as high as the estimated velocity. In the numerical method, the standard deviation of the surge velocity spectrum, which only included the wave frequent velocities, was used as an estimate for the platform surge velocity. When comparing with the surge velocities in the model tests, this estimate seemed to be too low.

Uncertainties in the two different methods were discussed. There is a large uncertainty related to the problem of breaking wave impact, especially for the high probability level defined by ALS.

The 8 slamming sensors on the Midgard model, measured the impact force on different locations on the column. The measurements done by each of these sensors has been compared to investigate if a pattern could be seen. This has been done by looking at vertical and horizontal correlation between the measurements done by the different sensors. Doing this showed that when all sensors was hit directly by a breaking wave, the sensors location in vertical direction was of importance for the measured impact force. The sensor located highest on the column would usually measure the largest impact force, while the sensor located lowest would usually measure the lowest. The sensors horizontal location on the column was of less importance.

The time variation for when each sensor measured its maximum impact force was also investigated. For the two largest slams in the model tests the same pattern could be seen. The maximum impact force occurred first for the sensors located highest on the column. It then occurred gradually downwards the column.

Based on the investigation of the measured impact force, two load configurations were suggested to be used in a structural analysis. The first one was a resultant of all the impact loads on the column, while the second one did account for how the impact loads vary in vertical direction. These two load

configuration was used to make four load models. The first two were made by using only the measured impact force from the sensors. The last two did also include the expected impact force from a larger area that was not covered by the sensors.

In the model test, 18 different realizations were used. During two of these realizations a really large slam occurred. These slams were used to estimate the global structural response for the ALS condition. Four different load models were therefore suggested. These load models were created using the measured impact force from these slams.

A simple structural model was made of the platform column. Static and dynamic analyses were performed using the four suggested load models. The bending moment at the column top, where it is attached to the platform deck, was obtained for each analysis.

These results showed that the dynamic magnification on the structural response is very small when hit by a breaking wave. This is because the platform column has a very high stiffness, causing the natural period to be much shorter than the duration of the impact load.

The largest bending moment obtained from the structural analyses was compared to the column's elastic moment capacity. This comparison showed that the bending moment caused by ALS breaking wave impacts was of little significance. This indicates that the impact load form ALS breaking waves do not give a significant contribution to the global structural response.

Preface

This report describes my thesis work for my Master of Science degree in Marin Technology at the Norwegian University of Science and Technology (NTNU). The work has been carried out during the spring semester of 2011.

I will like to express sincere thanks to my supervisor Professor Sverre Haver in Statoil. He has given me great support and guided me through the work in this report. Our meetings during the semester have been both inspiring and educational.

Furthermore, I will like to express thanks to Erik Lehn in MARINTEK who, through conversations, has provided me with valuable insight concerning slamming loads.

I would also like to thank Stein L. Rasmussen in Aker Solution for providing me with structural information about the platform column used in this project.

Finally, I will also thank Professor Jørgen Amdahl for helping me with the implementation of the USFOS model.

Trondheim, June 2011

Eirik Dalane

Table of Contents

List of Figures

List of Tables

Notations

Abbreviations:

ALS	Accidental Limit State
CFD	Computational Fluid Dynamics
DAF	Dynamic Amplification Factor
DNV	Det Norske Veritas
RAO	Response Amplitude Operator
VCG	Vertical Center of Gravity

Symbols:

a	Half of column width
A	Area
A_{11}	Surge added mass
A_S	Stiffener area
$c_B^{(n)}$	Phase velocity of the most probable highest breaking wave in n years
C_{Pa}	Space average slamming pressure coefficient
C_W	Phase velocity
d	Damping
DAF	Dynamic amplification factor
e	Residual
$E[\ ]$	Mean value
F	Sensors maximum measured impact force
$F_{\max}$	Maximum force
$F(t)$	Load history
$F_{X_{3h}}(x)$	Cummulative Gumbel distribution
$F_{X_{3h}}(x)$	Cummulative Frechet distribution
$\hat{F}_{X_{3h}}(x)$	Cummulative empirical distribution
g	Acceleration of gravity
$H_B^{(n)}$	Height of the most probable highest breaking wave in n years
H_S	Significant wave height
$H_S^{(n)}$	Most probable largest significant wave height in n years
I	Second moment of area
k	Stiffness
L	Length of column's submerged part

m	Mass
m_0	0th spectral moment
m_x	x-values mean
m_{x3h}	Mean of the 3-hour measured extremes
m_y	y-values mean
M	Bending moment
M_{el}	Elastic moment capacity
$p_{3h,10^{-4}}$	10^{-4} probability impact pressure
p_s	Space average slamming pressure
R	Vertical distance from force center of gravity to still water
$R_{\max}$	Maximum response force
$RAO_{surge,disp}$	Surge displacement RAO
$RAO_{surge,vel}$	Surge velocity RAO
s	Stiffener spacing
s_{x3h}	Standard deviation of the 3-hour measured extremes
$S_{surge,vel}$	Surge velocity spectrum
S_{wave}	Wave spectrum
t	Time
t	Thickness
t_e	Equivalent thickness
$t_{e,bulkhead}$	Equivalent bulkhead thickness
$t_{e,plate}$	Equivalent plate thickness
T	Wave period
T_0	Natural period
$T_B^{(n)}$	Wave period of the most probable highest breaking wave in n years
T_{dur}	Load duration
T_P	Spectral peak period
T_{rise}	Load rise time
u	Horizontal velocity of the water particles
$u_{\max}$	Maximum displacement
u_{static}	Static displacement
$u(t)$	Displacement
$\dot{u}(t)$	Velocity
$\ddot{u}(t)$	Acceleration
v	Relative horizontal velocity between water and column
W_{el}	Elastic section modulus
x	Impact force
x_{3h}	3-hour extreme impact force

$x_{3h,10^{-4}}$	10^{-4} probability impact force
y	Impact force
$\hat{y}$	Fitted regression line

α	Percentile in cumulative distribution
β	Scale parameter in Gumbel distribution
$\hat{\beta}_0$	Estimate of interception point
$\hat{\beta}_1$	Estimate of slope
ε	Global wave steepness
$\dot{\eta}_1$	Surge velocity
θ	Random number between 0 and 1
κ	Shape parameter in Frechet distribution
λ	Scale parameter in Frechet distribution
λ	Wave length
μ	Location parameter in Gumbel distribution
ρ	Density
ρ_{xy}	Correlation coefficient
σ	Standard deviation
σ_x	x-values standard deviation
σ_y	y-values standard deviation
σ_Y	Yield stress
ω	Angular frequency

Text that is directly taken from a reference is written using *italic* font.

1 Introduction

As a possible concept for the Midgard field in the Norwegian Sea, Aker Solutions came up with a compression platform named Midgard. Its task would be to ensure flow in the pipelines, and increase the gas production at the Midgard field. The structure is a four legged semi-submersible with ring pontoon.

When designing offshore structures like this, it is important to ensure that the structure can resist all the environmental loads that will be acting on it. Breaking waves that hits the structure is one of the largest loads acting on a platform during its lifetime. It is therefore important that the platform is designed to withstand these loads.

To be able to design for these large loads, the magnitude of the loads needs to be estimated. In connection with this MARINTEK performed model test on Midgard during the summer 2010. In addition to many other measurements, they instrumented one of the columns with sensors that were able to measure the impact force from breaking waves in severe sea states.

This report will present different methods used to predict the ALS design value for impact load from breaking waves. Design values will then be estimated using these methods.

By investigating the measured impact force from breaking waves, a model for the impact is suggested.

Impact loads from breaking waves are usually dealt with as a local structural problem. In this report, a simplified structural model of the platform column is made. This is used to investigate if the ALS impact loads from breaking waves will also give a significant global structural response.

Chapter 2 gives a brief introduction about the rules and regulations that needs to be fulfilled when designing offshore structures.

Chapter 3 gives a short introduction about breaking waves.

Chapter 4 describes two methods that can be used to predict the ALS impact loads from breaking waves. A numerical method based on DNVs recommended practice and stochastic analysis of model test data.

Chapter 5 gives the predicted ALS impact load from breaking waves using the numerical model based on DNVs recommended practice. An assessment of the uncertainties in this method is also given in this chapter.

Chapter 6 gives the predicted ALS impact load from breaking waves using stochastic analysis of model test data. An assessment of the uncertainties in this method is also given in this chapter.

Chapter 7 gives a discussion and comparison of the results obtained from the two methods used to predict the ALS impact loads from breaking waves.

Chapter 8 gives an investigation of the measured impact forces during the model test. Measurements done by different slamming sensors is compared, and based on this some simple load models are suggested.

Chapter 9 gives a simplified assessment of the global structural response from an ALS breaking wave impact.

Chapter 10 contains the conclusions from all the work in this report.

Chapter 11 proposes recommendations for further work.

2 Design of offshore structures

2.1 Rules and regulations – A brief introduction

When designing offshore structures, safety is an important part of the process. It is important that the structure can withstand all loads acting on the structure with an adequate safety factor. Higher safety is most often equal to larger costs. If an offshore structure was designed with cost optimization in focus there is a large chance it wouldn't have the sufficient safety level. To ensure that structural design is within the target safety level set by the authorities, the designer has to ensure that the design process is correct according to the rules and regulations for the location where the structure is going to be installed. Rules and regulations can vary from country to country, but similarity is recognized. Since Midgard was designed for the Norwegian Sea, the rules and regulations for the Norwegian Continental Shelf have been used in this report.

The rules and regulations consist of various laws, regulations, guidelines and standards. A regulation hierarchy is shown in Figure 2-1.

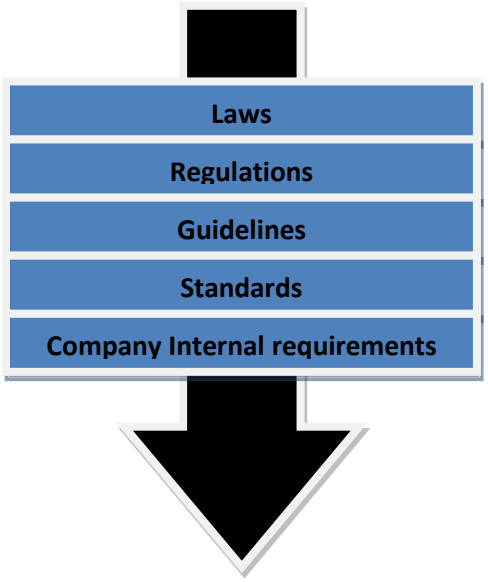

Figure 2-1: Norwegian regulation hierarchy (Haver, 2010)

NS-EN ISO 19900 (2003) is an international standard with general requirements for offshore structures. It contains some fundamental requirements for an offshore structure:

A structure and its structural components shall be designed, constructed and maintained so that it is suited to its intended use. In particular, it shall, with appropriate degrees of reliability, fullfil the following performance requirements:

a) *it shall withstand actions liable to occur during its construction and anticipated use (ULS requirement);*
b) *it shall perform adequately under all expected actions (SLS requirement);*
c) *it shall not fail under repeated actions (FLS);*

d) *in the case of hazards (accidental or abnormal events), it shall not be subsequently damaged disproportionately to the original cause (ALS);*
e) *appropriate degrees of reliability depend upon:*
   - *the cause and mode of failure;*
   - *the possible consequences of failure in terms of risk to life, environment and property.*
   - *the expense and effort required to reduce risk of failure;*
   - *different requirements at national, regional and local level.*

From this it can be seen that the structure need to comply with the requirements for four different limit states.

2.2 Accidental limit state (ALS)

In the fundamental requirements from NS-EN ISO 19900 (2003) four different limit states are mentioned. The limit state of interest in this report is the accidental limit state (ALS). In NS-EN ISO 19900 (2003) it is described as follows:

- *the accidental limit states (ALS) that correspond to situations of accidental or abnormal events.*

It also gives a more detailed explanation for the intentions for this limit state:

The intention of this limit state is to ensure that the structure can tolerate specified accidental and abnormal events and, where damage occurs, subsequently maintains structural integrity for a sufficient period under specified environmental conditions to enable evacuation to take place.

The structure need to withstand the characteristic environmental loads defined for the limit states. ALS corresponds to a characteristic environmental load effects with annual probability of exceedance not larger 10^{-4}. NORSOK N-003 (2007) contains an overview of different combinations that can be used to ensure that this requirement is satisfied. This overview is shown in Table 2-1.

Limit state	Wind	Waves	Current	Ice	Snow	Earthquake	Sea level [a]
Accidental Limit State	10^{-4}	10^{-2}	10^{-1}	-	-	-	m*
	10^{-2}	10^{-4}	10^{-1}	-	-	-	m*
	10^{-1}	10^{-1}	10^{-4}	-	-	-	m*
	-	-	-	10^{-4}	-	-	m
	-	-	-	-	-	10^{-4}	m

m - mean water level
m* - mean water level, including the effect of possible storm surge

Table 2-1: Combination of environmental quantities (NORSOK N-003, 2007)

It is clear that the waves are the most important environmental quantity for breaking waves. Based on this, waves with a 10^{-4} annual probability of exceedance have been used when investigating the breaking waves for the ALS condition.

3 Slamming from breaking waves

Breaking waves can give large impact loads on a structure. To estimate design values for impact load from breaking waves are therefore important. In this chapter a short explanation about why a wave breaks and how they induce impact forces in the structure will be given.

Breaking waves is a highly non linear phenomenon and the sea states investigated in this report are irregular. However, it is easier to explain a breaking wave using a two dimensional regular wave. A regular wave can be described as a sinusoidal wave as shown Figure 3-1.

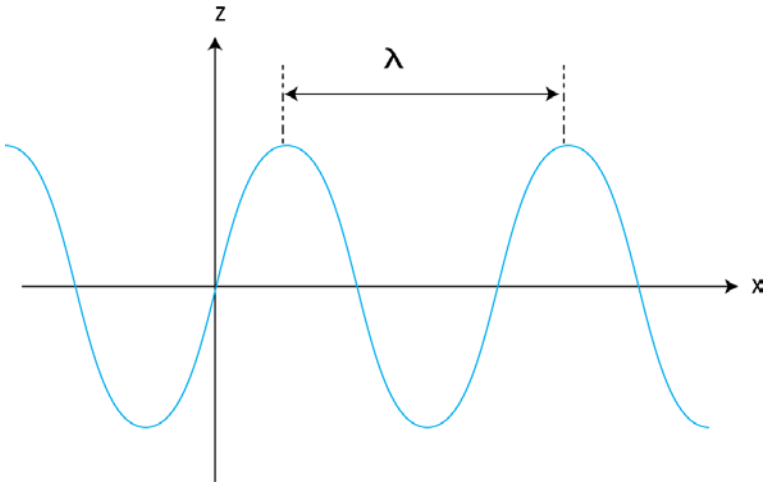

Figure 3-1: Regular sinusoidal wave

The wave length is the length of one wave cycle, as illustrated by λ in Figure 3-1. A wave will move this distance over a period of time defined by the wave period, T. The velocity of the wave, also called the phase velocity, is therefore defined by Eq.(3.1) (Pettersen, 2007).

$$C_w = \frac{\lambda}{T} \tag{3.1}$$

The water particles of a sinusoidal linear wave move in circles. The corresponding velocity can be decomposed in vertical and horizontal direction. Real ocean waves are nonlinear. Nonlinear effects can increase the horizontal velocity of the water particles at the top of a wave. If these water particles were to obtain a horizontal velocity which is larger than the wave's phase velocity, the water on the top would move faster than the wave itself and result in a breaking wave.

The velocity field under a near breaking wave is shown Figure 3-2.

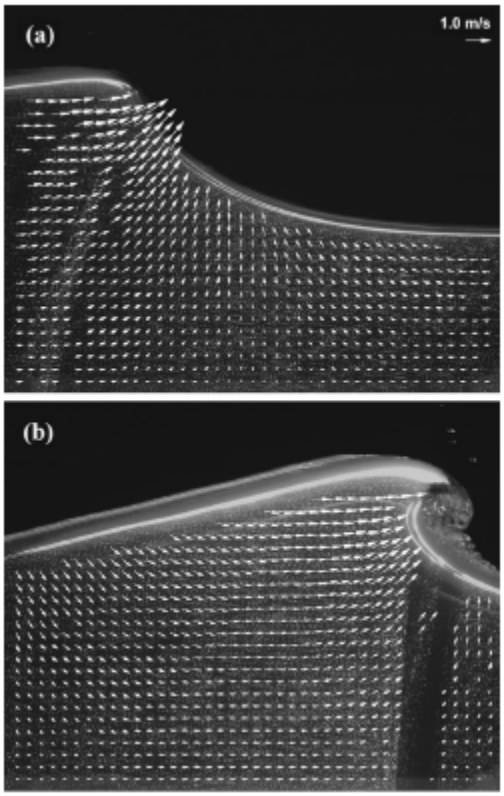

Figure 3-2: Velocity field under a near breaking wave (Chang and Liu, 1997)

It is the nonlinear interaction between different waves and between waves and currents that will give the water particles an increased velocity in a real situation.

When the water in these waves impacts with a structure, the water will act as a load on the structure. Impact loads from breaking waves hitting a column is also often referred to as slamming. The following is taken from Lehn (2003):

Impact loads due to impact between a body and water is often called "slamming". The slamming pressure generated on the body is essentially unsteady hydrodynamic pressure resulting from the direct contact between the body and the water.

4 Methods for predicting design impact load from breaking waves

Different methods can be used to estimate the ALS load event representing the impact loads from breaking waves against the column. It can be done numerically using recommendations in available recommended practice, by model test results or by CFD calculations.

In this report CDF calculations are not looked further into, while the two other methods will be explained and then used.

4.1 Numerical method based on DNV-RP-C205

In DNVs recommended practice, DNV-RP-C205 (2007), a method for predicting the characteristic impact pressures for a given probability level, are recommended. It shows how to calculate the space average slamming pressure. This pressure represents the average pressure over on strip of the platform column. The space average slamming pressure, p_s, is given by the following equation:

$$p_s = \frac{1}{2}\rho C_{Pa} v^2 \tag{4.1}$$

Where ρ is the mass density of the fluid

C_{Pa} is the space average slamming pressure coefficient

v is the relative horizontal velocity between water and column

4.1.1 Slamming coefficient

For slamming against an area on a flat column wall, the slamming coefficient has to be chosen such that it accounts for cushioning and three dimensional effects. In this case, DNV recommends a slamming coefficient equal to 2π.

4.1.2 Relative horizontal impact velocity

To estimate the relative horizontal velocity between water and column for a floating structure, the horizontal velocity of the water particles, u, and the surge velocity of the structure, $\dot{n}_1$, needs to be found. The relative horizontal velocity, v, is therefore given by Eq.(4.2).

$$v = u + \dot{n}_1 \tag{4.2}$$

The water particles impact velocity is defined positive toward the platform, while the surge velocity is defined positive toward the breaking wave.

4.1.2.1 Platform surge velocity

If assuming that the surge motion is of linear nature and only induced by loads in the wave frequent area, the surge velocity can be calculated in the frequency domain. This means that the platform's slowly varying motions are neglected. By using a linear diffraction computer program such as WADAM, it is possible to obtain the Response Amplitude Function (RAO) for surge displacement. The

RAO for the surge velocity is found by multiplying the surge motion RAO with ω^2 as shown in Eq.(4.3).

$$RAO_{surge,vel} = \omega^2 RAO_{surge,disp} \tag{4.3}$$

Where $RAO_{surge,vel}$ is the surge velocity RAO

$RAO_{surge,disp}$ is the surge displacement RAO

ω is the wave frequency

The surge velocity spectrum, $S_{surge,vel}$, can then be found by multiplying the surge velocity RAO to second power by the wave spectrum, S_{wave}, for the actual sea state.

$$S_{surge,vel} = RAO_{surge,vel}^{\ 2} \cdot S_{wave} \tag{4.4}$$

A more thorough explanation of RAO and spectral analysis is found in Dalane (2011).

In linear theory it is normal to assume that the wave field is a stationary and homogenous Gaussian process. The surge velocity will then also be a Gaussian process with a mean equal to zero. The 0th spectral moment, m_0, is found by Eq.(4.5).

$$m_0 = \int S_{surge,vel}(\omega) d\omega \tag{4.5}$$

The standard deviation, σ, is then found by Eq.(4.6).

$$\sigma = \sqrt{m_0} \tag{4.6}$$

It is reasonable to assume that the platforms surge velocity will be in the area limited by $\pm\sigma$ at the moment a breaking wave hits the column. This range corresponds to a 68.3% confidence band. If the direction of the surge velocity is unknown, both directions and therefore both limits should be used in the calculations.

$$\dot{\eta}_1 = \pm\sigma \tag{4.7}$$

4.1.2.2 Wave impact velocity

The wave impact velocity is represented by the water particles horizontal velocity. To estimate this is difficult, but DNV suggest that this impact velocity, u, for undisturbed waves should be taken as 1.2 times the phase velocity of the most probable highest breaking wave in n years.

$$u = 1.2 c_B^{(n)} \tag{4.8}$$

The phase velocity of the most probable highest breaking wave in n years, $c_B^{(n)}$, can be estimated using the relationship between wave period and phase velocity for a sinusoidal wave in deep water Eq.(4.9) (Dean and Dalrymple, 1984). The wave under consideration is far from a sinusoidal wave but this is used as an estimate.

$$c_B^{(n)} = \frac{g}{2\pi} T_B^{(n)} \tag{4.9}$$

Where g is the acceleration of gravity and the wave period, $T_B^{(n)}$, is found from a wave breaking criterion for limiting steepness.

$$\varepsilon = \frac{H_B^{(n)}}{g T_B^{(n)2}} \tag{4.10}$$

Where $H_B^{(n)}$ is the height of the most probable highest breaking wave in n years, and ε is the global wave steepness. In Ochi (1998) two values for the global wave steepness are given. A theoretical limit where $\varepsilon = 0.027$ and an experimental limit where $\varepsilon = 0.020$. The experimental limit is lower than the theoretical limit. Using the experimental limit will give a larger wave period, Eq.(4.10). Larger wave period will again give a larger phase velocity, Eq.(4.9). Using the experimental limit will therefore give the most unfavorable results.

According to DNV-RP-C205 (2007) the most probable highest breaking wave height should be taken as 1.4 times the most probable largest significant wave height in n years, $H_S^{(n)}$.

$$H_B^{(n)} = 1.4 H_S^{(n)} \tag{4.11}$$

4.2 Model test

The characteristic impact force for a given probability level can also be predicted by model tests.

A model test is trying to investigate the behavior of the full-scale platform in the real world. A scaled model of the platform is made and tested in a wave basin. This scaling is usually done using Froudes law (Steen and Aarsnes, 2010). The tests are performed in different environmental conditions to give a good understanding of the models behavior.

A large advantage with a model test is that it makes it possible to look at highly nonlinear problems.

To be able to predict the characteristic impact force from model test measurements, a stochastic analysis needs to be performed. How this is done will be explained in the following.

4.2.1 Environmental contour line method

The randomness of the sea states needs to be taken into account in the stochastic analysis. For a linear problem a full long term analysis based on a broad range of sea states would be the appropriate approach, see e.g. Haver and Winterstein (2008). But since impact loads from breaking waves is highly nonlinear, a full long term analysis is practically impossible to perform. A good approach for this kind of problem is to use the environmental contour line method. This method

makes it possible to estimate long term extremes by considering only some few short term conditions.

A sea state is described by the significant wave height, H_S, and the spectral peak period, T_P. Contour lines are lines in a H_S-T_P plot that gives a description of the sea states with the same probability of exceedance, e.g. the 10 000 year contour line give sets of H_S and T_P values that have a 10^{-4} probability of exceedance per year.

How the contour lines are produced is described in Haver and Winterstein (2008). The contour lines used for the Midgard model tests are shown in Figure 4-1:

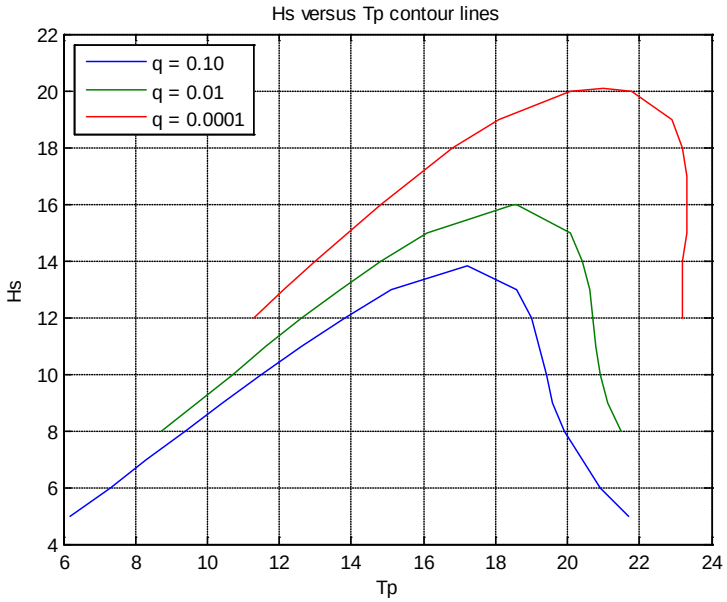

Figure 4-1: Contour lines for Åsgard MFP location (Mathiesen, 2010)

4.2.2 Estimation of characteristic impact force using contour lines and time series

When the environmental contour lines are established, the sea state that gives the most unfavorable results, i.e. the highest impact loads, needs to be determined. For the ALS condition, this is done by choosing a few sea states along the 10^{-4} probability contour line, and run some model tests for each of these. The results from the different sea states are compared and the worst sea state is determined.

All further model test realizations are then done with this so-called worst sea state. When investigating a response for a given sea state, it is necessary to have many realizations of the same sea state to get good statistical results. To be sure the realizations are independent from each other different seeds are used in the wave simulation. The wave elevation history generated by the wave maker will then be a different realization of the same wave spectrum. The common practice for the North Sea is that each realization represents a 3-hour interval in full scale.

The time series of the target response, in this case the impact loads from breaking waves, are measured during each of these tests. The extreme, or the largest peak, of the measured impact forces during one realization can be identified from these time series.

To estimate a design value for the impact force, a cumulative distribution of the impact force extremes must be established. A Gumbel distribution is found to be a good representation for these extreme values. The following is taken from Haver (2010). A cumulative Gumbel distribution with two parameters, μ and β, are given in Eq.(4.12).

$$F_{x_{3h}}(x) = \exp\left(-\exp\left(-\frac{x-\mu}{\beta}\right)\right) \tag{4.12}$$

Where μ and β are parameters that need to be estimated. These parameters are chosen so that the Gumbel distribution is fitted to the measured extremes. The estimation of these parameters can be done using the method of moments.

$$\beta = 0.7797 \cdot s_{x3h} \tag{4.13}$$

$$\mu = m_{x3h} - 0.57722 \cdot \beta \tag{4.14}$$

Where m_{x3h} is the mean and s_{x3h} is the standard deviation of the 3-hour measured extremes. They are found from the following equations:

$$m_{x3h} = \frac{1}{n}\sum_{i=1}^{n} x_{3h_i} \tag{4.15}$$

$$s_{x3h} = \left(\frac{1}{n-1}\sum_{i=1}^{n}\left(x_{3h_i} - m_{x3h}\right)^2\right)^{\frac{1}{2}} \tag{4.16}$$

Where n is the size of the sample, and x_{3h_i} are the *i*th 3-hour extreme value.

To verify the parameter estimation and choice of distribution a Gumbel probability paper can be used. This is done by rearranging the measured extreme values in ascending order, x_k. The cumulative distribution for the sample can then be found using Eq.(4.17).

$$\hat{F}_{x_{3h}}(x_k) = \frac{k}{n+1} \tag{4.17}$$

Where k is the number of observations less or equal to x_k and n is the size of the sample.

Eq.(4.12) is rearranged and results in the linear equation Eq.(4.18).

$$-\ln\left(-\ln\left(F_{x_{3h}}(x)\right)\right) = \frac{1}{\beta}x - \frac{\mu}{\beta} \tag{4.18}$$

Where the left side of Eq.(4.18) represents the y-axis in a Gumbel probability paper. When the fitted Gumbel distribution is plotted on a Gumbel probability paper it will be a straight line. If the empirical distribution, Eq.(4.17), is reasonably close to this straight line, the model can be a good representation of the underlying variable.

In Suyuthi (2009) another model was also used to represent the measured extremes, a two parameter Frechet distribution. The cumulative Frechet distribution is given in Eq.(4.19)

$$F_{x_{3h}}(x) = \exp\left(-\left(\frac{\lambda}{x}\right)^{\kappa}\right) \tag{4.19}$$

Where the parameters λ and κ can be estimated using the maximum likelihood estimation and iteration. Maximum likelihood estimation is explained in Walpole et al. (2007).

To verify these parameters a Frechet probability paper can be used. It is based on the same principle as the Gumbel probability paper. Rearranging Eq.(4.19) results in the linear equation Eq.(4.20).

$$-\ln\left(-\ln\left(F_{x_{3h}}(x)\right)\right) = \kappa \ln x - \kappa \ln \lambda \tag{4.20}$$

Where the left side in Eq.(4.20) represents the y-axis in a Frechet probability paper.

When a probability distribution of the 3-hour extremes is established for a given probability level, the design values can be found by selecting a proper α -percentiles.

The α -percentile is chosen so that it accounts for the total short term variability of extreme values. When using the environmental contour line method, there is a probability that the maximum response will occur in other sea states than the worst sea state. By using proper value of α , this is taken into account. NORSOK N-003 (2007) suggests using a percentile between the 90th and the 95th for 10^{-4} annual exceedence probability or a clearly nonlinear problem, such as the breaking wave problem. It is then assumed that the short term variability in the sea states are accounted for and that the α -percentile result will be a proper estimate for the target long term extreme value (i.e. the 10^{-4} annual probability impact force).

5 Prediction of impact loads based on DNV-RP-C205

In this chapter the impact loads will be predicted numerically, using the method based on DNVs recommended practice, DNV-RP-C205 (2007), which is explained in subchapter 4.1. The ALS loads are the loads of interest, therefore waves with a 10^{-4} annual probability of excedeence is used.

5.1 Estimated relative horizontal impact velocity

The most probable largest significant wave height in 10 000 years, $H_S^{(10000)}$, can be taken from the 10 000 year environmental contour line presented in Figure 4-1. Based on this, is set to 20.2m. When using this value, the most probable highest breaking wave height, $H_B^{(10000)}$ is found by Eq.(4.11). Further the breaking wave period, $T_B^{(10000)}$, is found from the wave breaking criterion for limiting steepness shown in Eq.(4.10). Since the experimental limit for the global wave steepness, $\varepsilon = 0.020$, gives the most unfavorable result, this has been used. The relationship between wave period and phase velocity for a sinusoidal wave in deep water, Eq.(4.9), is used to find the phase velocity of the most probable highest breaking wave in 10 000 years, $c_B^{(10000)}$. An estimate for the impact velocity of the water surface is then found by multiplying this phase velocity with 1.2, as shown in Eq.(4.8).

The platforms surge velocity is found using the method explained in subchapter 4.1. The platforms surge RAO is taken from the WADAM analysis presented in Dalane (2011). The surge velocity RAO is then found from Eq.(4.3). The surge velocity spectrum is then found by multiplying this RAO raised to second power by the actual sea states wave spectrum. The actual sea state is set to the peak of the 10 000 year environmental contour line in Figure 4-1. The significant wave height and the peak period are therefore set to 20.2m and 21.0s respectively. The wave spectrum used is a Pierson Moskowitz wave spectrum for fully developed sea (Haver, 2010).

The wave spectrum, surge velocity RAO and the following surge velocity spectrum is shown in Figure 5-1.

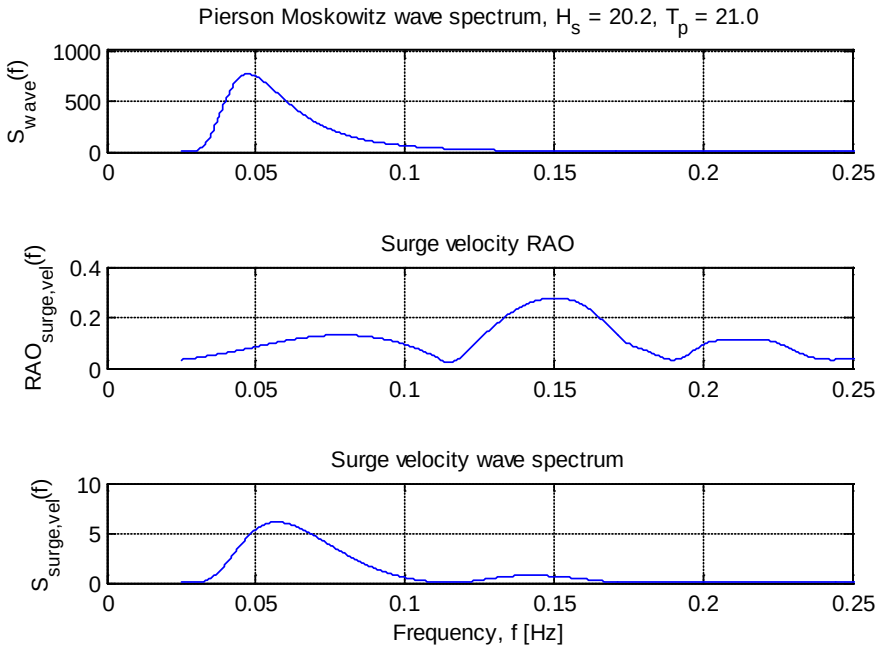

Figure 5-1: Wave spectrum, surge velocity RAO and surge velocity spectrum

The standard deviation is then found using Eq.(4.5) and Eq.(4.6). This is used as an estimate for the platform surge velocity. The surge velocity can be in both positive and negative direction so two relative horizontal velocities are calculated. The estimated velocities are presented in Table 5-1.

H_s (m)	H_B (m)	T_B (s)	c_B (m/s)	u (m/s)	$\dot{\eta}_1$ (m/s)	v^- (m/s)	v^+ (m/s)
20.20	28.28	12.01	18.74	22.49	0.50	**21.99**	**22.99**

Table 5-1: Estimated relative horizontal velocity

It can be seen that the platform surge velocity is relative small compared to the wave velocity.

5.2 Estimated impact force based on DNV-RP-C205

When the relative horizontal velocity is estimated, a slamming coefficient needs to be decided. DNVs recommended value for the space average slamming pressure coefficient, $C_{Pa} = 2\pi$, is used. The mass density of seawater, ρ, is set to 1025 kg/m^3.

All the values needed to calculated the space average slamming pressure, p_s, with 10^{-4} annual probability of exceedence is now found. The results obtained from using Eq.(4.1) are shown in Table 5-2.

ρ (kg/m^3)	C_s (-)	v^- (m/s)	v^+ (m/s)	p_s^- (kPa)	p_s^+ (kPa)
1025	6.28	21.99	22.99	**1 557.1**	**1 702.0**

Table 5-2: Predicted ALS space average slamming pressure using DNV-RP-C205

5.3 Uncertainties in the method based on DNV-RP-C205

The estimation of the slamming coefficient and the relative impact velocity introduce a lot of uncertainties in DNVs method. These will be further discussed in this subchapter.

The slamming coefficient is set equal to 2π in these calculations. In the real world a lot of parameters will influence the slamming coefficients. By using this value it is assumed that the wave represents water that hits a completely vertical area on a column, with a direction normal on the column in both the vertical and horizontal direction.

During a real slam it is reasonable to assume that the platform, which is a floating structure, will move in all 6 degrees of freedom. It is likely that the platform will have at least a small offset angle in both pitch and jaw when a wave hits the column. In addition, the water from the wave might hit the column with an angle different from 90 degrees in both vertical and horizontal direction. This is factors that would influence the slamming coefficient. However, it would be very hard to estimate a slamming coefficient that includes this, especially since it would be different for each breaking wave impact.

When finding the phase velocity it is assumed that the wave is a regular sinusoidal wave by using Eq.(4.9). A breaking wave is usually very asymmetric and to assume a sinusoidal wave is therefore a bad assumption.

The phase velocity is multiplied with a factor 1.2 to get an estimate of the wave impact velocity. DNV suggest using this factor for undisturbed waves. In the case of Midgard, the impact happens in the vicinity of a large volume structure, and the impact velocity will be affected by diffraction effects. This is not accounted for here.

6 Prediction of impact loads based on model test data

During the summer 2010 MARINTEK performed model tests with the Midgard platform. The model test was performed at the ocean basin at the Marine Technology Centre in Trondheim. The model was built at a scale of 1:55. A picture of the model is shown in Figure 6-1.

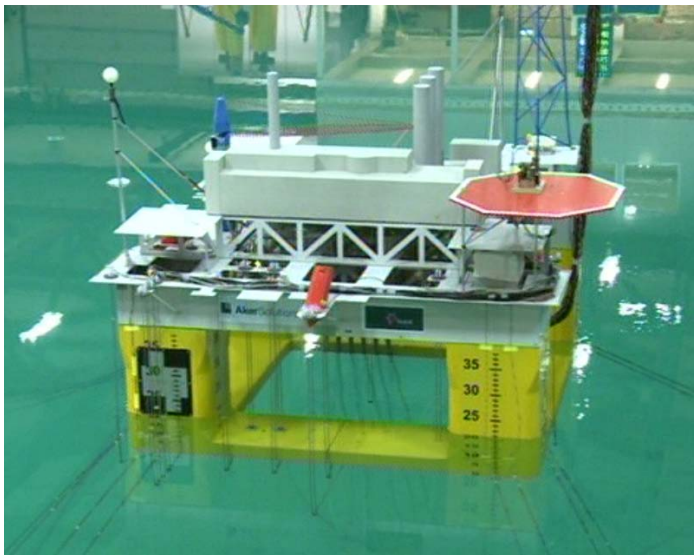

Figure 6-1: Snapshot of Midgard model from recordings of the model tests performed by MARINTEK 2010.

In the model test performed by MARINTEK, four sea states were chosen from the 10 000 year environmental contour line from the metocean report (Mathiesen, 2010). Two realizations were performed for each of them. The duration of each realization corresponds to 3 hours in full scale.

For the 10 000 year condition, relevant for impact loads in this report, it was determined to use a sea state with $H_S = 20.2m$ and $T_P = 21.0s$ as the worst sea state. Further, 18 model test realizations was performed for this sea state.

In this model test the worst sea state was chosen based on which sea state that gave the worst air-gap response. If the worst sea state had been chosen based on the worst impact force from breaking waves, it is possible that a different sea state had been chosen. It is possible that a sea state with a lower T_P on the right side of the peak in the 10 000 year contour line, would be chosen. A lower spectral peak period would result in steeper waves, and it is therefore possible that it would increase the number of breaking waves. However, the significant wave height would then also be lower and the impacts would probably be less severe.

The breaking wave impacts were measured by 8 slamming sensors located at the North-West column. Each slamming sensor had an area of $9m^2$. The sensors were arranged as in Figure 6-2:

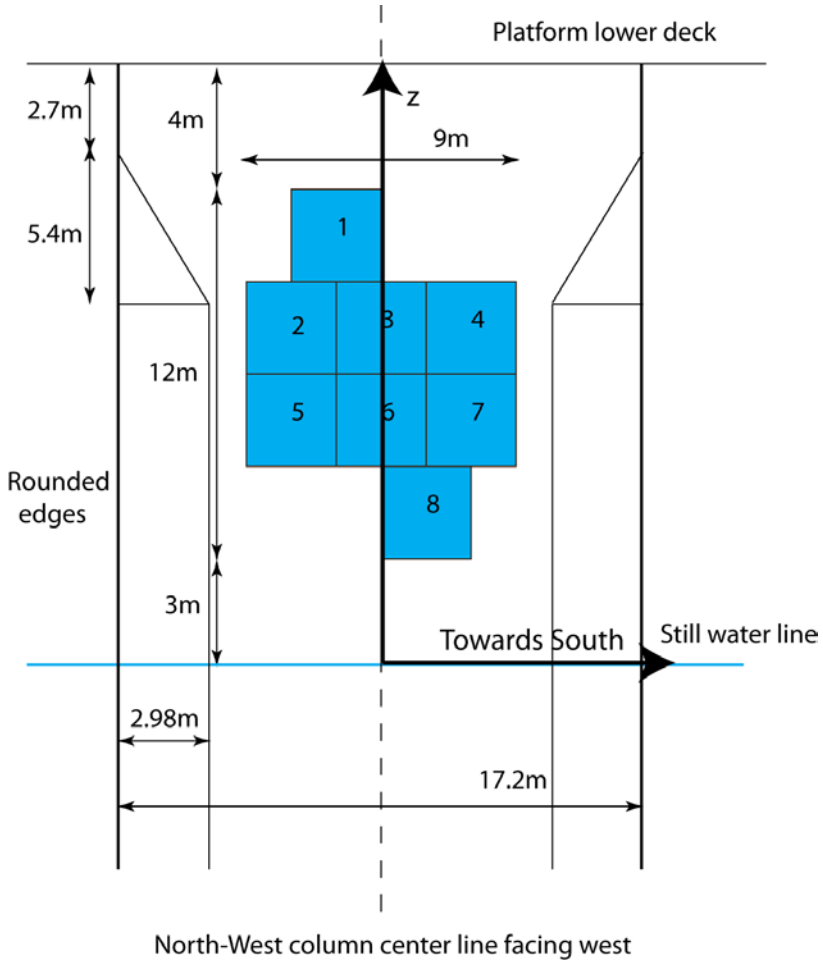

Figure 6-2: Overview of slamming sensors

The slamming event is transient. The slamming forces occur infrequently, and the number of large slams caused by breaking waves in a 3-hour realization varies, typically between two and ten. The model test data received by MARINTEK only includes slamming measurements for slams that gave impact force larger than 1 000kN.

6.1 Elimination of slamming sensor dynamics

The slamming sensors used, consist of a slamming panel connected to a transducer. A slamming sensor is a dynamic system and the data measured from the sensors are therefore not the exact load, but the response caused by the load. When a slamming sensor experiences an impact force, the response will be of transient nature. This will result in a dynamic amplification of the response signal. Denoting the maximum response force, $R_{\max}$, and the maximum impact force, $F_{\max}$, the dynamic amplification factor, DAF, is defined as:

$$DAF = \frac{R_{\max}}{F_{\max}} \tag{6.1}$$

Since it is the actual impact loads that are of interest, the dynamic amplification factor needs to be found. A method to estimate the impact load was suggested by Erik Lehn (2011) and is described in the following.

At first the actual impact force history is guessed based on the measured force. Figure 6-3 shows an example for sensor 1 during the largest slam in test 3124.

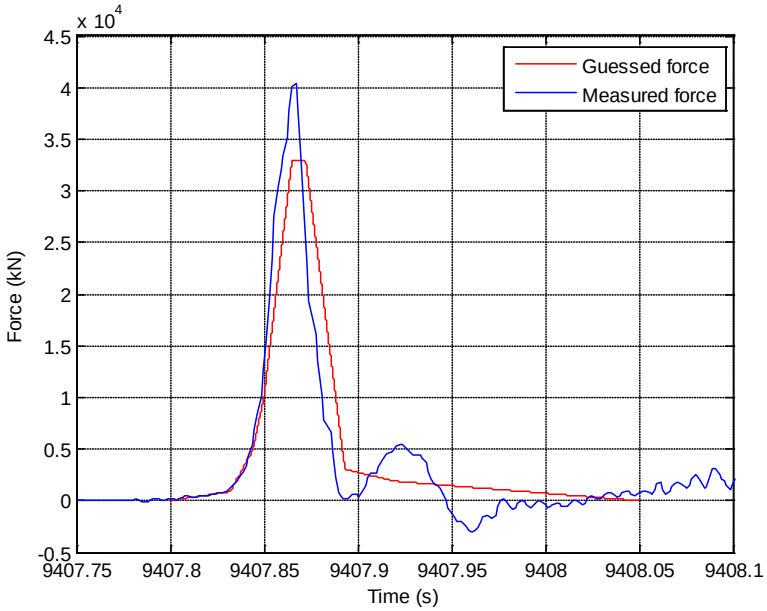

Figure 6-3: Guessed force and measured force for largest slam in test 3124

A time domain simulation for a one mass system with the guessed impact force is performed. This has been solved using the Runge-Kutta method explained in Langen and Sigbjörnsson (1979). The response force is then compared with the measured force. If the differences are large, the impact force history is changed, and a new simulation is run. This is done until the two responses look similar. Similarity at the largest peak is most important. The magnitude of the dynamic response depends on (Lehn, 2003):

- T_{rise}/T_{dur} *the ratio of the rise time to the load duration*
- T_{rise}/T_0 *the ratio of the rise time to the natural period of the structure*
- T_{dur}/T_0 *the ratio of the load duration to the natural period of the structure*
- *The shape of the load*

The rise time is defined as the time interval from impact starts until it reaches its maximum value.

From Figure 6-3 it can be seen from the measured force that the dynamic system has two resonance frequencies. These frequencies are given in MARINTEK (2010). The first one is the resonance frequency of the slamming sensor itself, and is equal to 80 Hz, while the second one is caused by some instrumentation at the NW column, and is equal to 37 Hz. To get the time domain simulations to be correct, a two mass system should be used. For simplicity two simulations are done for each of the mass systems. The results from the two simulations can be seen in the following figures:

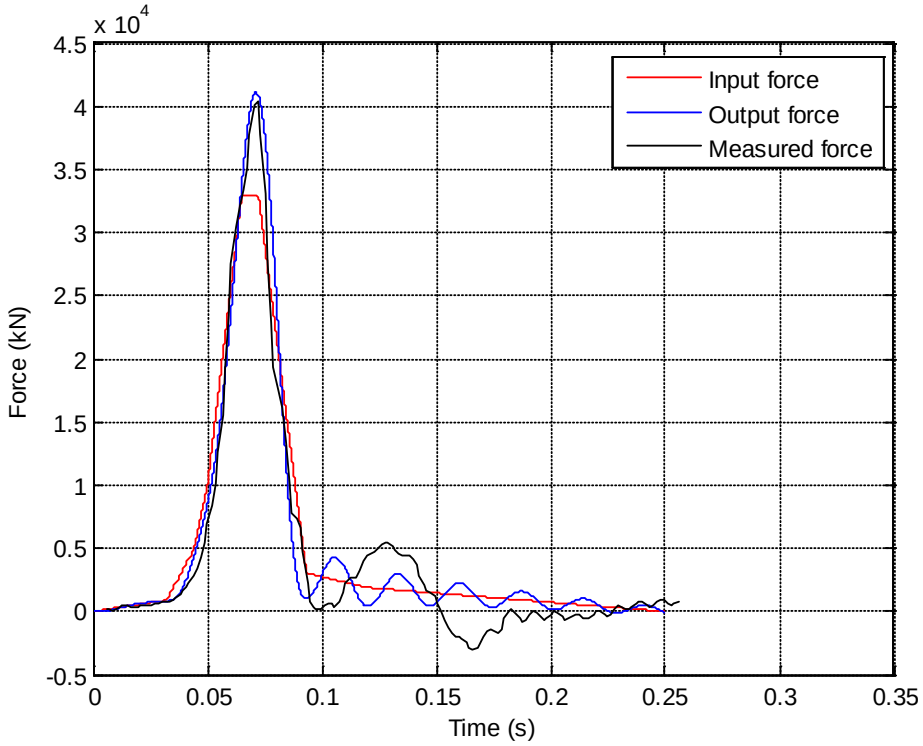

Figure 6-4: Time domain simulation with resonance frequency 37 Hz

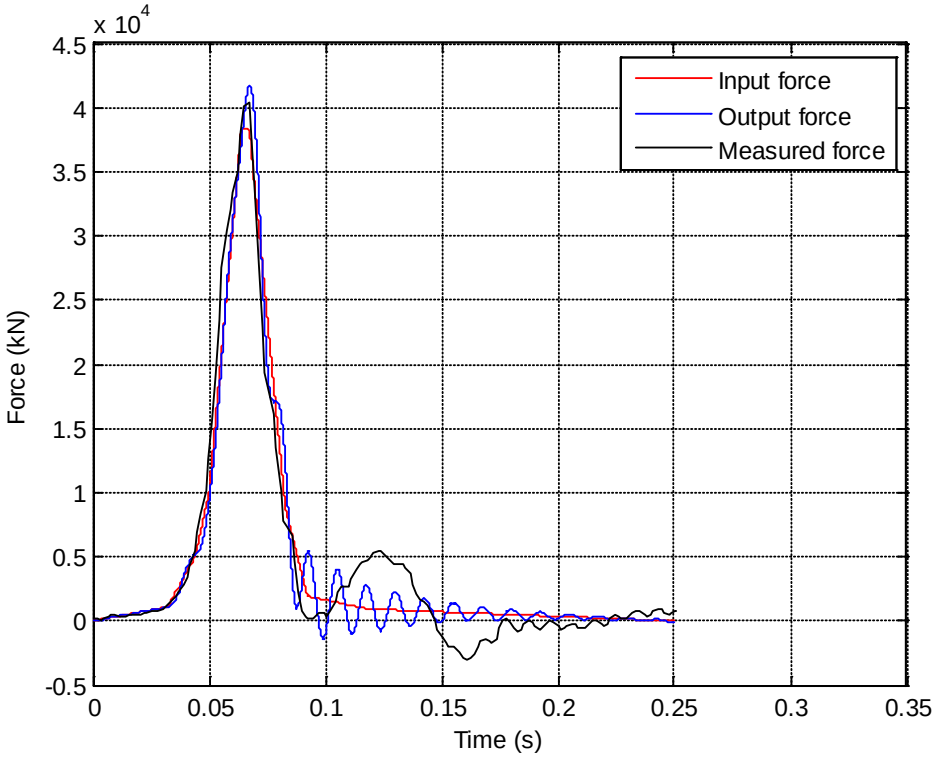

Figure 6-5: Time domain simulation with resonance frequency 80 Hz

Figure 6-4 and Figure 6-5 shows the estimated impact forces when using the two resonance frequencies. Using the peak of the measured force in Figure 6-3 combined with the results from the time domain simulations the dynamic amplification factors can be found. For the system where the resonance frequency is 37 Hz the dynamic amplification factor is estimated to 1.22, while for the system where the resonance frequency is 80 Hz it is estimated to 1.05. Based on these estimations it can be anticipated that the system's dynamic amplification factor will be in between these two values. Based on this, the dynamic amplification factor is set equal to 1.16.

The dynamic amplification factor is very dependent on the four points mentioned earlier. Therefore sensor 1 will have different dynamic amplification for each slam. The factor will vary between 1.0 and 2.0. For simplicity, the factor estimated in the example above will be used for all impact loads on sensor 1. For many slams the estimated force will then probably become smaller than it should since this dynamic amplification was as low as 1.16.

6.2 Establishing the cumulative distribution

The measured maximum impact forces at panel 1 from each test and the estimated maximum forces found using 1.16 as dynamic amplification factor, are given the following table:

Test	Measured force [kN]	Estimated force (DAF = 1.16) [kN]
3100	40 645	35 039
3111	2 398	2 067
3120	4 726	4 074
3121	6 083	5 244
3122	3 463	2 985
3124	40 352	34 786
3126	7 874	6 788
3129	2 633	2 270
3131	2 616	2 255
3133	3 907	3 368
3135	2 147	1 851
3137	2 543	2 192
3139	10 395	8 961
3141	5 044	4 348
3142	11 241	9 691
3144	8 573	7 391
3146	6 294	5 426
3148	2 043	1 761

Table 6-1: Measured and estimated maximum forces for panel 1

When using the method described in subchapter 4.2, the cumulative Gumbel distribution will become as follows:

$$F_{x_{3h}}(x) = \exp\left(-\exp\left(-\frac{x-3233.073}{7921.271}\right)\right) \tag{6.2}$$

Figure 6-6 shows the fitted Gumbel distribution, Eq.(6.2), and the sample data plotted in a Gumbel probability paper.

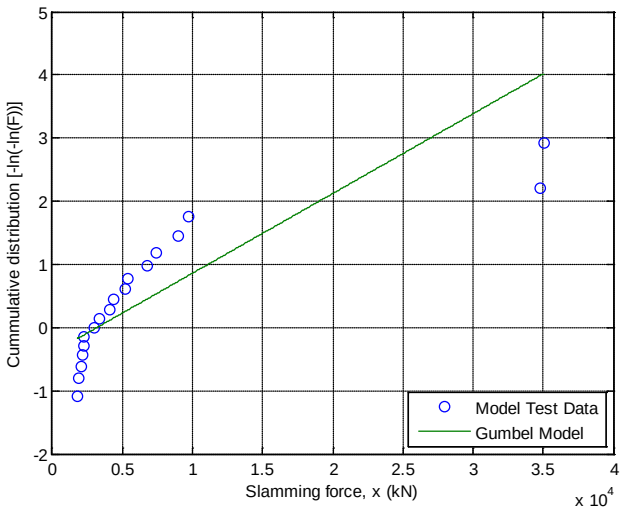

Figure 6-6: Gumbel probability paper with fitted Gumbel distribution and sample data

From Figure 6-6 it can be seen that the estimated Gumbel distribution are not representing the model test data very well. There is some deviation between the measured values and the straight line in the Gumbel probability plot. Especially the values from test 3100 and 3124 stand out.

A cumulative Frechet distribution is also established to see if it would represent the model test data better than the Gumbel distribution. The cumulative Frechet distribution fitted to the 3-hour maximum values become as follows:

$$F_{x_{3h}}(x) = \exp\left(-\left(\frac{2925.1}{x}\right)^{1.3461}\right) \tag{6.3}$$

Figure 6-7 shows the fitted Frechet distribution and the sample data plotted in a Frechet probability paper.

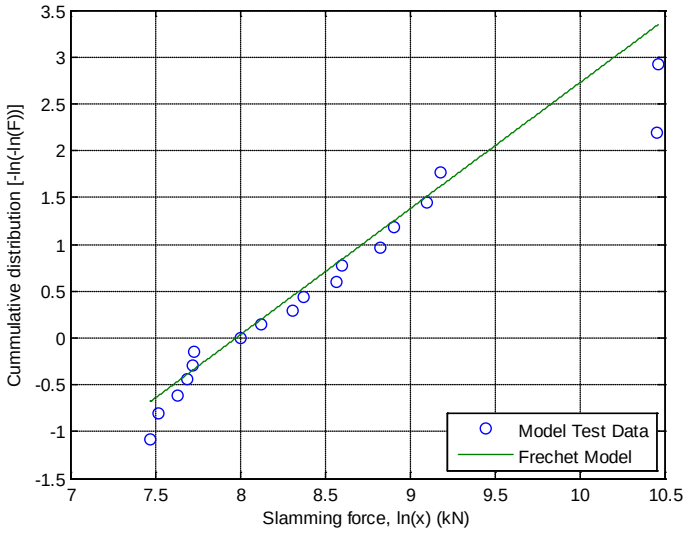

Figure 6-7: Frechet probability paper with fitted Frechet model and sample data

Figure 6-7 shows that the Frechet distribution is a better model for the model test data than the Gumbel distribution. However, the values from test 3100 and 3124 are not represented very well using neither of the distributions.

There can be different reasons why the large slams from test 3100 and test 3124 stands out when compared with the other slams. It is possible that when a slam gets so large there can be some nonlinear effects that trigger mechanisms different from the smaller slams. These slams would then belong to a different population than the smaller slams. This would explain why these values deviate from both the Gumbel and Frechet model. A probabilistic model that accounts for this should then be used. The probabilistic model could be a hybrid model, consisting of two distributions with a reasonable transition. The distribution that describes the large slams should then have a thicker and longer tail than the Gumbel and Frechet distributions in Figure 6-6 and Figure 6-7. The idea is that the probabilistic model should describe the whole range of slams in a better way. Figure 6-8 contains two drawn lines that illustrate this idea.

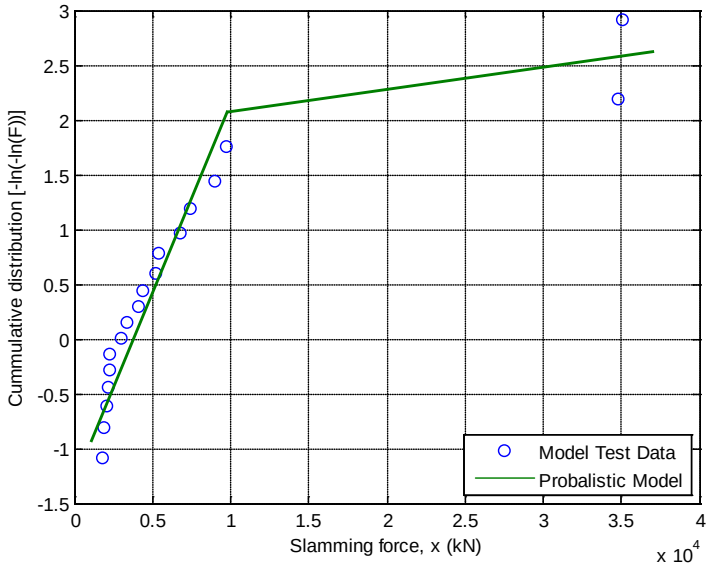

Figure 6-8: Illustration of a probabilistic model describing two populations

6.3 Design value for the impact force using model test data

When the distribution function of the 3-hour extremes is established, the design value for the impact force can be found by the distributions α -percentiles.

According to NORSOK N-003 (2007), a percentile between 90th and 95th should be used when predicting characteristic values for this kind of problem. Since using the 95th percentile gives the worst result, this has been used. By solving Eq.(6.2) and Eq.(6.3) using the 95th percentile the predicted 10^{-4} probability impact force, $X_{3h,10^{-4}}$, is found. This can be transformed into pressure, $p_{3h,10^{-4}}$, by dividing the force on the area of panel 1, equal to 9m^2. The results are shown in Table 6-2:

Distribution	$X_{3h,10\text{-}4}$ [kN]	$p_{3h,10\text{-}4}$ [kPa]
Gumbel	26 761	2 973
Frechet	26 572	2 952

Table 6-2: Predicted ALS impact force and pressure from stochastic analysis

Table 6-2 shows that the predicted impact force using the 95th percentile is almost identical for the two distributions. In MARINTEK (2010) they have chosen to use a Gumbel distribution instead of a Frechet distribution since it is well established and the preferred extreme value distribution. Based on this, the value obtained from the Gumbel distribution is chosen as the design value for ALS impact force based on model test data.

As mentioned earlier, the two largest values are not represented well by any of these two distributions. Two values are a not insignificant amount in a sample with a total of 18 values. If a cumulative distribution is made for the sample using Eq.(4.17), the largest measured impact force would represent the 95th percentile in this distribution, while the second largest would represent the 90th percentile. Since these impact forces are so much higher than all the other measured forces

during the model test, the load histories for these two slams will be used when investigating global structural effects later in the report.

6.4 Assessment of uncertainties in model test predictions

When predicting the design impact load from breaking waves using stochastic analysis of model test data, there will be uncertainties involved.

The measurements from the model test itself may introduce some uncertainties, like model effects and measurement uncertainties.

The dynamic effects in the slamming sensors should be removed for all sensors. In this report the dynamic amplification factor was only estimated for one breaking wave impact, and for simplicity it was assumed that this could be used for all slams. The correct thing to do would be to estimate this dynamic amplification factor for all the measured slams.

In addition to the dynamic in the sensors, the panel size of the sensor may introduce some uncertainties. From investigating the different sensors during several slams, it is seen that there is differences in measurements for sensors at different location on the column. If looking at a horizontal strip on the column it seems like there can be some small differences in the peak impact force along this strip. If a very small panel size is used, it is possible that this sensor measure a local peak impact force that is not representing the impact force averaged over the entire strip. On the other hand it is likely that too small panels will miss the local peak force. To assure that neither of this is happening Lehn (2003) suggests to use sensors with panel size between $5m^2$ and $10m^2$. The panel size used in this model test is $9m^2$ and is therefore in range of these suggested sizes. It is also seen during investigation of the different sensors, that the differences in horizontal direction gets less for large slams. This is further described in subchapter 8.3.

In DNV-RP-C205 (2007) it is mentioned that Froude scaling of the slamming measurements might also give some errors. Entrained air in the water will reduce the impact pressure. The model test is performed in freshwater. Freshwater has different properties than seawater. Because of this the entrapped air will escape faster in freshwater than in seawater. Scaling by Froudes law does not account for this and will therefore overestimate the measured pressure peaks.

However, if assuming that the data from the model test was correct, the stochastic analysis would still introduce a lot of uncertainties. Two clear uncertainties involved in an approach like this are the selected probabilistic model and the estimation of parameters of the model. These uncertainties will be showed in the following.

6.4.1 Bootstrapping

One method that can be used to estimate statistical uncertainty is the Bootstrapping method. It is a statistical resampling method that can be used to determine the confidence band of a statistical variable. This method is described in Efron (1979).

To determine the confidence band of the measured impact force extremes, a large amount of measurements should be used to get a confidence band with certain accuracy. During the model test only 18 realizations was run, and therefore only 18 extreme values was obtained. The advantage with the bootstrapping method is that it makes it possible to determine the confidence band when the

number of measured data points is insufficient for the normal way of determining these characteristics. With the bootstrapping method, new samples containing 18 data points are created using the 18 extreme values measured during the model tests.

It is assumed that there is an equal probability for each of the 18 measured extreme values to occur. 18 values are then picked randomly with replacement, from the measured sample. A new data set is then created. Since there is an equal probability for the measured extremes to occur, it is possible that the same value can be picked more than one time. This new data set will then contain values that are physical possible since they are measured in the model tests. This procedure can be repeated many times to get as many as possible data sets. The cumulative distribution for each value in these new data sets can be found using Eq.(4.17). The new data sets can then be plotted in a Gumbel probability paper that also includes the original sample. This is shown in Figure 6-9.

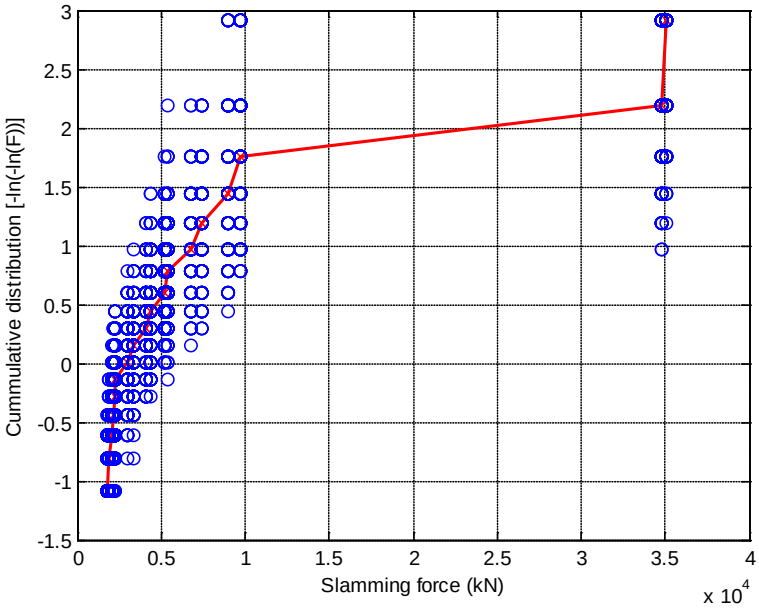

Figure 6-9: Values from 200 samples generated with Bootstrapping method and the original sample

The figure shows the data points generated with the Bootstrapping method. The original data sample is linked together by the red line. Since all the data sets contain 18 values, the values will be distributed over the same probability levels found by Eq.(4.17). It is therefore possible to determine the confidence band for each of these probability levels. It is assumed that the values at each probability level follow a normal distribution. The mean and variance is found at each probability level and the confidence band is estimated using a normal distribution. The 90% confidence band determined using this method is shown in the following figure.

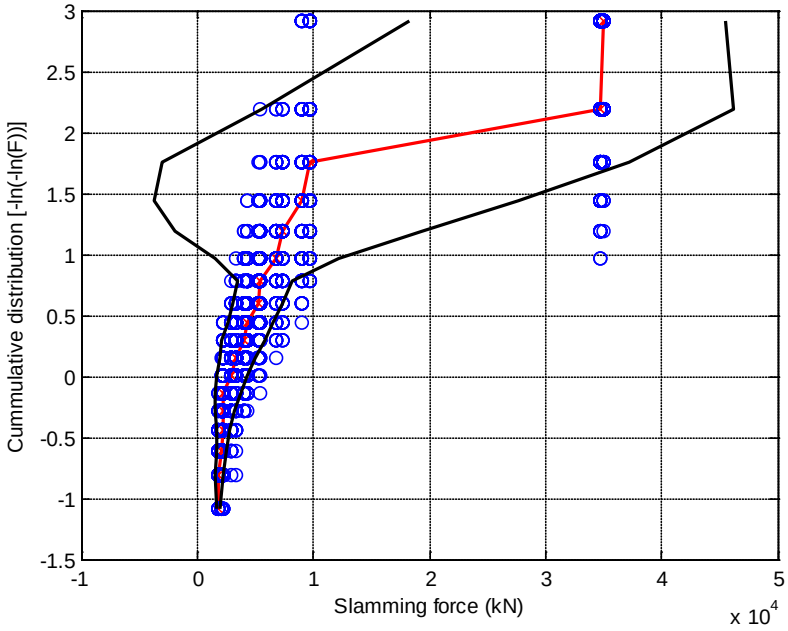

Figure 6-10: Values from 200 samples generated with Bootstrapping method, and the associated 90% confidence band

The 90% confidence band is shown in Figure 6-10 as the area between the two black lines. The confidence band is very narrow for lower probabilities while it widens out for the higher probabilities. This means that the uncertainty gets larger for higher probability levels.

For the highest probability level it can be seen that the confidence band is narrower than for the second highest probability level. This is caused by a short-coming of the Bootstrapping method. When the largest of the measured extremes is picked to a data set, it will always be appointed the highest probability from Eq.(4.17). This will cause a small tightening of the confidence band for this probability level. Unfortunately this probability level is equal to the 95th percentile where the design impact force is found. However, the confidence band shows us that high probability levels have large uncertainties. The 90% confidence band for the 95th percentile found using the Bootstrapping method is given in Table 6-3.

	90% confidence band		
$X_{3h,10-4}$ [kN]	lower limit [kN]	upper limit [kN]	mean value [kN]
26 761	18 224	45 573	31 898

Table 6-3: 90% confidence band and mean value from the Bootstrapping method at the 95th percentile

It can be seen that the 90% confidence bands upper limit is a factor 1.7 larger than the predicted value from the Gumbel distribution.

6.4.2 Parametric Bootstrapping

Another method that can be used to estimate the statistical uncertainty, is the Parametric Bootstrapping method. While the Bootstrapping method only used the measured values to generate new samples, the parametric bootstrapping method uses the distribution established based on the measured values. The Gumbel distribution, Eq.(6.2), is set as the “true” distribution when using this method. New samples of 18 values will then be generated based on this distribution using the Monte

Carlo method. This method is described in Haver (2010). A new sample is generated by drawing random numbers between 0 and 1. The x-values, in this case the impact force, are then found by the following formula.

$$x_j = F_X^{-1}\left(\theta_j\right) \tag{6.4}$$

Where θ_j is a random number between 0 and 1

F_X^{-1} is the inverted cumulative distribution function

x_j is the generated value

j is each value's number in the sample

In this case the inverted cumulative distribution function, F_X^{-1}, is the inverted Gumbel distribution in Eq.(6.2). Samples are generated by doing this for 18 values. This sample is then sorted in ascending order, and each value is given a cumulative probability by Eq.(4.17). 200 samples are generated by using this method. They are then plotted in a Gumbel probability paper together with the original sample and the "true" Gumbel distribution.

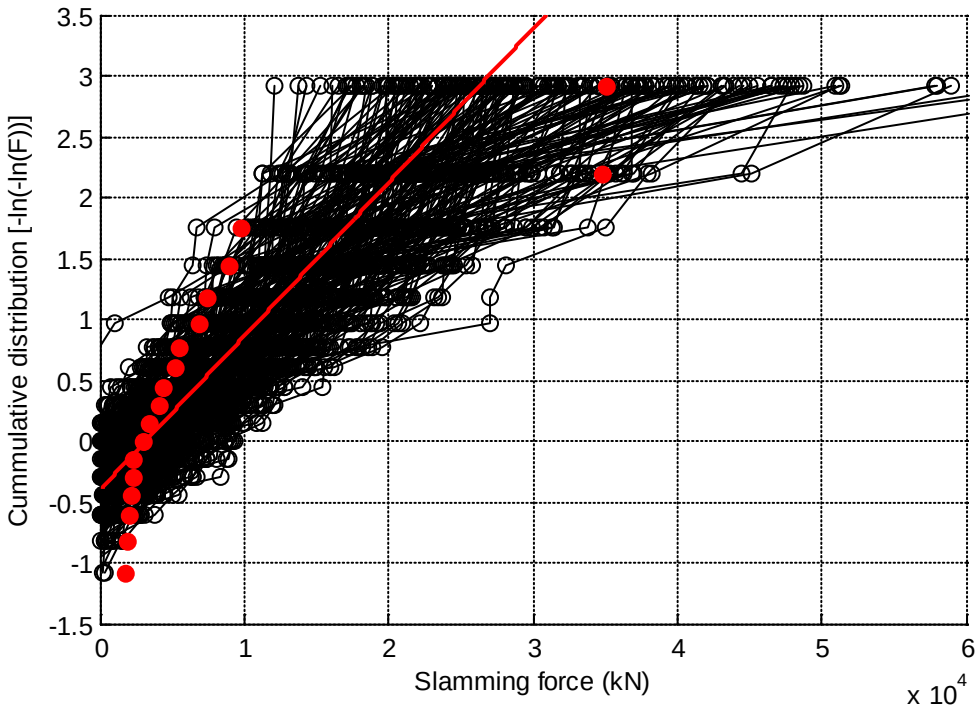

Figure 6-11: 200 samples generated with Monte Carlo method, original sample and fitted Gumbel model

From Figure 6-11 it can be seen that the original sample is enveloped by the generated samples. This means that the spreading of the original sample can to some extend be explained by the uncertainty in the estimated Gumbel model.

In Figure 6-11 a large spreading of the generated samples can be seen, especially for the high probability levels.

The 90% confidence band based on the generated values is shown in Figure 6-12.

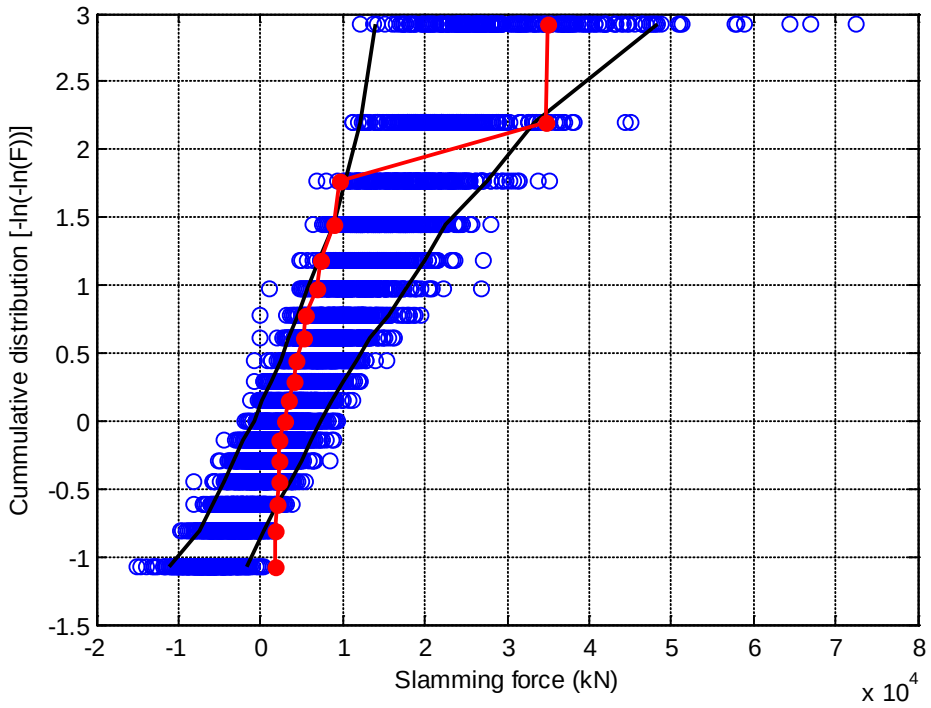

Figure 6-12: Values from 200 samples generated with Monte Carlo method, and the associated 90% confidence band

From this it can be seen that the confidence band gets wider for higher probabilities. It can therefore be concluded that the uncertainty rises for higher probability levels.

The 90% confidence band found by using the Monte Carlo method is much smoother than the one found using the Bootstrapping method. In addition, it doesn't have the short-coming at the highest probability level as the Bootstrapping method.

The 90% confidence band and mean value at the 95th percentile are given in Table 6-4.

	90% confidence band		
$X_{3h,10-4}$ [kN]	lower limit [kN]	upper limit [kN]	mean value [kN]
26 761	12 233	48 350	30 292

Table 6-4: 90% confidence band and mean value from the Monte Carlo method at the 95th percentile

Using this method the 90% confidence bands upper limit is a factor 1.8 larger than the predicted value.

The 90% confidence band found using the Monte Carlo method seems to be much more consistent than the one found from the Bootstrapping method. Therefore, this confidence band has been used later, when comparing with the predicted value based on DNVs recommended practice.

7 Discussion: Numerical method vs. Model test

In this chapter the differences in the predicted impact force from the two different methods will be discussed.

The predicted impact pressures with a 10^{-4} annual probability of exceedence from both of these methods are given in Table 7-1.

Design impact pressures from breaking wave impact		
Model Test [kPa]	**90% confidence band [kPa]**	**DNV [kPa]**
2 973	2 025 - 5 064	1 557 - 1 702

Table 7-1: Predicted ALS impact pressure from breaking waves

The design impact pressure predicted from the model test is almost twice as large as the pressure obtained using DNVs recommended practice. The lower limit in the 90% confidence band from the model test estimations is also larger than the results from DNVs recommended practice.

Uncertainties in the two different methods are discussed earlier. Are these uncertainties enough to explain the large difference in the results? To investigate the difference a bit further, the values used in the numerical method will be compared with measured values from the model test.

7.1 Discussion: Slamming coefficient

The slamming coefficient used in Eq.(4.1) was assumed to be equal to 2π based on recommendations. Is it possible that this slamming coefficient is too small? The predicted impact pressure from the model test data was 2 973kPa. To obtain this impact pressure using Eq.(4.1), with a slamming coefficient equal to 2π, the relative impact velocity must be 30.4m/s. Is it reasonable with impact velocities as large as this? Is it possible that the slamming coefficient should have been higher under the conditions of a breaking wave impact?

7.2 Discussion: Relative horizontal impact velocity

The relative horizontal impact velocity based on DNVs recommended practice was estimated to be between 21.99m/s and 22.99m/s. When calculating the impact pressure based on DNVs recommendations this velocity is raised to second power. It is therefore the most important parameter by Eq.(4.1). This relative impact velocity accounts for both the wave impact velocity and the platform surge velocity. These two quantities will be discussed in the following.

7.2.1 Discussion: Surge velocity

The platforms surge velocity used in the numerical method was estimated using the frequency domain. The slowly varying surge velocity was therefore neglected. First the platforms surge velocity spectrum was found. This was then used to find the standard deviation to the surge velocity. The standard deviation was then used as an estimate for the surge velocity. By this method the surge velocity is set equal to 0.5m/s in both positive and negative surge direction. Is it possible that the estimated surge velocity is wrong? To see if this is a realistic estimate, the platform surge velocity at the moment a breaking wave hits the column is found from the model tests.

During each realization in the model test, the platform surge displacement is measured as a time series. The surge velocity can then be found by differentiating the surge displacement with respect to time. The surge velocity can then be identified at the time instance when a breaking wave hits the column. The measured impact force can then be plotted together with the platform surge velocity at the same time. A plot like this, for the largest slam in test 3100, is shown in Figure 7-1. Same type of plots from the largest slam in each realization can be found in Appendix B. Positive surge velocity is toward the breaking wave.

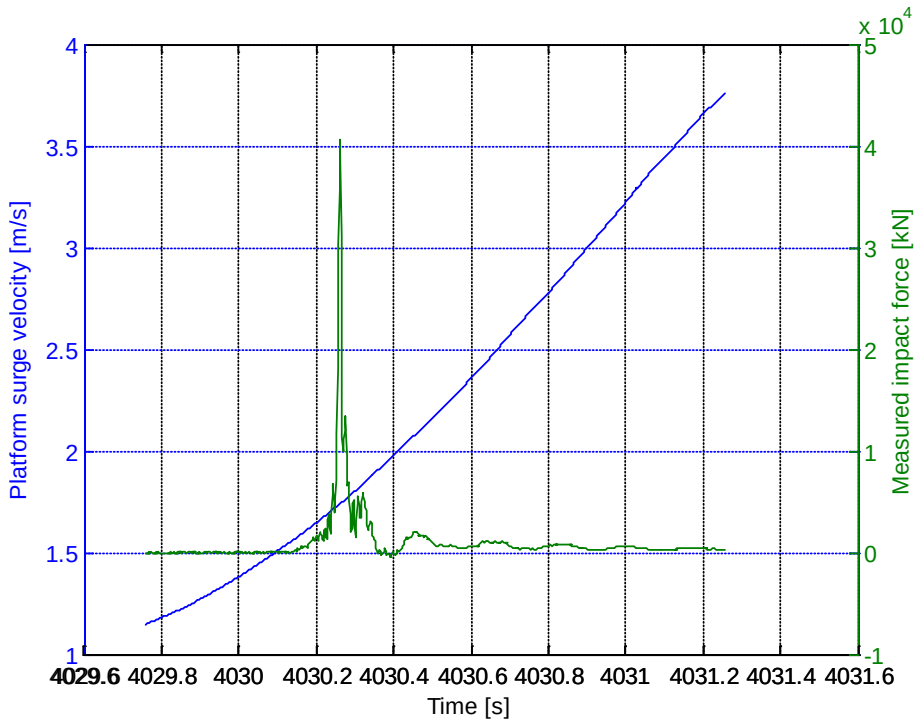

Figure 7-1: Platform surge velocity and measured impact force for largest slam in test 3100

By using these plots it is possible to manually find the surge velocity at the time instance when the wave hits the column. This has been done for the largest slam in each of the 18 realizations run in the model test. These surge velocities are presented in Table 7-2. A positive value means that the platform is moving toward the breaking wave, while a negative value means that it is moving away from the wave.

Test	Surge velocity [m/s]
3100	1.6
3111	0.8
3120	0.7
3121	0.7
3122	-0.3
3124	1.5
3126	1.8
3129	0.9
3131	0.4
3133	0.6
3135	1.7
3137	0.1
3139	3.8
3141	-0.5
3142	1.2
3144	0.9
3146	0.8
3148	0.9

Table 7-2: Platform surge velocity at the time instance the breaking wave hits the column for the largest slam in each test

The surge velocities vary between 3.8m/s toward the breaking wave and 0.5m/s away from the breaking wave. When the platform has a surge velocity toward the breaking wave it will increase the relative horizontal impact velocity, and therefore also increase the impact force. This is the case for all velocities shown in Table 7-2 except two. During these two slams the surge velocity is away from the breaking wave and will therefore reduce the impact force.

It is then interesting to see if the surge velocity is an important parameter. If it is an important parameter, it is expected that larger surge velocity toward the breaking wave should give larger impact force. To investigate this, a plot is made where the maximum measured impact force is plotted against the surge velocity at the time the wave hits the column. This is done for the largest slam in each of the 18 realizations.

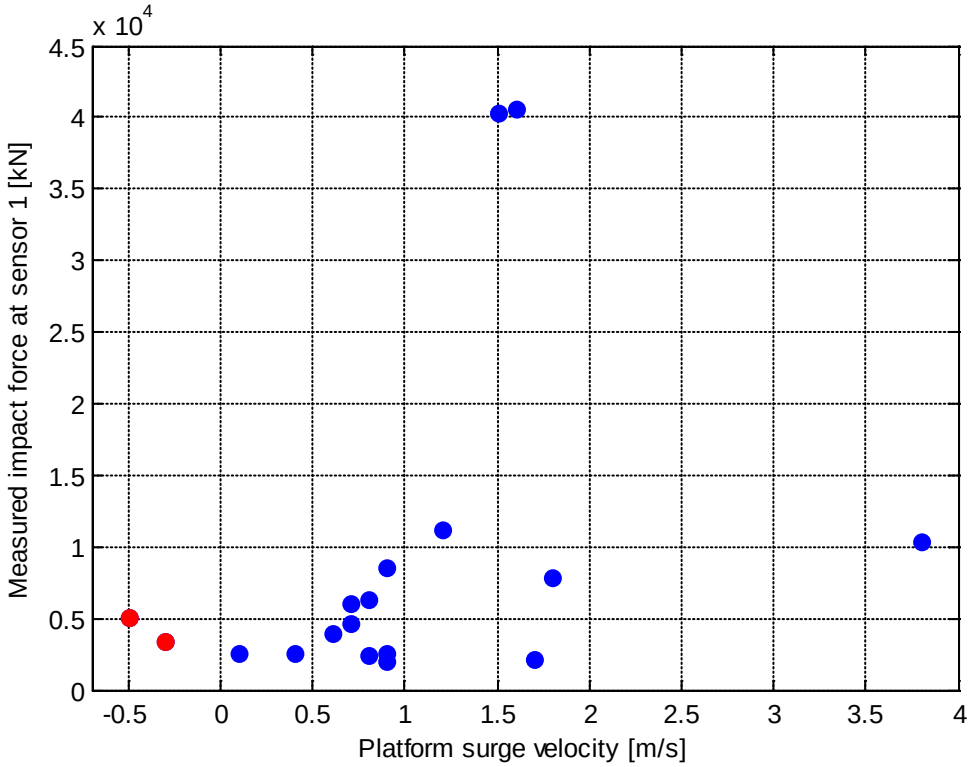

Figure 7-2: Maximum measured impact force plotted against the platform surge velocity at impact

The two cases where the platform surge velocity was away from the breaking wave are marked as red dots in Figure 7-2. It can be seen that the measured impact force for these two slams are not very high compared to the others. It should also be noted that the 6 largest measured slams have some of the highest positive surge velocities. It is difficult to see a clear pattern from the plot, but is seems like the surge velocity is of some importance for the impact force. When the relative horizontal velocity, in Eq.(4.2), is squared, the equation becomes as follows:

$$v^2 = \left(u + \dot{n}_1\right)^2 = u^2 + 2u\dot{n}_1 + \dot{n}_1^2 \tag{7.1}$$

From this equation it is clear that the cross term will give an important contribution, even if the surge velocity is much smaller than the wave velocity. Assuming that the wave velocity estimated in the numerical method was the true velocity. If using the estimated surge velocity equal to 0.5m/s toward the wave, the relevant horizontal velocity squared in Eq.(7.1) will become 528.5m^2/s^2. If the largest positive surge velocity from the model test was used, this value would become 691.25m^2/s^2. Using Eq.(4.1), the latter would give an impact pressure 1.3 times larger than if the estimated surge velocity was used.

Compared to the surge velocities from the model tests it seems like the estimated surge velocity is too low. This can explain some of the differences in the predicted impact force from the two methods.

7.2.2 Discussion: Wave impact velocity

In the numerical method based on DNVs recommended practice, the wave impact velocity was estimated to 22.49m/s. This was estimated by first finding the phase velocity of the most probable

highest breaking wave in 10 000 years. This phase velocity was then multiplied with a factor 1.2 to get an estimate of the horizontal velocity of the wave. By investigating measurements done in the model test it is possible to get an idea of the wave velocity at impact. This can then be compared with the estimated velocity.

In the model test, three probes were placed in front of the platform. These were attached to the platform deck and measured the relative wave elevation. The three probes was placed 10m, 6m and 3m away from the column. An illustration of the setup is shown in Figure 7-3.

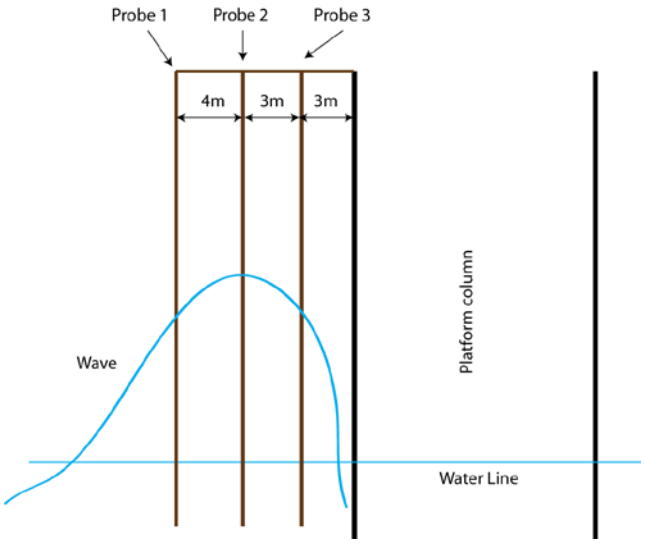

Figure 7-3: Illustration of relative wave elevation probes setup

By comparing the time series measured by each of these probes it is possible to see how fast the wave is moving before it hits the column. It is also possible to see the height and how the wave "builds up" before impact. Zero wave elevation is defined at the still water line. Plots with the measured time series for these three probes are made for time intervals corresponding to the largest slam in each realization. These plots can be found in Appendix C. The plot for the largest slam in test 3100 is shown in Figure 7-4.

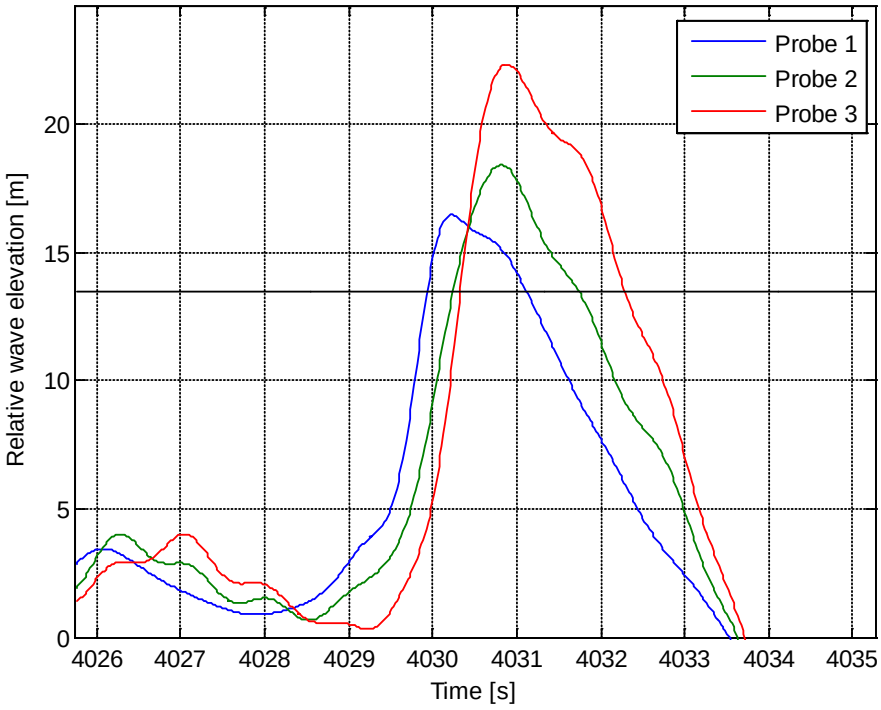

Figure 7-4: Relative wave elevation in front of column during the largest slam in test 3100

The black line in Figure 7-4 is representing the location of sensor 1. To find the velocity of the wave at this height, the time at the intersection between the black line and the probe measurement are found for each of the probes. Since the distance between each probe is known, the velocity can then be calculated.

The wave in Figure 7-4 has a velocity equal to 40.42m/s between probe 2 and 3. This is almost twice as fast as the estimated wave velocity. It is clear that this will give a much higher impact force.

The phase velocity of the most probable highest breaking wave in 10 000 years was used to estimate the wave velocity. This phase velocity was estimated to 18.74m/s under the assumption of a regular sinusoidal wave. The breaking waves are very nonlinear and asymmetric. However, it is reasonable to assume that the main part of a breaking wave is carried by a sinusoidal wave. If this sinusoidal wave could be found for the breaking waves in the model test, it is possible to compare the phase velocities under the same assumption. To do this, a regular sinusoidal wave has been fitted to the breaking wave shown in Figure 7-4. The sinusoidal wave is fitted so that the wave period is equal to the time between the two zero-up-crossings for the breaking wave. This is shown in Figure 7-5.

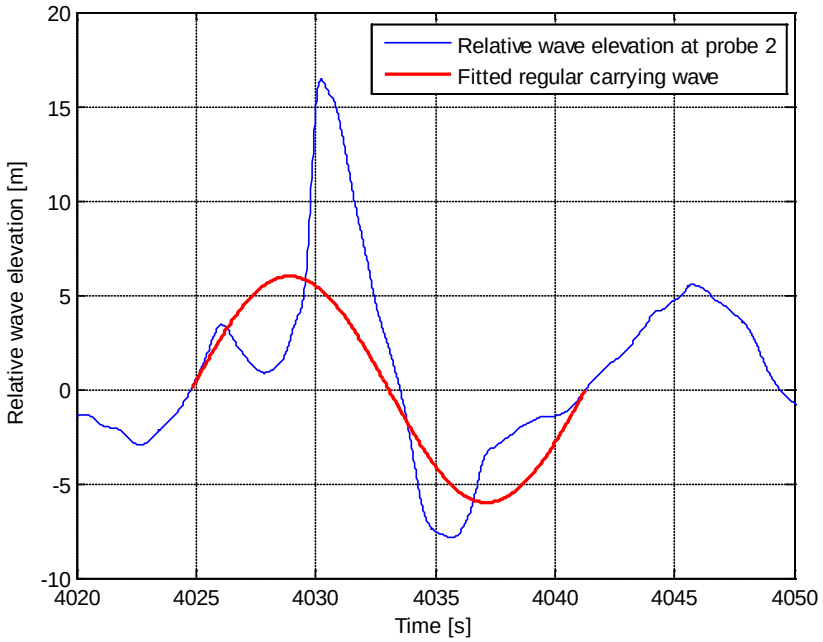

Figure 7-5: Regular wave fitted to breaking wave in largest slam in test 3100

The fitted regular wave has a wave period equal to 16.5s. The carrying wave's phase velocity can then be found using the relationship between period and phase velocity given by Eq.(4.9). This gives a phase velocity equal to 25.76m/s. This is higher than the phase velocity estimated in the method based on DNVs recommended practice. Is it possible that the phase velocity estimated with this method is too small? If so, this would be an obvious reason for why the estimated impact force is smaller than the measured impact force.

Looking back on Figure 7-4, it is clear that the wave elevation is much higher for probe 3, which is closest to the column. Comparing this with probe 2 it is obvious that something happens to the wave at this moment. Probe 3 measures a much higher peak almost at the same time as probe 2 measures its peak. Since probe 2 are located 3m in front of probe 3 it seems like the wave is breaking in between the probes and a water jet "shoots" out from the wave crest with high velocity. An illustration of this is shown in Figure 7-6.

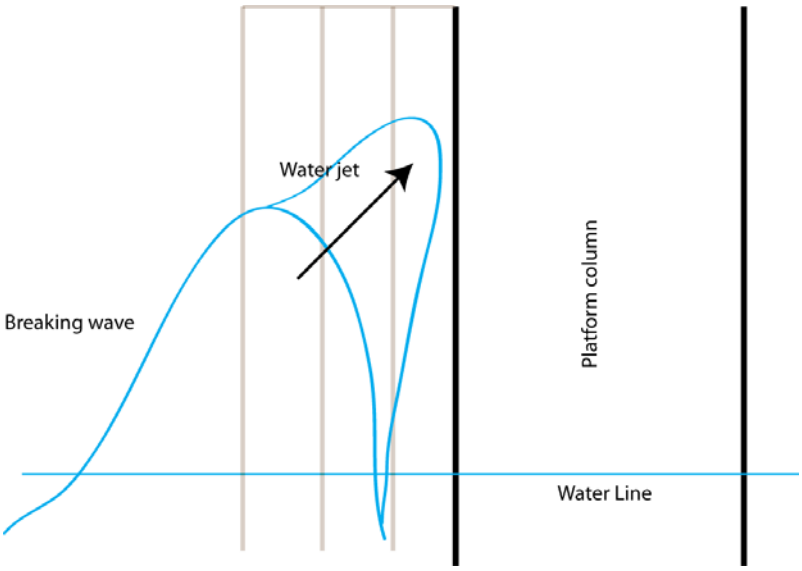

Figure 7-6: Illustration of water jet shooting out of the wave

It is this phenomenon that is the main reason to why breaking waves give much larger impact forces than non breaking waves. The velocity of the water particles that “shoots” out from the wave can be very high, much higher than the phase velocity of the waves. DNV recommends multiplying the phase velocity with a factor 1.2 to account for this, assuming undisturbed waves. For the breaking wave shown in Figure 7-4 the wave velocity was found to be 40.42m/s. When assuming that this wave could be represented by a sinusoidal wave, the phase velocity became 25.76m/s. This phase velocity needs to be multiplied with a factor 1.57 to get the measured wave velocity. This is higher than 1.2 suggested by DNV. Is it possible that the factor suggested by DNV is too small? The problem with deciding this factor is that it varies a lot for different slams. It is also very dependent on where the wave breaks. It seems like the worst scenario is when the wave breaks just in front of the column.

Based on all this, it seems like it is the wave impact velocity which is causing most of the difference in the results obtained from the two methods.

8 Investigation of measured impact forces

During the model tests, performed by MARINTEK, impact forces were measured at 8 locations on the column using 8 sensors as described in chapter 6. The sensors are spread out both vertical and horizontal at the column. This makes it possible to investigate how the measured impact forces vary at the different locations on the instrumented column.

This investigation has been performed by looking into the spatial correlation and variation of time for the maximum measured force for the different sensors. For simplicity the measured impact forces have been used. This means that the slamming sensors dynamic has not been eliminated. This could have been done by using the method explained in subchapter 6.1. This is an iteration process that needs to be done manually. To get a good understanding of the spatial correlation and variation in time, a large number of impact force time histories needs to be investigated. To eliminate the slamming sensors dynamic for all of these would have been very time consuming and is therefore not done.

The target of this investigation is to see if a similar pattern can be found for the different breaking wave impacts measured in the model test, and suggest a model for the impact forces on the column.

8.1 Theory used in impact force investigation

In order to describe the method used when investigating correlation in vertical and horizontal direction some theory will be presented.

8.1.1 Correlation

The term correlation means in general the similarity between two sets of data. The best way to describe the concept of correlation is to use a mathematically approach. Consider a set of data points (x_n, y_n). These data points can be plotted in a 2 dimensional plot with x and y-axis. It is then possible to see if there exist a correlation between the x and y values. Figure 8-1 illustrates correlation between two variables:

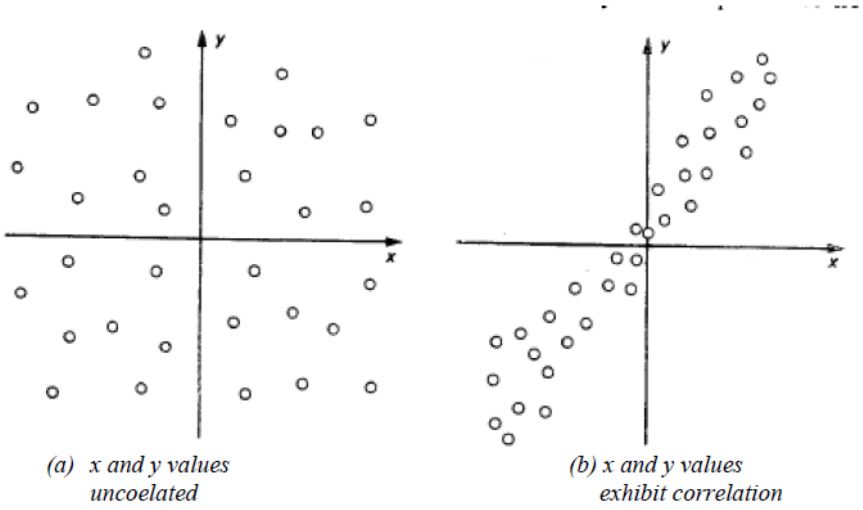

Figure 8-1: Illustrating correlation between two random variables (Newland, 1993)

To see if the *x* and *y* values exhibit a correlation a correlation coefficient can be found. The deviation of this coefficient can be found in Newland (1993). The correlation coefficient, ρ_{xy}, can be expressed as Eq.(8.1).

$$\rho_{xy} = \frac{E\left[\left(x - m_x\right)\left(y - m_y\right)\right]}{\sigma_x \sigma_y} \tag{8.1}$$

Where m_x and m_y are the mean values of *x* and *y* respectively, and σ_x and σ_y are the standard deviation of *x* and *y* respectively. If $\rho_{xy} = \pm 1$ it exists a perfect correlation and the relationship between the *x* and *y* values can be presented as a straight line. If $\rho_{xy} = 0$ there is no linear correlation between the data points. This is shown in Figure 8-2.

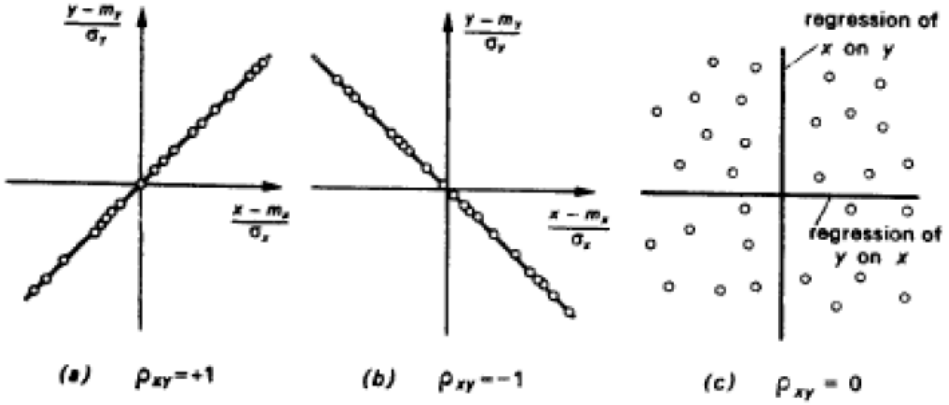

Figure 8-2: Regression lines for different values of the correlation coefficient (Newland, 1993)

8.1.2 Simple linear regression

As shown in Figure 8-2, if it exists a perfect correlation between two data sets, they can be presented by a single line. However, a regression line can also be estimated if the data sets are not perfect correlated. This is done by fitting a line to the data sets. One method used for this is the method of least squares. This method is explained in detail in Montgomery and Runger (1994). An estimated regression line is then given by Eq.(8.2).

$$\hat{y} = \hat{\beta}_0 + \hat{\beta}_1 x \tag{8.2}$$

Where $\hat{y}$ is the value on the y-axis for the fitted line for a given x value. $\hat{\beta}_0$ and $\hat{\beta}_1$ is the least square estimates of the intercept and slope to the fitted line. They are again given by Eq.(8.3) and Eq.(8.4)

$$\hat{\beta}_0 = m_y - \hat{\beta}_1 m_x \tag{8.3}$$

$$\hat{\beta}_1 = \frac{\sum_{i=1}^{n} y_i x_i - \frac{\left(\sum_{i=1}^{n} y_i\right)\left(\sum_{i=1}^{n} x_i\right)}{n}}{\sum_{i=1}^{n} x_i^2 - \frac{\left(\sum_{i=1}^{n} x_i\right)^2}{n}} \tag{8.4}$$

Where $m_y = \left(\frac{1}{n}\right)\sum_{i=1}^{n} y_i$ and $m_x = \left(\frac{1}{n}\right)\sum_{i=1}^{n} x_i$. Where y_i and x_i are the data set for $i = 1, 2, 3, ..., n$ with n as the size of the data set.

Each pair of *x* and *y* values from the data set will then satisfy the relationship in Eq.(8.5).

$$y_i = \hat{\beta}_0 + \hat{\beta}_1 x_i + e_i \tag{8.5}$$

Where $e_i = y_i - \hat{y}_i$ is called the residual. This describes the error in the fitted line for the *i*th observation y_i. The higher the correlation between the *x* and *y* values are, the lower residuals. As shown in Figure 8-2, perfect correlation gives no residuals.

8.2 Relevant slams

The slamming data from the model tests, provided by MARINTEK, are given as measured time series for each slam. As mentioned earlier, only slams that had measured impact force larger than 1 000kN were provided. The number of slams giving an impact force larger than 1 000kN varies for the different realizations in the model test. For some realizations this number was large, around 10 slams, and even higher. For the 10 000 year condition, 18 realizations were run. With 8 slamming sensors this gives a large amount of time series.

When trying to find a pattern in spatial correlation and the variation in time, a large number of these slams should be looked into. To make it easier to work with this large number of time series MATLAB has been used.

The measured impact force on the different sensors during one slam, is dependent on the location where the wave hits the column. If a wave hits the lower part of the column, like illustrated in Figure 8-3, the lower sensors can measure an impact force larger than 1 000kN while the sensors higher on the column might not, and the data for these sensors are therefore not available.

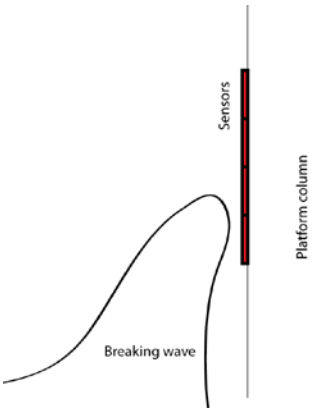

Figure 8-3: Illustration of breaking wave impact on the lower sensors

To take this into account when looking at spatial correlation and variation in time, only slams that have maximum measured impact force larger than 1 000kN on all the relevant sensors will be used. A MATLAB script was made to sort out the relevant sensors for each slam.

8.3 Spatial correlation

The arrangement of the sensors is shown in Figure 6-2. From this figure it can be seen that measurements are done for four different vertical positions, where the two middle positions also measures in three different horizontal positions. The spatial correlation can therefore be investigated by comparing the measurements done for the different positions in both vertical and horizontal direction.

8.3.1 Sensors used when investigating spatial correlation

Three different correlations have been investigated. The first one is in vertical direction. This is done by using the maximum measured impact forces from sensors 1, 3, 6 and 8. The two others are for horizontal direction, one by using the values from sensors 2, 3 and 4, and one for sensors 5, 6 and 7. The sensors used in the three correlations are shown in Figure 8-4:

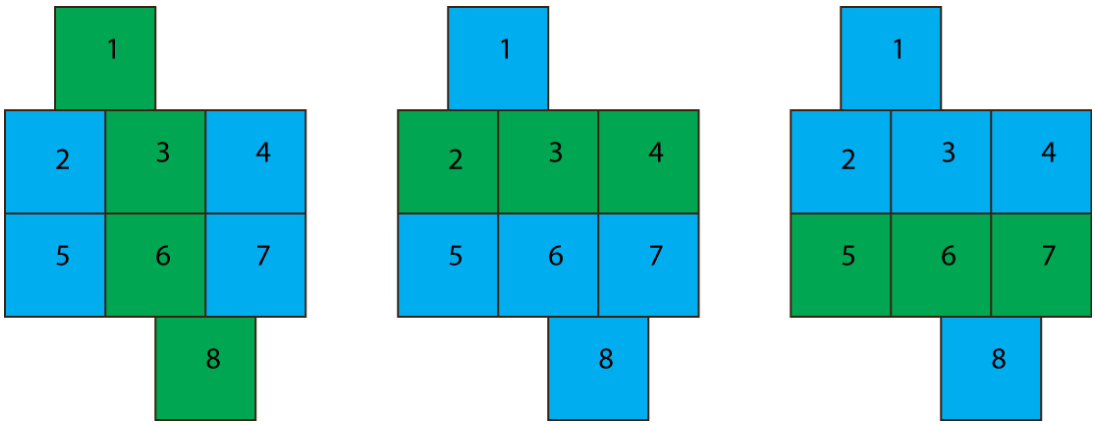

Figure 8-4: Overview of the three correlations investigated

8.3.2 Spatial correlation in vertical direction

When looking for correlation in vertical direction, the maximum measured impact force from sensors 1, 3, 6, and 8 has been used as shown in Figure 8-4. Sensor 8, the lowest of the sensors, has been chosen as the x-values. This means that the impact force in this sensor has been investigated for

correlation with the three other sensors. Three correlation coefficients have been calculated, and three plots with scatter diagram and a straight line fitted to these values have been produced.

The correlation coefficients calculated are given in Table 8-1:

X values	Y values	Correlation coefficient
Sensor 8	Sensor 1	0.9187
Sensor 8	Sensor 3	0.8968
Sensor 8	Sensor 6	0.9584

Table 8-1: Correlation coefficients for sensors in vertical direction, all slams

According to the correlation coefficients it seems like there is a good linear correlation between the measurements done by sensor 8 and the other vertical sensors. However, to conclude this only based on these coefficients would be wrong. To get a better understanding if there is a pattern between the sensors, scatter plots should also be investigated. Plots with both scatter diagrams and fitted lines for the vertical sensors are shown in Figure 8-5.

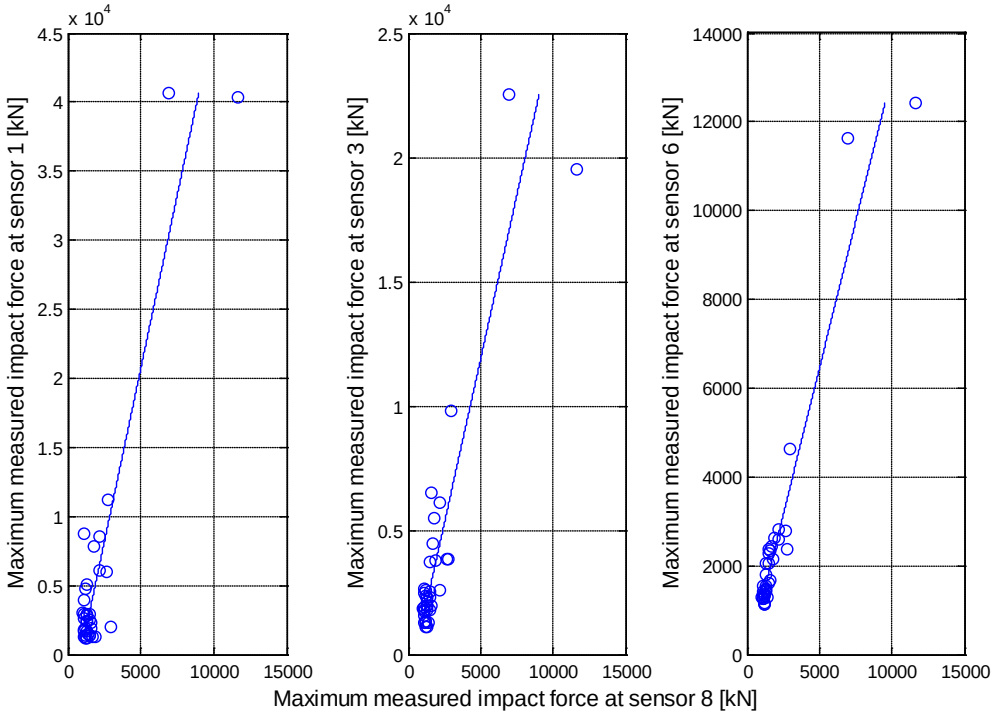

Figure 8-5: Scatter plots and fitted lines for vertical sensors, all slams

From the scatter diagrams it can be seen that there is two measured values that are much larger than all the others. As shown in chapter 6, two slams during the model tests induced much larger impact forces than all the others slams. These two outliers will influence both the mean and standard deviation for both *x* and *y* values, hence the correlation coefficient given by Eq.(8.1) will become larger than if they were not there. It would therefore be misleading to report of good correlation on all of the data based on the correlation coefficients given in Table 8-1. This is because it would not represent the behavior of the bulk of the lower valued data.

It could therefore be of interest to see how the correlation would become if the measurement from these two large slams were removed. When removing these two slams the new correlation coefficients will become as shown in Table 8-2.

X values	Y values	Correlation coefficient
Sensor 8	Sensor 1	0.4539
Sensor 8	Sensor 3	0.7318
Sensor 8	Sensor 6	0.8719

Table 8-2: Correlation coefficients for sensors in vertical direction, without two largest slams

The new correlation coefficients clearly shows a difference from the coefficient when the two largest slams were included. The correlation between sensor 8 and the two sensors above, sensor 3 and 6 are a little lower than before. But the main difference is in the correlation between sensor 8 and sensor 1.

Plots with scatter diagrams and fitted straight lines are presented in Figure 8-6.

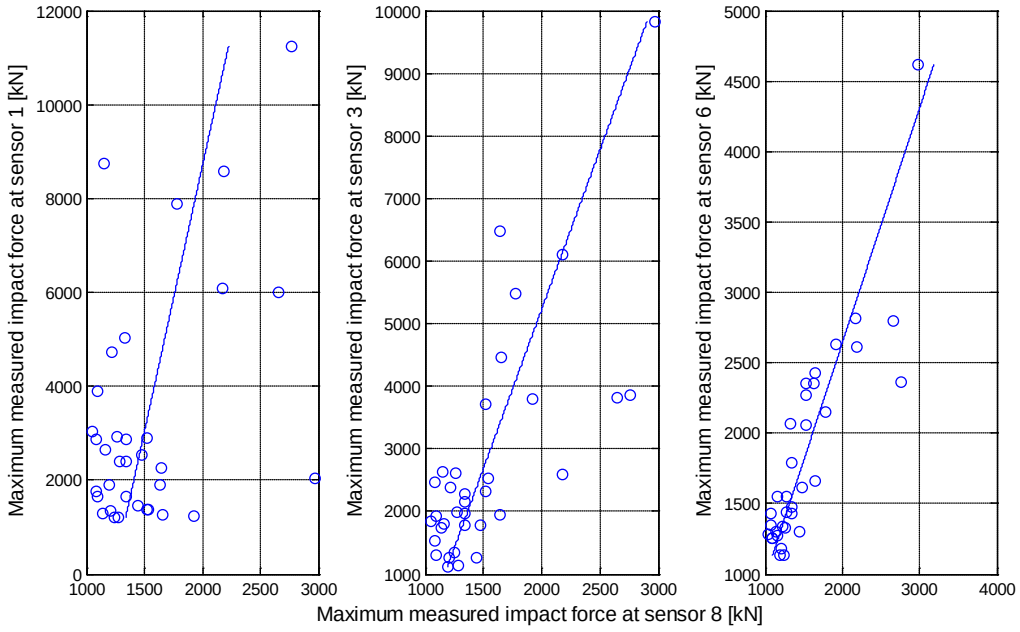

Figure 8-6: Scatter plots and fitted lines for vertical sensors, without two largest slams

From the new scatter plots it is now easier to see that the measured forces from the smallest slams are less correlated.

One reason for the spreading of the data points might be the problem that is mentioned earlier in subchapter 8.2. The measurements from the different sensors are dependent on where the wave hits the column. A breaking wave may hit the lower sensors and induce a relative high impact force for these sensors. The higher sensors will then register lower impact forces, since they will not be directly hit by the wave. They will only be affected by the water that is pushed away. This is illustrated in Figure 8-7.

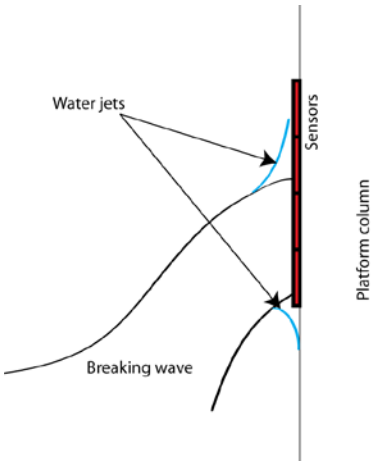

Figure 8-7: Illustration of water jet in vertical direction from breaking waves

When the relevant slams where sorted out as explained in subchapter 8.2, slams where at least one sensor did not register impact forces larger than 1 000kN were removed. In Table 8-2 it can be seen that the correlation gets worse for larger vertical distance between the sensors. Could the reason for this be that many waves are too small to directly hit the highest sensors? To investigate this, the correlation coefficient is calculated for all combinations of the sensors. The two largest slams are excluded in these calculations as well. The calculated correlation coefficients are given in Table 8-3:

X values	Y values	Correlation coefficient
Sensor 1	Sensor 3	0.2071
Sensor 1	Sensor 6	0.2383
Sensor 1	Sensor 8	0.4539
Sensor 3	Sensor 1	0.2071
Sensor 3	Sensor 6	0.8705
Sensor 3	Sensor 8	0.7318
Sensor 6	Sensor 1	0.2383
Sensor 6	Sensor 3	0.8705
Sensor 6	Sensor 8	0.8719
Sensor 8	Sensor 1	0.4539
Sensor 8	Sensor 3	0.7318
Sensor 8	Sensor 6	0.8719

Table 8-3: Correlation coefficients for sensors in vertical direction, all sensor combinations, without two largest slams

From Table 8-3 it can be seen that the measurements done at sensor 1 have a bad correlation with the measurements done by the other sensors. The correlation for sensor 1 and the other sensors are colored blue. In Table 8-3 six rows are colored blue. However there are really only three combinations since changing the x and y-axis will give the same coefficient. The measurements done by sensor 1 and sensor 3 are least correlated. A scatter diagram for maximum measured impact force at sensor 1 and sensor 3 is shown in Figure 8-8.

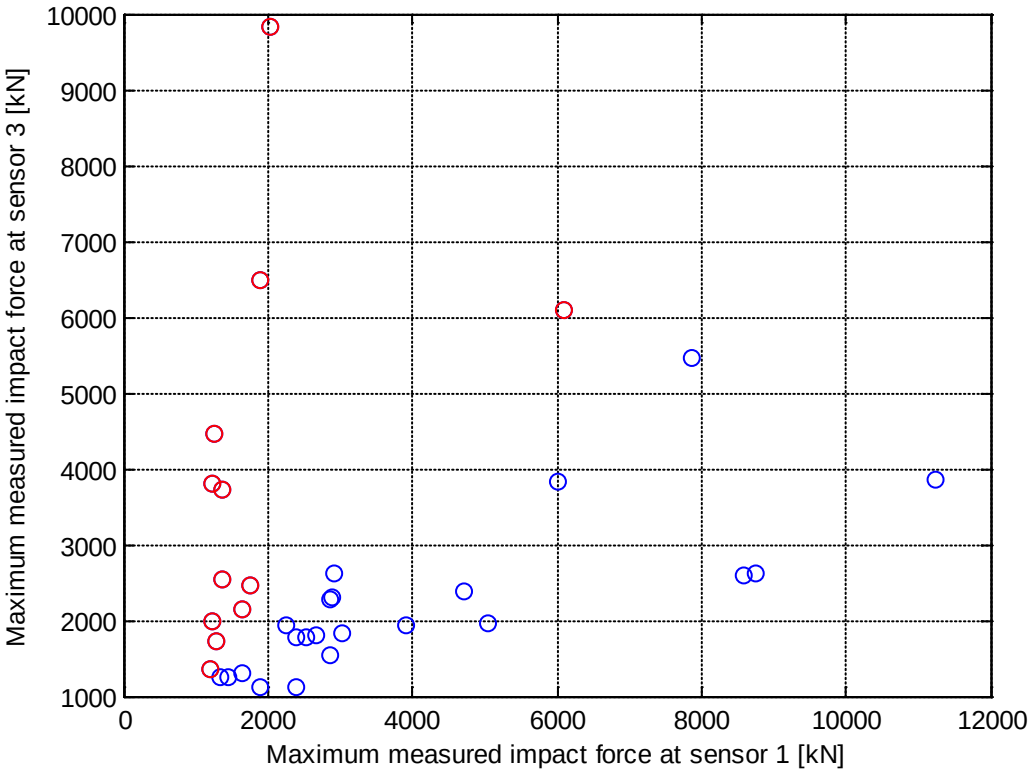

Figure 8-8: Scatter diagram for measured impact forces at sensor 1 and sensor 3, without two largest slams

The red dots represent slams where the maximum measured impact force was larger at sensor 3 than in sensor 1. The slam where the difference was largest is identified as a slam that occurs in test number 3148. The impact forces measured by sensor 1 and 3 during this slam are plotted in Figure 8-9.

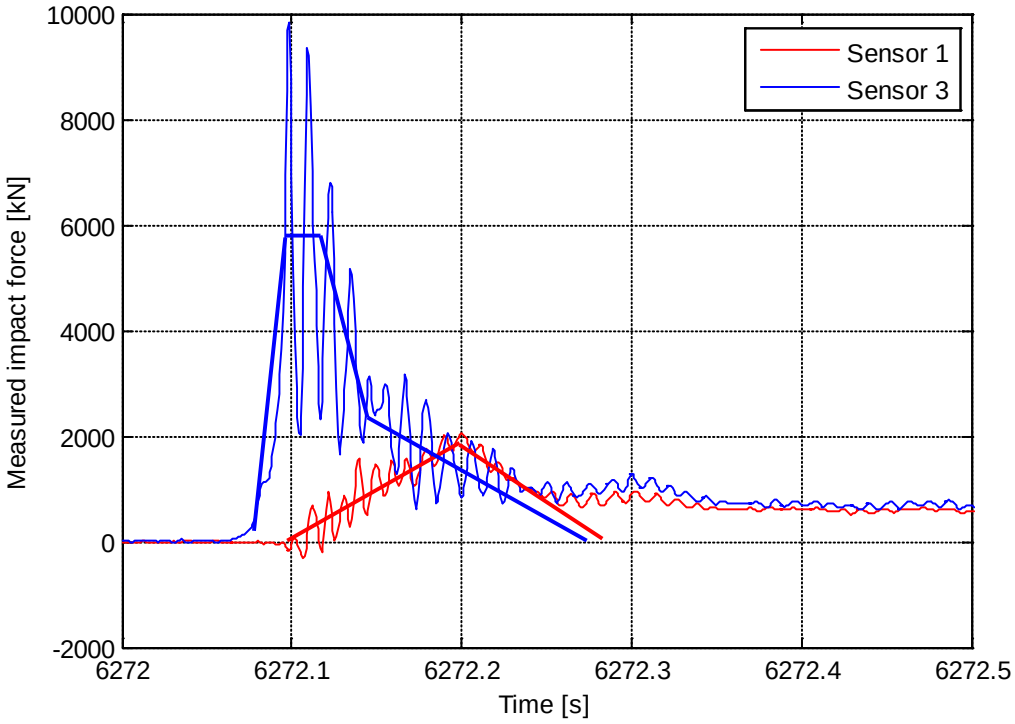

Figure 8-9: Measured impact force for sensor 1 and sensor 3, slam in test 3148

Figure 8-9 shows that there is a lot of dynamics in the two sensors measured impact force. An approximated load history is drawn for each sensor. Since the dynamic amplification varies for different sensors and different slams, it will give worse correlation than if the dynamics was removed.

If the dynamics in the two sensors was removed as shown in Figure 8-9, the difference between the maximum impact forces would be less than in Figure 8-8. However, it would still be larger for sensor 3 than for sensor 1. In addition the peak for sensor 1 occurs later than for sensor 3. It seems like that the wave hits sensor 3, while sensor 1 only experience water running over it as illustrated in Figure 8-7. Visual inspection of movie recordings from the model test is also done to verify this. Figure 8-10 is a snapshot from the recordings of this slam. It shows that sensor 1 is above the wave when the wave hits the column.

Figure 8-10: Snapshot of test 3148 from recordings of model test performed by MARINTEK 2010

Slams like this one will give more spreading in the scatter diagram and the values will get less correlated. The ideal thing would be to only investigate slams where the breaking wave covered all the sensors. By looking at the movie recordings from the model tests it seems like sensor 3, 6 and 8 are covered for most slams. This is probably why they show higher correlation with each other than sensor 1.

Based on the correlation coefficients and scatter diagrams a suggested pattern can be introduced for the sensors. If a straight line is fitted to the data, with values from sensor 8 as x-axis, it can be seen that the lines slope gets larger for the lines describing sensors located higher. This is shown in Figure 8-11.

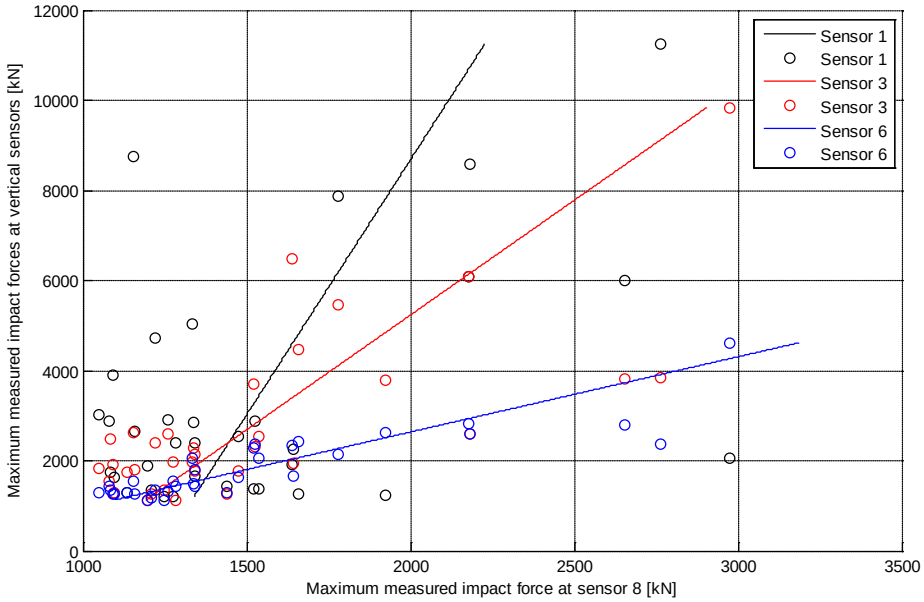

Figure 8-11: Linear regression lines for vertical sensors

Figure 8-11 tells us that if sensor 8 measures a maximum impact force of 2 000kN, it could be expected that sensor 6 measures around 2 800kN, sensor 3 around 5 100kN and sensor 1 around 8 800kN. These values would only be the true values if the correlation coefficient was exactly 1. Therefore, it would be wrong to predict values using this figure. Especially for sensor 1 that have much less correlation with measurements from sensor 8 than the two other sensors. However, it seems to give an indication of how the impact force from a breaking wave is distributed in vertical direction on a column.

As mentioned earlier, two of the slams in the model test gave much larger impact loads than the other slams. The maximum measured impact forces at sensors 1, 3, 6 and 8 for these two slams are shown in Table 8-4.

Sensor	test 3100	test 3124
Sensor 1	40 645	40 352
Sensor 3	22 501	19 515
Sensor 6	11 623	12 420
Sensor 8	6 927	11 636

Table 8-4: Maximum measured impact force [kN] for the two largest slams

It can be seen that the two largest slams also have the suggested pattern. The measured impact force is largest at the top and gets lower downwards the column.

Discussion

It is clear that breaking waves in an irregular sea is a highly nonlinear phenomenon, involving many different parameters. DNVs formula for slamming pressure Eq.(4.1), says that the impact pressure is dependent on the relative impact velocity squared. The relative velocity is defined as the velocity between the water particles and the platform column. The velocity of the water particles are therefore one of the most important parameters concerning the magnitude of the impact force from a breaking wave.

The horizontal velocity of the water particles varies over the height of a breaking wave. As explained in chapter 3, a wave breaks because the horizontal velocity of the water particles at the top of the wave becomes larger than the wave's phase velocity. In Chang and Liu (1997) they measured fluid particles velocity at the tip of the overturning jet in a breaking wave. They did measurements where this velocity reached 1.68 times the phase velocity calculated with linear theory.

From Figure 3-2 it can be seen that the horizontal velocity is largest at the top and gets lower downwards in the wave. Since the impact force are so dependent on this velocity, these pictures support the pattern observed from investigating the vertical sensors measurements in the model test. It seems likely that the highest sensors would measure the highest impact force and it would gradually be reduced downwards the column.

Conclusion

It seems like there is a linear correlation in vertical direction between the sensors, except for sensor 1 at the top. The reason for the low correlation between sensor 1 and the other sensors might be that many of the breaking waves are not covering all of the sensors during impact. The

measurements from impacts like these might just be water splashing onto the sensors from the impact below. This might be a problem for the other sensors too, and result in a slightly lower correlation than if all slams were “full” slams. However, it seems like that the maximum measured impact force as a direct consequence of the slam itself, gets larger higher on the column and is reduced downwards along the column.

8.3.3 Spatial correlation in horizontal direction

When looking for correlation in horizontal direction, two configurations have been used. Those are shown in Figure 8-4. The middle sensor has been chosen as the as the x-values. For the first configuration this would be sensor 3 while for the other sensor 6. Two correlation coefficients have been calculated for both horizontal levels. In addition scatter plots with straight lines fitted to the values are produced.

The correlation coefficients are given in the following table.

X values	Y values	Correlation coefficient
Sensor 3	Sensor 2	0.9150
Sensor 3	Sensor 4	0.9296
Sensor 6	Sensor 5	0.9684
Sensor 6	Sensor 7	0.9172

Table 8-5: Correlation coefficients for sensors in horizontal direction, all slams

From the correlation coefficients it seems like the sensors are highly correlated in horizontal direction. The scatter diagrams with fitted lines are shown in Figure 8-12 and Figure 8-13.

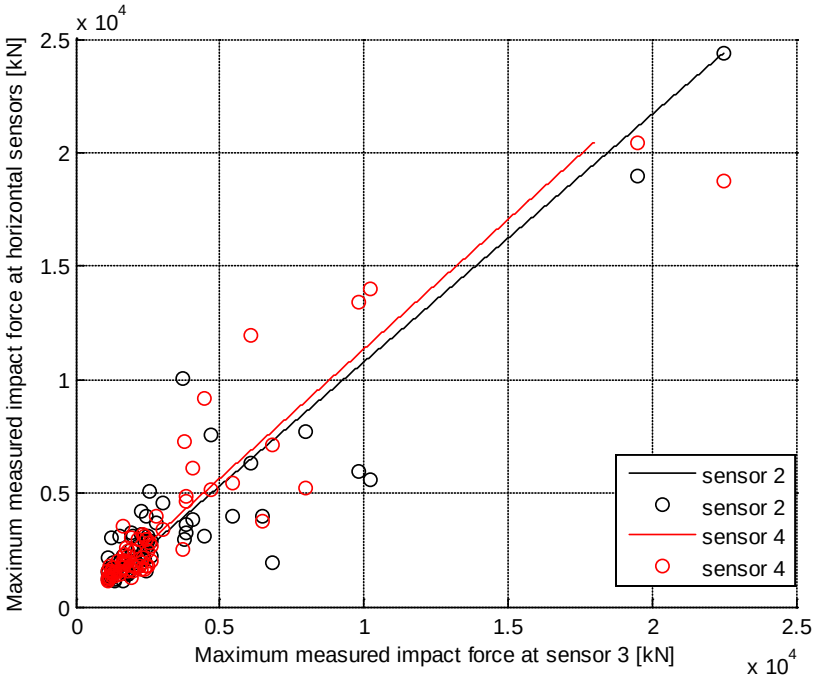

Figure 8-12: Scatter plots and fitted lines for horizontal sensors 2, 3 and 4, all slams

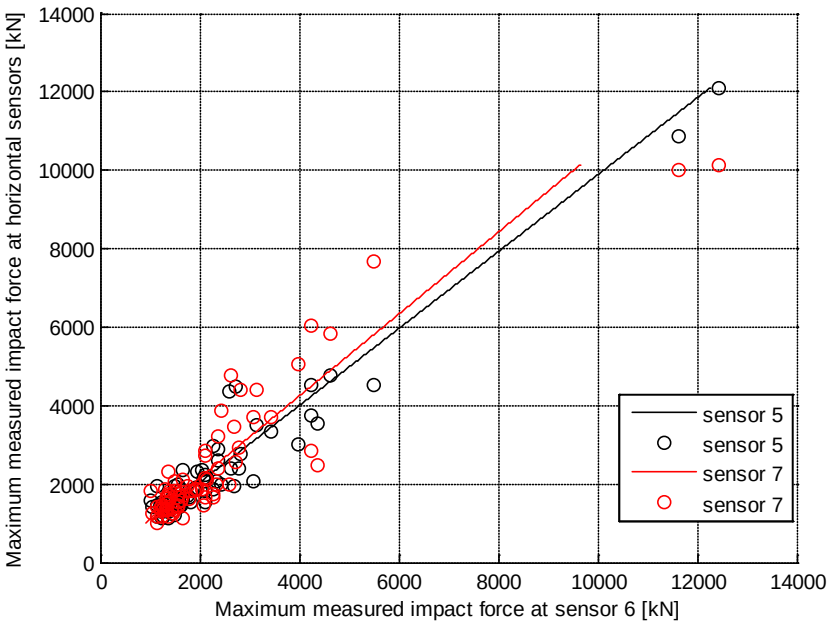

Figure 8-13: Scatter plots and fitted lines for horizontal sensors 5, 6 and 7, all slams

From these figures it can be seen that the two largest slams probably makes the correlation coefficient larger, as they did for the vertical correlation. When removing these two slams the new correlation coefficients becomes.

X values	Y values	Correlation coefficient
Sensor 3	Sensor 2	0.6704
Sensor 3	Sensor 4	0.8821
Sensor 6	Sensor 5	0.8740
Sensor 6	Sensor 7	0.8620

Table 8-6: Correlation coefficients for sensors in horizontal direction, without two largest slams

From Table 8-6 it can be seen that correlation coefficients gets smaller. However, the coefficients still suggest that there is some correlation between the sensors. Scatter diagrams and fitted lines are given in Figure 8-14 and Figure 8-15.

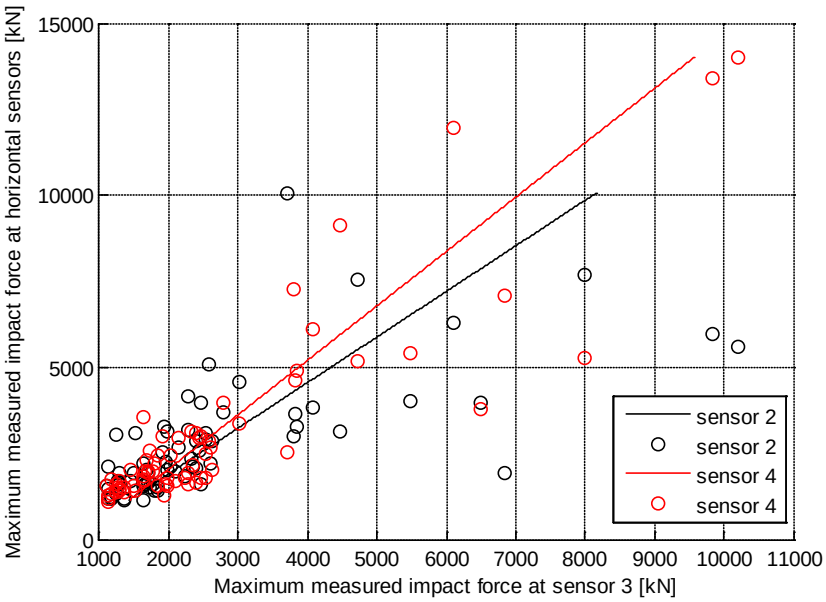

Figure 8-14: Scatter plots and fitted lines for horizontal sensors 2, 3 and 4, without two largest slams

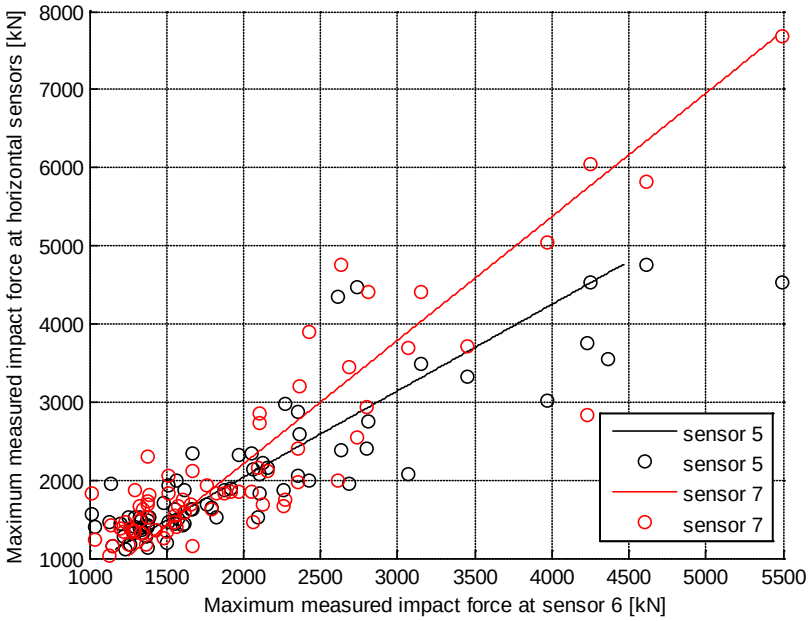

Figure 8-15: Scatter plots and fitted lines for horizontal sensors 5, 6 and 7, without two largest slams

From the linear regression lines it can be seen that the intercepts are almost the same and the slopes are close to 1 for the different lines. It can therefore be suggested that the measurements done by the horizontal sensors are quite similar.

Discussion

Similar measurements for sensors located at the same vertical height are expected. This is most likely because of the horizontal velocity of the water particles does not vary that much in a wave's horizontal level. However, the measurements are dependent on where the wave hits the column.

This might give some variation in measured impact forces. When a wave hits the column, the water needs to go somewhere afterwards. The water will not only get pushed away in vertical direction as illustrated in Figure 8-7. It will be pushed away in horizontal direction as well. How close the sensors are to the column edge might also have influence on the impact force, as water will then be allowed to travel around the edges.

Conclusion

It seems like there is correlation between the sensors in horizontal direction. From the scatter diagrams a pattern can be suggested. It seems like the maximum measured impact force as a direct consequence of the slam itself, is very similar for a given height level on the column. A larger difference in horizontal direction might be observed if there had been sensors closer to the radius of the cornered edges.

8.4 Time variation

To get a better understanding of how the waves hit the column, the time for when the maximum measured impact load occur for each sensor has been compared. This will show if there is any pattern for when each sensor reach their measured peak value.

To investigate this, the two largest slams in the model test are used. They occur during test 3100 and test 3124. By visual inspection of recorded movies from the model test, it is known that all sensors are hit directly by the breaking waves during these two slams. This makes them very suitable to use when comparing the time variation in the maximum measured impact force for the different sensors. The dynamics of the sensors are not accounted for here either. This might introduce some errors in both the peak value and the time this occur.

By use of MATLAB, the maximum value and the time for when this occur is found for each sensor during a slam. These are plotted as data points with a label that tells which sensor it represents. The numbering of the sensors is done after Figure 6-2.

The plot of the largest slam in test 3100 is given in Figure 8-16.

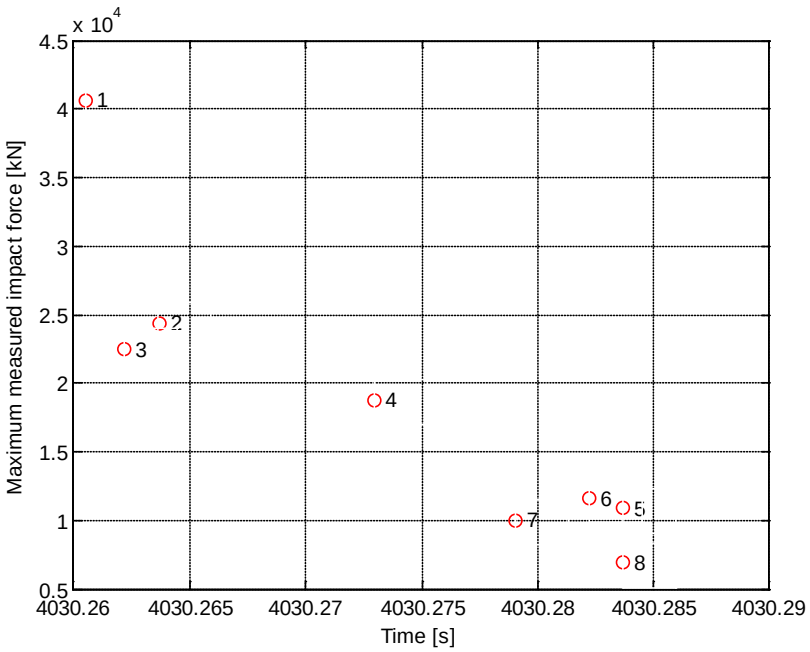

Figure 8-16: Max measured impact force vs. time for largest slam in test 3100

From this plot it can be seen that the peak value of sensor 1 occurs first. After this the peak occurs for the three sensors 2, 3 and 4, then sensors 5, 6 and 7, and sensor 8 reach its peak value last. From this plot it looks like that the top of the column reach their maximum measured impact force first, and it occurs later and later further down on the column. The plot for the largest slam in test 3124 is given in Figure 8-17.

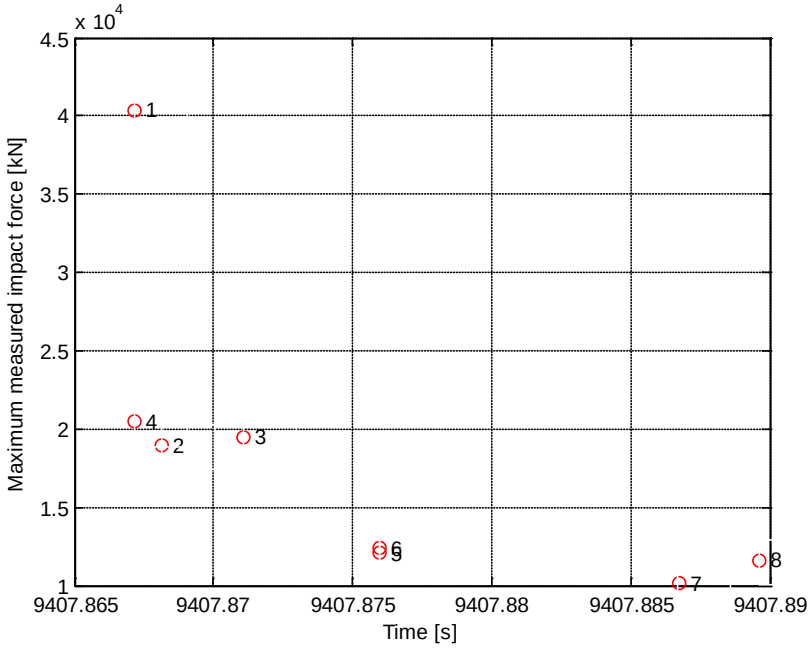

Figure 8-17: Max measured impact force vs. time for largest slam in test 3124

The same pattern can be seen for the slam in test 3124. The sensors can be categorized into four levels, one for each horizontal level as shown in Figure 8-18. It then seems like the maximum

measured impact force will occur for the different levels in the following order; level 1, level 2, level 3 and level 4.

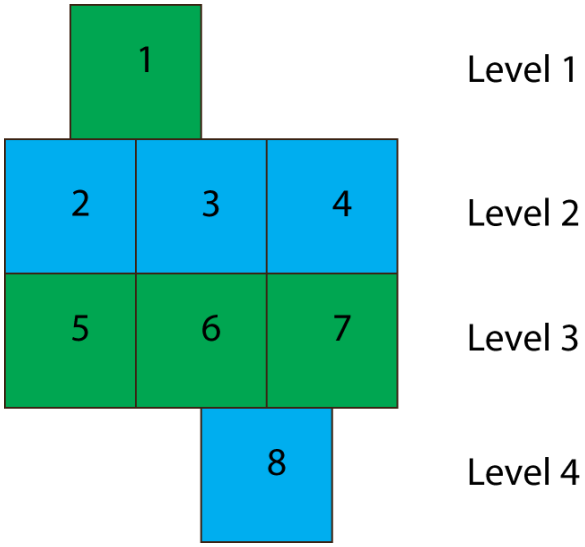

Figure 8-18: Sensors categorized into four levels

That the sensor will measure the maximum impact force in this order seems reasonable. A breaking wave will have an overturning water jet on the top that will hit the column first. Although a small difference is shown for the different levels in Figure 8-16 and Figure 8-17, it also shows that the time differences are very short. For the two slams investigated the difference between the first sensor's peak to the last sensor's peak, which is sensor 1 and sensor 8 for both slams, are less than 0.025s or 25ms.

8.5 Load models to be used in simplified structural analysis

To be able to use the measured force histories in a simplified two dimensional structural analysis, a reasonable load model needs to be established. In this subchapter, load models will be suggested based on the above results. Models that include only the measured values from the model tests and models that also accounts for the area without sensors will be suggested. The load models are made using the impact force histories from the model tests directly. This means that dynamic in the sensors has not been eliminated. The load histories used to explain the load models are taken from the largest slam in test 3124.

Two different load configurations are suggested. They are as follows:

1. All load histories are added together. The resulting time history is then applied as a time dependent point load, $F(t)$. The point load acts in the "center of gravity" of the measured forces. The height above still water is referred to as R. This is shown in Figure 8-19.

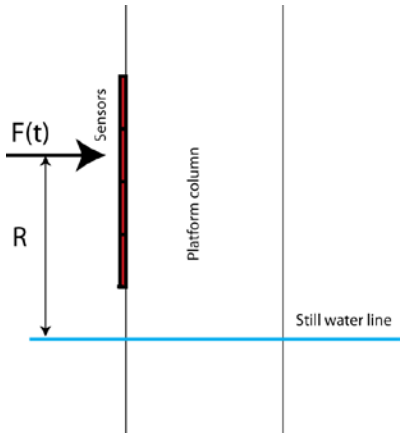

Figure 8-19: Illustration of load configuration 1

The distance, R, is found by the use of the "Center of Gravity theorem for force origin" given in Amdahl et al. (2005). The formula is given in Eq.(8.6).

$$R \cdot \sum_{i=1}^{n} F_i = \sum_{i=1}^{n} F_i \cdot R_i \tag{8.6}$$

Where i is the index for each max load

R is the distance from the still water line to the origin of force for the total force

R_i is the distance from the still water line to the origin of force for each force F_i

F_i each sensors maximum measured force

n is the total number of forces

2. The load histories are added together for each horizontal level. The resulting time histories are applied as time dependent point loads, $F_1(t)$, $F_2(t)$, $F_3(t)$ and $F_4(t)$. The point loads for each level acts in the middle of the relevant sensors height. This configuration is illustrated in Figure 8-20.

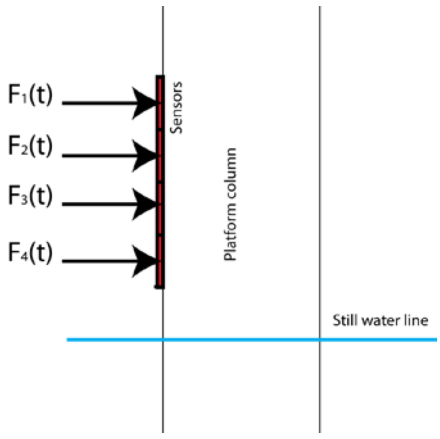

Figure 8-20: Illustration of load configuration 2

8.5.1 Load models with only measured values from the model test

When adding all sensors measured force histories together, the load history, $F(t)$, for the largest slam in test 3124 will become as shown in Figure 8-21.

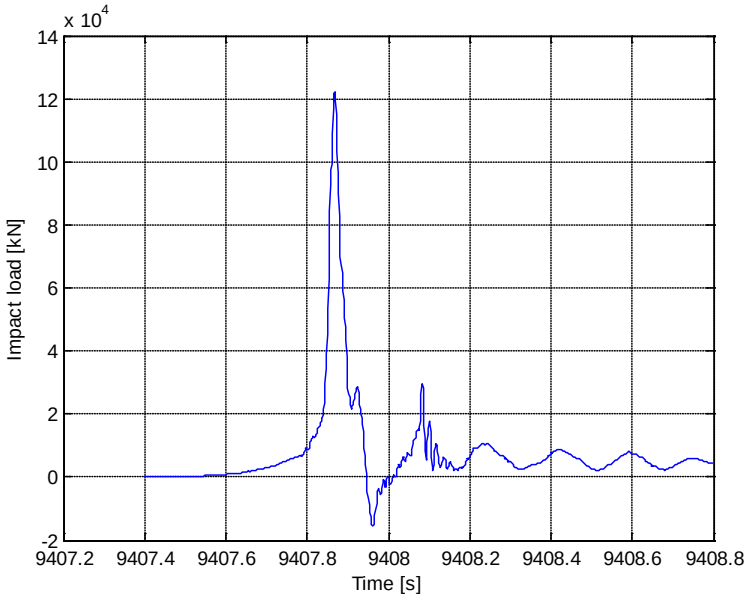

Figure 8-21: All sensors measured force histories added together for largest slam in test 3124

This load is applied as a point load. The vertical position where this load acts is found using Eq.(8.6). The calculations can be found in Appendix F. This is from now on referred to as load model 1.

When the measured impact force for each sensor row in vertical direction are added together, the load histories $F_1(t)$, $F_2(t)$, $F_3(t)$ and $F_4(t)$, for the largest slam in test 3124 will become as shown in Figure 8-22.

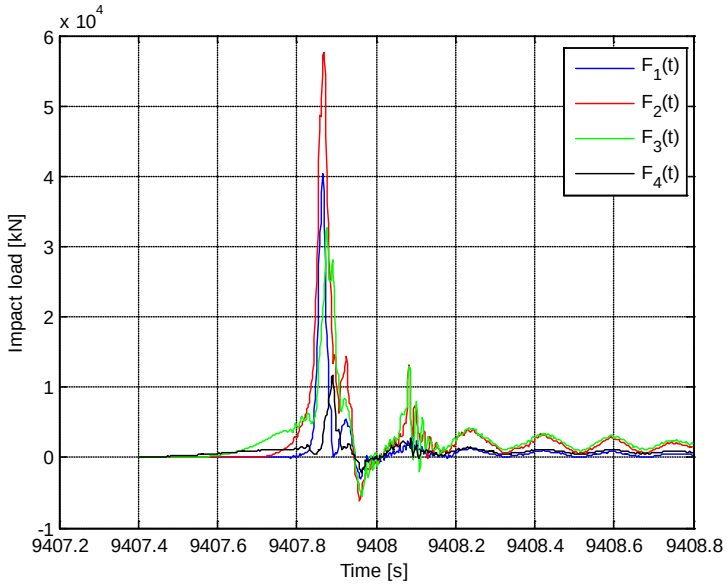

Figure 8-22: Each sensor row measured force histories added together for largest slam in test 3124

Each load history is applied at the middle of the corresponding sensor row. This is from now on referred to as load model 2.

8.5.2 Load models that also account for area without sensors

It is reasonable to believe that some of the area on the column that does not have sensors will experience impact force from the breaking waves. It is difficult to say something about what happens above the highest sensor, sensor 1, since no measurement exists. In chapter 8 it was concluded that the impact forces got less downwards the column. It is therefore reasonable to assume the area below sensor 8 will not experience impact forces of significance. Based on this the area both above sensor 1 and below sensor 8 are neglected. The two sensor rows containing sensors 2, 3 and 4, and sensors 5, 6 and 7, measured impact force almost out to the rounded edges on the column. On both sides there is just above 1m from the edge of the sensors to the start of the rounded edges. Further out on the sides, it is likely that water will run of the column along the edges during an impact. The impact forces will then become lower, and the area further out against the edges are therefore neglected. Based on this, the area that can be assumed to experience significant impact forces during a slam is shown in Figure 8-23.

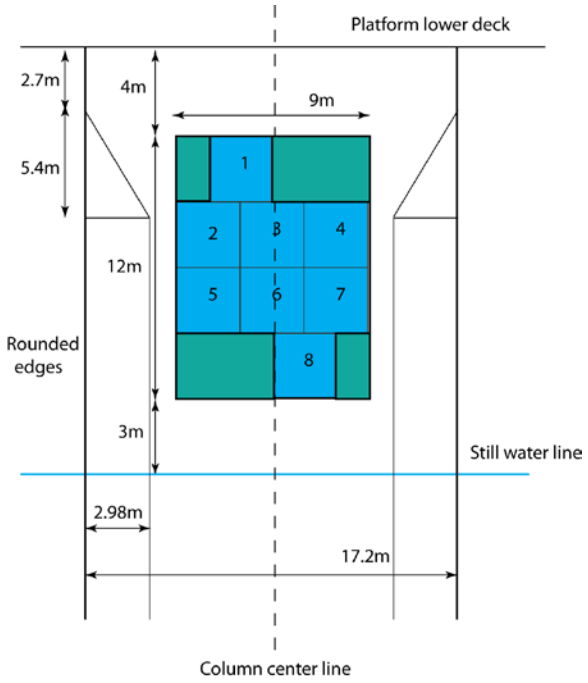

Figure 8-23: Illustration of assumed area that experience impact force

In Figure 8-23 the area of the sensors are shown in blue, while the other area were significant impact forces are expected is green.

Since there are no measurements for the green area in Figure 8-23, some assumptions need to be done. The green area on top is at the same height as sensor 1, while the green area at the bottom is at the same height as sensor 8. In chapter 8 it was shown that there is little difference between the sensors at the same height. It is therefore assumed that the impact pressure is the same for a horizontal level. The green areas next to sensor 1 have a total area twice as large as sensor 1 itself. The impact force history for the green area at this height is therefore assumed to be the measured impact force history for sensor 1, multiplied with 2. The same is done for the green area at the

bottom. The impact force history for this area is found by multiplying the measured impact force at sensor 8 with 2.

For load configuration 1, where all load histories are added together, the load history, $F(t)$, will be as shown in Figure 8-24 for the largest slam in test 3124.

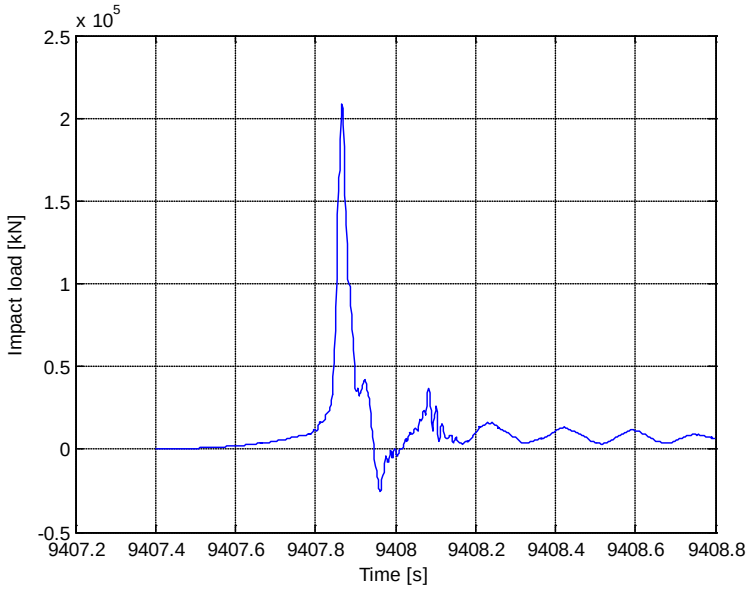

Figure 8-24: Total force history for assumed significant impact area for largest slam in test 3124

This is from now on referred to as load model 3.

When the measured force histories for each horizontal level are added together, the load histories $F_1(t)$, $F_2(t)$, $F_3(t)$ and $F_4(t)$, for the largest slam in test 3124 will become as shown in Figure 8-25. This is from now on referred to as load model 4.

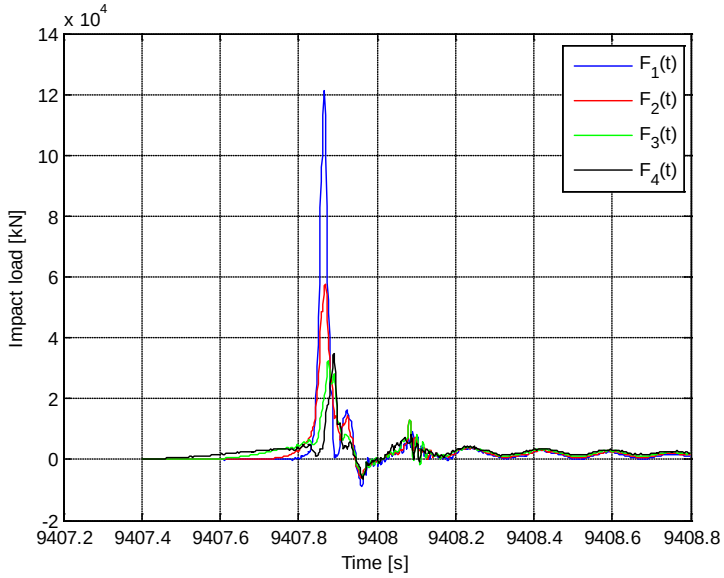

Figure 8-25: Assumed force histories for each horizontal level for largest slam in test 3124

9 Simplified assessment of global structural response

Impacts from breaking wave on a platform column give high loads of a short duration. The loads from breaking wave impacts are usually handled as a local structural problem. Local reinforcements on the columns are used to withstand these loads. When impact loads are as high as the largest loads measured during the model test, it is clear that they will give large local structural response. In this chapter it will be investigated if these large impact loads also can contribute to a significant global structural response.

To investigate this, a simplified assessment of the global structural response will be performed. This will be done by using a simplified structural model of the platform column, and expose it for an estimated load history representing the ALS impact loads from breaking waves. In this report the bending moment at the top of the column, where it is attached to the deck, is the quantity used as a measure for global structural response.

9.1 Impact loads

An impact load is a load that suddenly acts on the system and lasts for a relatively short period of time. To get a better understanding of how a system responds when exposed to an impact load a single degree of freedom system will be studied.

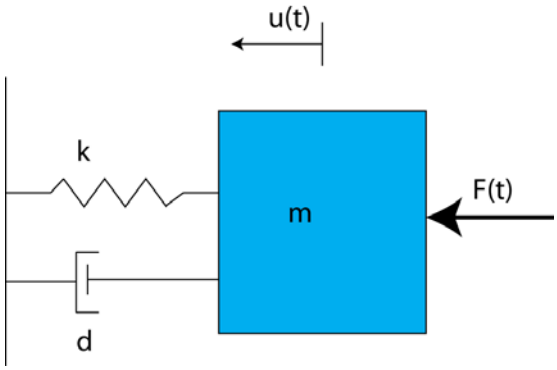

Figure 9-1: Illustration of single degree of freedom system

The dynamic equilibrium for this system will then be given as:

$$m\ddot{u}(t) + c\dot{u}(t) + ku(t) = F(t) \tag{9.1}$$

Where m is the system mass

d is the system damping

k is the system stiffness

$u(t)$ is the displacement

$\dot{u}(t)$ is the velocity

$\ddot{u}(t)$ is the acceleration

$F(t)$ is the load

By solving this equation it is possible to determine the system's response, e.g. the displacement.

When an impact load acts on the system it will induce a response. In Larsen (2009) the time lapse of an event like this is divided into two phases. Phase 1 is when the load act on the system and the system is exposed to a forced oscillation. Phase 2 is the time after, when the system oscillates freely.

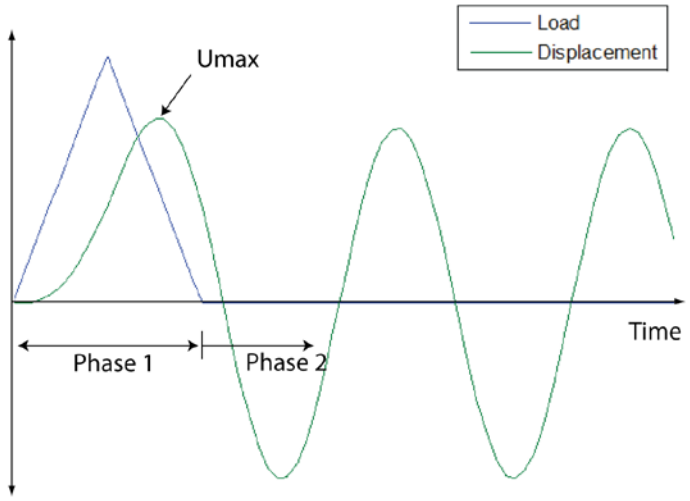

Figure 9-2: Illustration of response from impact load

For impact loads it is usually the maximum response that is off interest. The maximum response usually occurs during the first oscillation, as shown in Figure 9-2.

For systems with relative small damping, the damping will give little effect on the first oscillation. It will get more important for the next oscillations. In addition to the impact load itself, the systems mass and stiffness are the most important parameters for the first oscillation and therefore the maximum response. Since the system's natural period is given by these two parameters as shown in Eq.(9.2), it can be said that the maximum response is dependent on this period.

$$T_0 = 2\pi\sqrt{\frac{m}{k}} \tag{9.2}$$

Where m is the mass and k is the stiffness.

It is also possible to calculate the static response. This is done by dividing the maximum load, $F_{\max}$, on the stiffness, k, as shown in Eq.(9.3).

$$u_{static} = \frac{F_{\max}}{k} \tag{9.3}$$

The relationship between the maximum displacement, obtained by solving Eq.(9.1), and the static displacement gives the dynamic amplification factor, DAF.

$$DAF = \frac{u_{\max}}{u_{static}} \tag{9.4}$$

As mentioned earlier, the dynamic amplification depends on (Lehn, 2003):

- T_{rise}/T_{dur} *the ratio of the rise time to the load duration*
- T_{rise}/T_0 *the ratio of the rise time to the natural period of the system*
- T_{dur}/T_0 *the ratio of the load duration to the natural period of the system*
- *The shape of the load*

Figure 9-3 shows the DAF for different ratios between the load duration and the natural period of the system for four different load shapes.

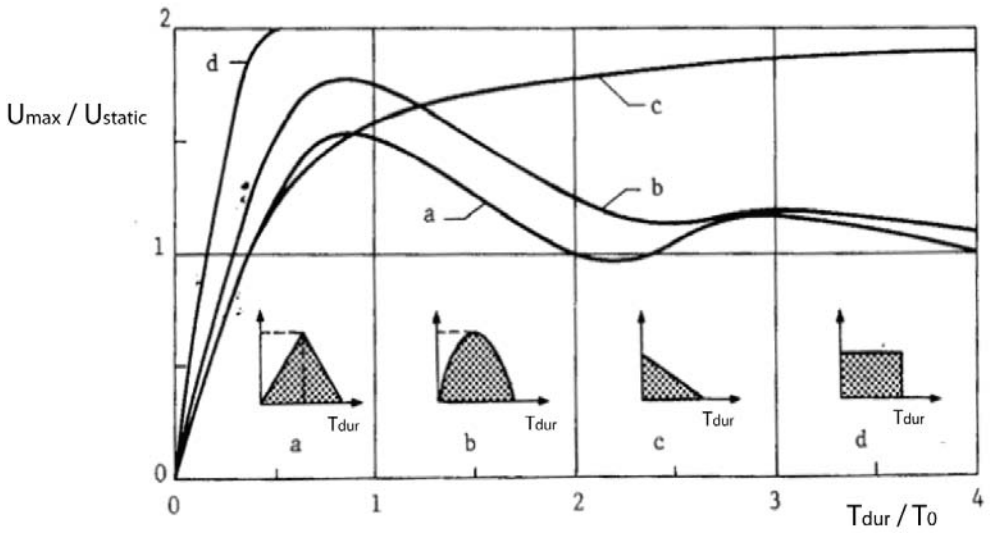

Figure 9-3: DAF for single degree of freedom system for 4 different load shapes (Larsen, 2009)

Impact loads from breaking waves have a load shape that looks similar to the triangle load (a) in Figure 9-3. For this load shape it can be seen that a low ratio between the load duration and the natural period gives a DAF lower than 1. As the ratio becomes higher the DAF becomes larger than 1 and peaks at around 1.5. For large ratios it can be seen that the DAF gets close to 1.

In Lehn (2003) the response is classified into three categories according to the duration of the impact load, T_{dur}, relative to the natural period of vibration of the structural component, T_0. The following is taken from Lehn (2003):

1. *<u>The impulsive domain:</u> the response is dependent on the impulse of the force, only. The duration of the impact is typically less than a third of the resonance period of the structure, i.e. $T_{dur} < 0.3\ T_0$*
2. *<u>The dynamic domain:</u> the resonant motions of the structure results in a dynamic amplification to the input force. The duration of the impact is typically between 0.3 and 3 to 6 times the resonance period of the structure, i.e. $0.3\ T_0 < T_{dur} < 3\text{-}6\ T_0$. The dynamic magnification factor depends principally on the rate of increase of the load to its maximum value. A steep loading of sufficient duration produces a magnification factor of 2; a very gradual increase causes a magnification factor of 1.*

3. *The quasi-static domain: the shape of the impact load can normally be detected from the response itself. The duration of the impact is typically larger than three to six times the resonance period of the structure, i.e. $T_{dur} > 3\text{-}6\ T_0$*

9.2 Structural analysis

The computer program USFOS is used to perform the simplified structural analysis. USFOS is a program that performs nonlinear static and dynamic analysis of space frame structures. The theory used by the program is given in the theory manual (Søreide et al. 1988).

Although USFOS is capable of running advanced nonlinear analyses, only simple linear structural analyses is performed.

When performing the structural analyses several simplifications will be assumed. The results will therefore only work as an indication on whether ALS breaking wave impacts will give a significant contribution to a global structural response.

9.2.1 Structural model

A simplified two dimensional structural model is used to represent the platform column. The model will be described in the following.

Beam model

The column has been modeled as a vertical beam with length 30.875m that is fixed in both ends. To model the connections from column to deck and column to pontoon as fixed is not completely true. However, the connection is probably so stiff that it can be used as reasonable assumption.

Cross-section properties

The beam used in the model is a general beam, where all the relevant cross-section properties must be defined. Based on the structural drawings of the column, provided by Aker Solutions (Rasmussen, 2011), a simplified cross-section can be assumed. A snapshot from one of the cross-section drawings is shown in Figure 9-4.

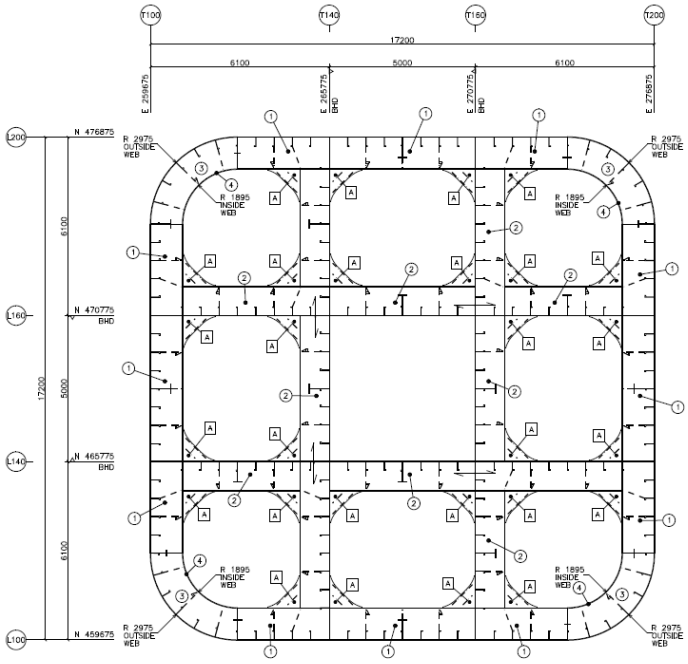

Figure 9-4: Snapshot from drawing of column cross-section (Rasmussen, 2011)

The columns cross-section is not uniform, and varies for different levels along the column. A simplified cross-section is therefore used. This is shown in Figure 9-5.

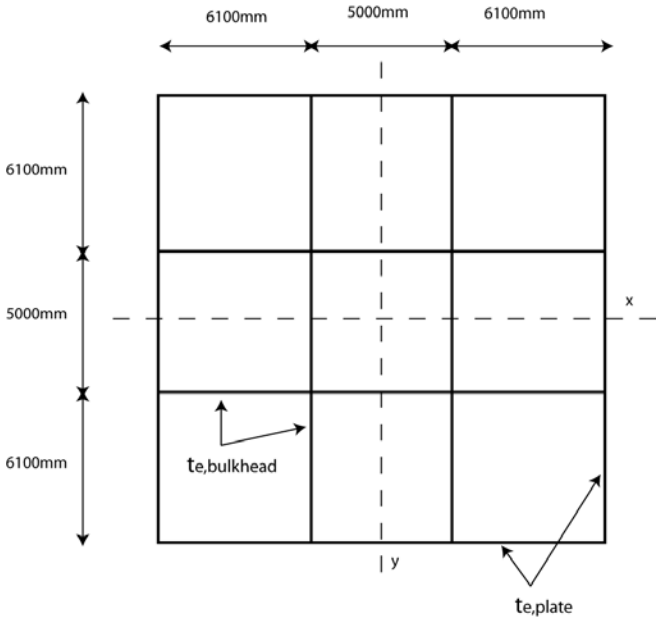

Figure 9-5: Illustration of simplified column cross-section

Where $t_{e,plate}$ and $t_{e,bulkhead}$ are the equivalent thickness for the column outer plates and the bulkheads respectively. Equivalent thicknesses are used to account for the vertical stiffeners. The formula for the equivalent thickness is taken from Amdahl (2011) and is shown in Eq.(9.5).

$$t_e = t + \frac{A_S}{s} \tag{9.5}$$

Where t_e is the equivalent thickness

t is the plate thickness

A_S is the area of one vertical stiffener

s is the stiffeners spacing

The vertical stiffeners used in the column are of type HP 260x10. According to Ruukki (2006) this type of stiffeners has area 36.11cm^2. The stiffeners spacing is equal to 625mm on both the outer plates and the bulkheads. Based on the column drawings the outer plate thickness is set to 12mm and the bulkheads thickness is set to 14mm. When using Eq.(9.5) the equivalent thicknesses becomes; $t_{e,plate} = 17.78mm$ and $t_{e,bulkhead} = 19.78mm$.

The dimensions needed to estimate the cross-section properties for the simplified cross-section, shown in Figure 9-5, are then found. The properties will be as follow:

Area - $A = 2.584m^2$

The second moment of area - $I = 127.398m^4$

Mass distribution

A short overview of the dry weights and their corresponding center of gravity for the platform hull was provided by Aker Solutions (Rasmussen, 2011). Based on this, the mass and vertical center of gravity (VCG) for the column was found.

Item	Mass	VCG
Upper column	530.0 tonne	24.025 m
Middle column	375.8 tonne	12.375 m
Lower column	247.0 tonne	3.685 m
Column bulk	72.2 tonne	15.935 m
Total	**1 225.0 tonne**	**15.873 m**

Table 9-1: Mass and VCG for column

The vertical centers of gravity in Table 9-1 are given as the distance from the lower end of the column. The height of the column is 30.875m. The column's estimated vertical center of gravity is located only 0.44m above the middle of the column. It is therefore assumed that the mass can be represented by a uniform equivalent density for the beam material. This assumed density becomes 15354.5 kg/m^3.

Damping

The structural damping is modeled by defining a constant damping ratio of 2% (Amdahl, 2011).

Water level

A lower part of the column will be underwater when the breaking wave hits the column. To find exactly how much of the column that is submerged during a breaking wave impact is difficult. A simplification has therefore been done. It is assumed that the water level during a breaking wave

impact is equal to the still water line. The lowest 11.9m of the column will then be submerged.This assumption is found reasonable by looking at the movie recordings from the model tests.

The most important effect from the water in this analysis is the added mass. The column has a large volume, hence a large added mass. Hydrodynamic damping will be of little importance since the column displacement will be really small. Since the structural model is two dimensional, it is only the surge added mass that will be of importance. This is found from Faltinsen (1990).The added mass is calculated from the following equation.

$$A_{11} = \rho \pi a^2 L \tag{9.6}$$

Where A_{11} is the surge added mass

ρ is the water density

a is equal to half of the column width

L is the length of the column's submerged part

When using Eq.(9.6) the column's added mass in surge becomes 2828 tonne. The added mass is modeled by defining an equivalent material density for the submerged part that is added to the equivalent density that represents the column mass.

9.2.2 Load models

In subchapter 8.5, four different load models were suggested. Static and dynamic analyses are performed with these load models.

During the model tests there were two slams that gave much larger impact forces than all other measured slams. When the ALS impact force was predicted from the model test data, these two large slams were 2 of 18 extreme values used. It was mentioned earlier that if looking at the cumulative empirical distribution, Eq.(4.17), for these 18 extremes, these two slams would represent the 90th and 95th percentile. This is the probability level used for the ALS breaking wave problem. Based on this, it has been chosen to run structural analyses with the measured impact force from both of these slams. These slams are from now on referred to as slam 3100 and slam 3124.

To get the four load models for each of these slams, the time series of the measured impact forces are added together as explained in subchapter 8.5. As mentioned before, these time series are the response measured by the sensors. To get the real impact force history, the dynamic in the sensors should be eliminated. The important part of the impact force is the large peak. The actual impact force will rise faster than the response. The actual impact force would therefore have given a larger dynamic amplification. However, the peak of the sensor response is larger than the actual force's peak. These two differences will therefore to some extent equalize each other. To use the measured impact force would therefore not introduce large errors.

In the dynamic analyses the point loads in the different load models are whole load histories. These load histories are shown in Appendix D. In the static analyses, the point loads are set to the maximum load in each relevant load history.

9.2.3 Result from structural analyses

A total of 16 analyses were performed; static and dynamic analyses for slam 3100 and slam 3124 using all four load models.

The quantity used to investigate for global structural response is the bending moment. The maximum bending moment at the top of the column, where it is attached to the deck, is therefore found for each of these analyses. The results are given in Table 9-2.

Slam	Bending moment at column top [MNm]							
	Load model 1		Load model 2		Load model 3		Load model 4	
	Static	Dynamic	Static	Dynamic	Static	Dynamic	Static	Dynamic
3100	549.4	569.3	585.7	521.7	902.2	950.9	944.2	849.0
3124	550.6	539.9	602.6	502.4	926.2	908.8	997.3	816.0

Table 9-2: Bending moments from structural analyses

Plots with the bending moment response from these analyses can be found in Appendix E.

9.3 Discussion: Results

The results from the analyses presented in Table 9-2 shows that there is some difference in the results obtained from the static analysis versus dynamic analyses. The reason for these differences will now be discussed.

Load models 1 and 3 both consist of a single point load, while load models 2 and 4 have four point loads. For the dynamic analyses, the value of these point loads is given as load histories, while for the static analyses the point loads is equal to the maximum load in each load history. For load models 1 and 3 the dynamic amplification factor varies between 0.98 and 1.05. For load models 2 and 4 the dynamic amplification varies between 0.82 and 0.89.

It could be of interest to see what the dynamic amplification was expected to be, based on the theory in subchapter 9.1. To do this the natural period of the structure and the load duration needs to be found.

The natural period of the structure is found by performing an eigenvalue analysis, using USFOS. The lowest eigenvalue that is relevant for this problem is then found. The eigenperiod that corresponds to this eigenvalue is 0.017s. The natural period of the structure is characterized by this eigenperiod. In Rasmussen (2011) a natural period of 0.01s was suggested for the column, if modeled as a fixed beam and not including added mass. If the added mass is removed, the eigenvalue analysis gives a natural period equal to 0.01s. This is in accordance with the suggestion. When added mass is included, the total mass in the system will be increased and therefore give a larger natural period. Based on this the natural period of the structure is set to 0.017s.

The load history used in load model 1 for slam 3100 is shown in Figure 9-6.

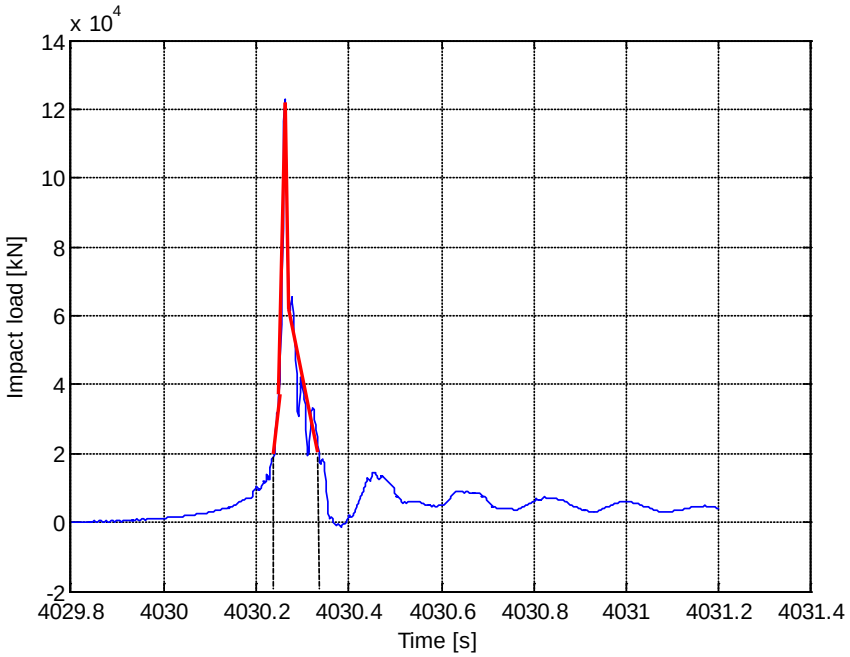

Figure 9-6: Load history for load model 1, slam 3100

From Figure 9-6 it can be seen that the main part of the load have a duration of approximately 0.1s. The load duration seems to be in a time range close to this, for all the load histories used in the different load models. The load duration is therefore sat to 0.1s.

It can be seen from Figure 9-6 that the main part of the load has some sort of a triangular shape. The load can therefore by idealized by a triangular load. Three idealized triangular load histories with different rise time are given in Figure 9-7.

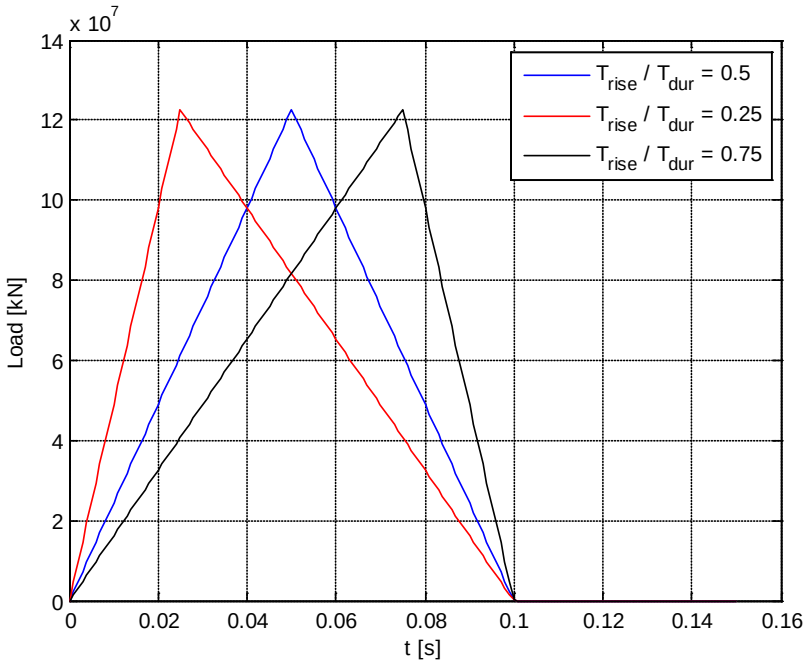

Figure 9-7: Idealized triangular loads with different rise time, based on load model 1 for slam 3100

Triangular load histories, like those shown in Figure 9-7, are used to investigate how the bending moment's dynamic amplification factor varies with the ratio between the load duration and the natural period. Several dynamic analyses were run with these triangular loads but with different load durations. The maximum bending moment at the top of the column is found for each analysis and compared with the static bending moment to find the dynamic amplification. The results are shown in Figure 9-8.

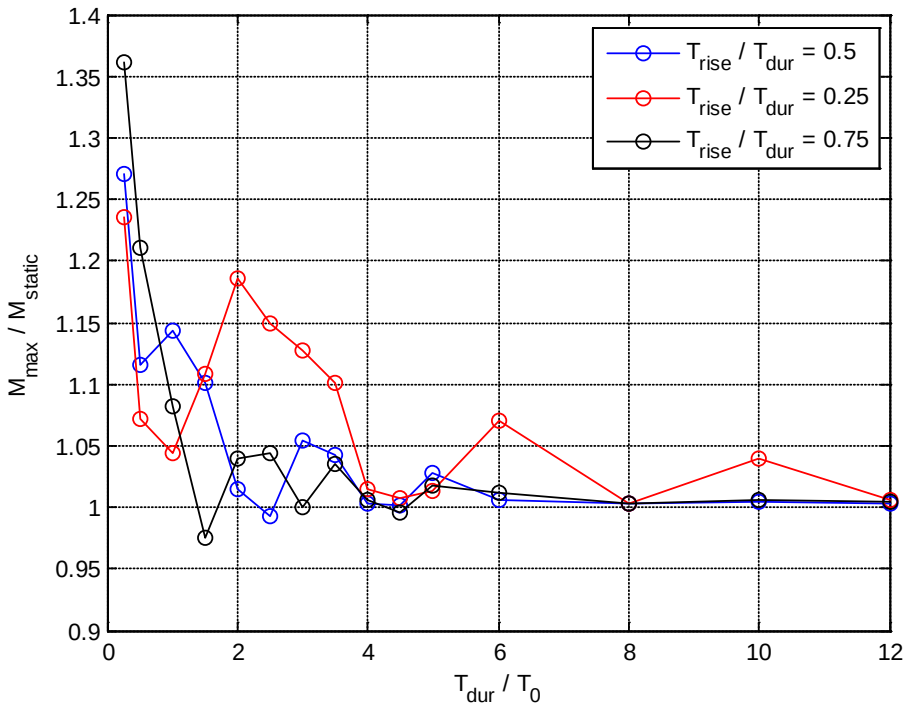

Figure 9-8: DAF for bending moment at column top for triangular loads

When the load duration is 0.1s and the natural period is 0.017s, the ratio will become 5.9. The response can therefore be said to be in the quasi-static domain, with only small dynamic amplifications. For this ratio the dynamic amplification in Figure 9-8 will become between 1.02 and 1.06, depending on the rise time. The largest dynamic amplification from the analyses using load models 1 and 3 was 1.05. This seems to be reasonable.

The lowest dynamic amplification factor for load model 1 and 3 was 0.98. This is most likely because the load history used in the analyses is not a perfect triangle. The load history has small distortions that might cause the maximum bending moment to become a little less than the static bending moment. However, this difference is of little significance.

These distortions in the load histories is probably causing some of the difference in the results between static and dynamic analysis using load models 2 and 4 as well. However, there was a larger difference between static and dynamic results when using these load models. Since the load histories used in these two load models also have load duration that can be approximated to around 0.1s, the static and dynamic results should be more similar. There seems to be something else that is causing these differences.

In subchapter 8.4, the time variation of the measured maximum impact force for the different sensors was investigated. It was found that for slam 3100 and slam 3124 the sensors located higher on the column experienced their maximum impact force earlier than the sensors below. The load histories used in load models 2 and 4, were found by adding together the measured impact force for the sensors at each horizontal level. This means that the maximum loads in the resulting load histories will also have a time variation like this. Since the response is in the quasi-static domain, the maximum response will occur at the same time as the maximum load. The maximum load for the point load that represents the top level on the column is larger than the maximum loads for the levels below. Since this maximum load occurs before the others, the maximum response will therefore occur before the column has been exposed to the other levels maximum load. When performing the static analysis the maximum load for each horizontal level was set to act simultaneously. This is probably the main reason for the differences in static and dynamic results for load model 2 and 4.

If looking back on Figure 9-8, it can be seen that for triangular loads with load duration larger than 2.5 times the natural period, a very small dynamic amplification can be present. It gets higher when the rise time is short, meaning a steeper loading. It is expected that a steep loading will give larger dynamic effects than a load that increases more slowly. When the load duration gets less than 2.5 times the natural period, the dynamic amplification is not according to the behavior expected. When the ratio is 2.5, the load duration will be 0.043s. When the load duration becomes less than this, it seems like it will start to affect other mode shapes than the one corresponding to the natural period. From the eigenvalue analysis performed in USFOS, the eigenperiods for the two next relevant mode shapes were found. These eigenperiods were 0.006s and 0.003s. The shape of these mode shapes is shown in Figure 9-9.

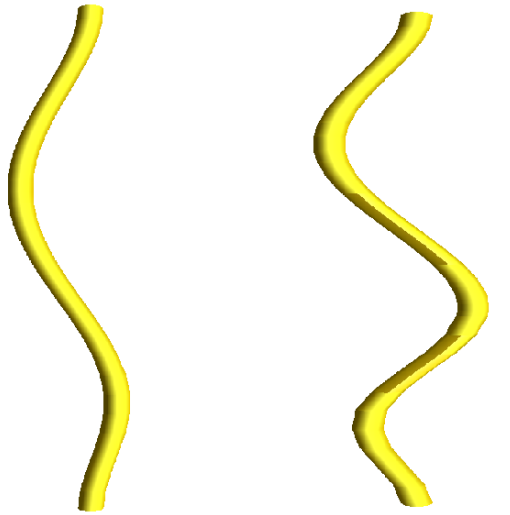

Figure 9-9: Second and third mode shape

In Larsen (2009) it is said that there are two conditions that determines which modes that will give the dominating response; the modal load, and the relationship between the load duration and the modes eigenperiods. The location of the point loads used in the different load models seems to generate large modal loads for the two shapes shown in Figure 9-9. As the relationship between the

load duration and these modes eigenperiods gets smaller, they will give more and more contribution to the response. Based on all this, it is likely that it is the response from these modes that is causing the unexpected dynamic amplification when the load duration gets lower.

The structural model of the platform column is a system with many degrees of freedom. Based on this, Figure 9-8 cannot be compared with the dynamic amplification for a single degree of freedom as shown in Figure 9-3. If the mass was uniform over the entire column and a point load acted at the middle of the beam, the displacement at the middle would only act in one degree of freedom. Doing this to the column, by removing the added mass and set an idealized triangular load to act on the middle, would give the same dynamic amplification for the displacement. This is shown in Figure 9-10.

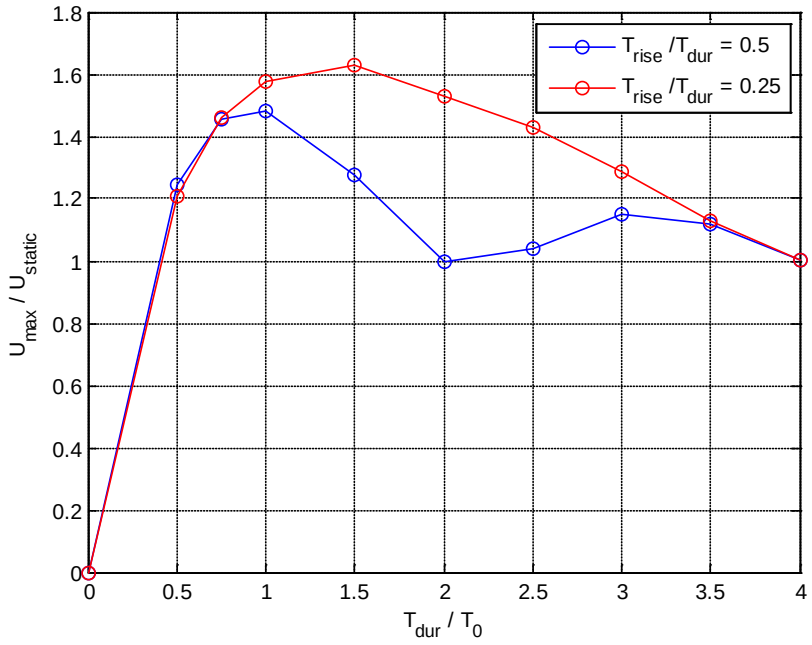

Figure 9-10: DAF for displacement at the middle of the column when symmetrical conditions are fulfilled

This looks very similar to Figure 9-3. It also shows the effect from having a steeper loading.

The platform model, which was used in the model tests, had three force transducers that connected the North-West column to the rest of the platform. These force transducers could measure the global forces and moments of the North-West column. Unfortunately this was only done for one damage condition. If these global responses had been measured during the 10 000 year tests, the measurements could have been compared with the results presented in Table 9-2.

9.4 Discussion: Global structural response

The bending moment that the structure needs to withstand is set to 997.3MNm. This is taken from the static analysis using load model 4 for slam 3124. The static analysis does not account for the time variation of the maximum loads. Using the bending moment from this analysis is therefore conservative.

To see if this bending moment is of any significance, it is compared with the column's elastic moment capacity. This moment capacity, M_{el}, is found from the following equation (Moan, 2004).

$$M_{el} = \sigma_Y W_{el} \tag{9.7}$$

Where σ_Y is the yield stress and W_{el} is the elastic section modulus.

It is assumed that column has steel with yield stress 300MPa. The elastic section modulus for the columns simplified cross section is 14.81m^3. When using these values the elastic moment capacity becomes 4443.0MNm.

It is then possible to see how much of this capacity that is utilized by the bending moment from the breaking wave impact.

$$\frac{M}{M_{el}} = \frac{997.3MNm}{4443.0MNm} = 0.22 \tag{9.8}$$

The bending moment from the breaking wave impact only utilize 22% of the elastic moment capacity. This is when disregarding all other forces. Interaction with other forces would probably give a larger moment. However, since the global structural response is investigated for the ALS condition the capacity could probably be set even higher. It is acceptable with some plastic deformation as long as the structure survives in the damaged condition under functional and environmental loads. Based on this, the bending moment from the breaking wave impact does not seem to be of significant magnitude concerning the structural capacity of the column.

Although a lot of simplifications have been done, this assessment indicates that the ALS impact loads from breaking waves do not give a significant contribution to global structural response.

10 Conclusion

In this report different problems in connection with ALS breaking wave impact have been assessed. Two different methods have been used to estimate the ALS impact loads from breaking waves. The impact force on different locations on a platform column has been studied, and a simple assessment of the global structural response has been performed.

The most important results were as following:

- Estimating the ALS impact loads from breaking wave using stochastic analysis of model test data, gave an impact load almost twice as large as when using the numerical method based on DNV-RP-C205 (2007).
- The largest breaking waves in the model test had much higher wave velocity than estimated with the numerical method.
- The platform surge velocities measured in the model test could be quite large and gave significant contribution to the impact force.
- There is a lot of uncertainty involved when predicting design values for impact loads from breaking waves, especially for high probability levels.
- A breaking wave that hits the column will give higher impact force where the upper part of the wave hits than the lower parts of the wave.
- A breaking wave that hits the column will give similar impact force for a certain horizontal level on the column.
- The very stiff platform column had a natural period much smaller than the impact load duration.
- Since the load duration was much longer than the structures natural period the dynamic effects in the structural response became very small.
- A load model that accounted for the variation in impact load over the column's height gave larger bending moment at the column top.
- When the column was exposed to ALS impact loads from breaking waves the associated global structural response was of little importance.

11 Recommendations for further work

The work in this report has revealed many aspects that need further investigation.

The two large slams that occurred during test 3100 and 3124 should be investigated closer. They should be compared with the smaller slams to see if there is other mechanism that is causing them to be so large. If it was found that these large slams belong to a different population, a probabilistic model that accounts for this should be established.

The ALS impact load from breaking waves should also be estimated using a CFD method. The results from this could then be compared with the results from the numerical method based on DNV-RP-C205 (2007) and the stochastic analysis of model test data.

When investigating the correlation in the measured impact force between the different sensors, many slams were used. However, more slams with a size between the two largest and the other slams would be preferable. More slam data could be obtained from more model tests or CFD simulations.

If a similar model test should be performed, more slamming sensors should have been used. If slamming sensors did cover a larger area on the column wall it would be possible to see how large area that experiences significant impact force during each slam.

The global moments obtained in this report could have been validated if there was model test data of the global forces and moments for the column. The Midgard model was instrumented to perform these measurements, but this was not done for the 10 000 year condition. If a similar model test should be performed, these global forces and moments should have been measured.

When performing the structural analysis in this report, a lot of simplifications were done. To get more realistic results a more detailed model of the platform should have been used.

12 References

Amdahl, J., Endal, A., Fuglerud, G., Minsaas, K., Rasmussen, M., Sillerud, B., Sortland, B. and Valland, H. (2005). TMR 4100 – Marin teknikk 1. Marinteknisk senter, NTNU, Trondheim, Norway.

Amdahl, J. (2011). Personal conversation 2011-05-10 in Trondheim, Norway.

Chang, K.-A. and Liu, P.L.-F. (1997). Velocity, acceleration and vorticity under a breaking wave. School of Civil and Environmental Engineering. Cornell University. Ithaca. New York.

Dalane, E. (2011). Air-gap Estimation Methods for Semi-Platforms. Project Thesis. NTNU, Department of Marine Technology.

Dean, R.G. and Dalrymple, R.A. (1984). Water wave mechanics for engineers and scientists. Advanced Series on Ocean Engineering – Volume 2. World Scientific.

DNV-RP-C205 (2007). Environmental conditions and environmental loads. DNV.

Efron, B. (1979). Bootstrap Methods: Another Look at the Jackknife. The Annals of Statistics, Vol. 7, No. 1, pp. 1 – 26.

Faltinsen,O.M. (1990). Sea loads on ships and offshore structures. Cambridge Ocean Technologies Series.

Haver, S. and Winterstein, S.R. (2008). Environmetal Contour Lines: A Method for Estimating Long Term Extremes by a Short Term Analysis, Proceedings of SNAME Maritime Technology Conference (SMTC) 2008. Houston, Texas.

Haver, S. (2010). Prediction of Characteristic Response for Design Purposes. Lecture Notes TMR 4195, Department of Marine Technology, NTNU.

Langen, I. and Sigbjörnsson, R. (1979). Dynamisk analyse av konstruksjoner. Tapir.

Larsen, C.M. (2009). TMR 4180 – Marin Dynamikk. Marinteknisk senter, NTNU, Trondheim, Norway.

Lehn, E. (2003). On Water Impact Loads, Publication P-09.03 March 2003, MARINTEK.

Lehn, E. (2011). Personal conversation 2011-02-17 in Trondheim, Norway.

MARINTEK (2010). AKER Midgard Model Tests – Main Report

Mathiesen, M. (2010). Åsgard MFP – Metocean Design Basis. Revision 1. Statoil internal document.

Moan, T. (2004). TMR 4195 – Design of offshore structures, Vol.1, Design procedures and criteria. Marinteknisk senter, NTNU, Trondheim, Norway.

Montgomery, D.C. and Runger, G.C. (1994). Applied Statistics and Probability for Engineers. John Wiley & Sons Inc.

Newland, D.E. (1993). An introduction to random vibrations, spectral and wavelet analysis. Dover Publications, Inc. Mineola. New York.

NORSOK N-003 (2007). Actions and action effects. Standards Norway.

NS-EN ISO 19900 (2003). Petroleums- og naturgassindustri, Generelle krav til offshore-konstruksjoner. Standards Norway.

Ochi, M.K. (1998). Ocean waves – The stochastic approach. Cambridge Ocean Technology Series.

Pettersen, B. (2007). TMR 4247 – Marin Teknikk 3, Hydrodynamikk. Marinteknisk senter, NTNU, Trondheim, Norway.

Rasmussen, S.L. (2011). Email, received 2011-03-24. Aker Solutions.

Ruukki (2006). Hot Rolled Shipbuilding profiles. www.ruukki.com.

Steen, S. and Aarsnes, J.V. (2010). TMR 7 – Experimental Methods in Marine Hydrodynamics. Marinteknisk senter, NTNU, Trondheim, Norway.

Suyuthi,A. (2009). Extreme loads due to Wave Breaking Against Platform Column. Proceedings of the Nineteenth International Offshore and Polar Engineering Conference 2009. Osaka, Japan.

Søreide, T.H., Amdahl, J., Eberg, E., Holmås. T. and Hellan, Ø. (1988). USFOS – A Computer Program for Progressive Collapse Analysis of Steel Offshore Structures. Theory Manual. SINTEF, Division of Structural Engineering, Trondheim, Norway.

Walpole, R.E., Myers, R.H., Myers, S.L. and Ye, K. (2007). Probability & Statistics for Engineers & Scientists - Eighth Edition. Pearson Education International. Prentice Hall

Appendix A Plots of measured impact force

This appendix contains plots of the measured impact force for all 8 sensors during the two largest slams in the model test, slam 3100 and slam 3124.

Slam 3100

Sensor 1:

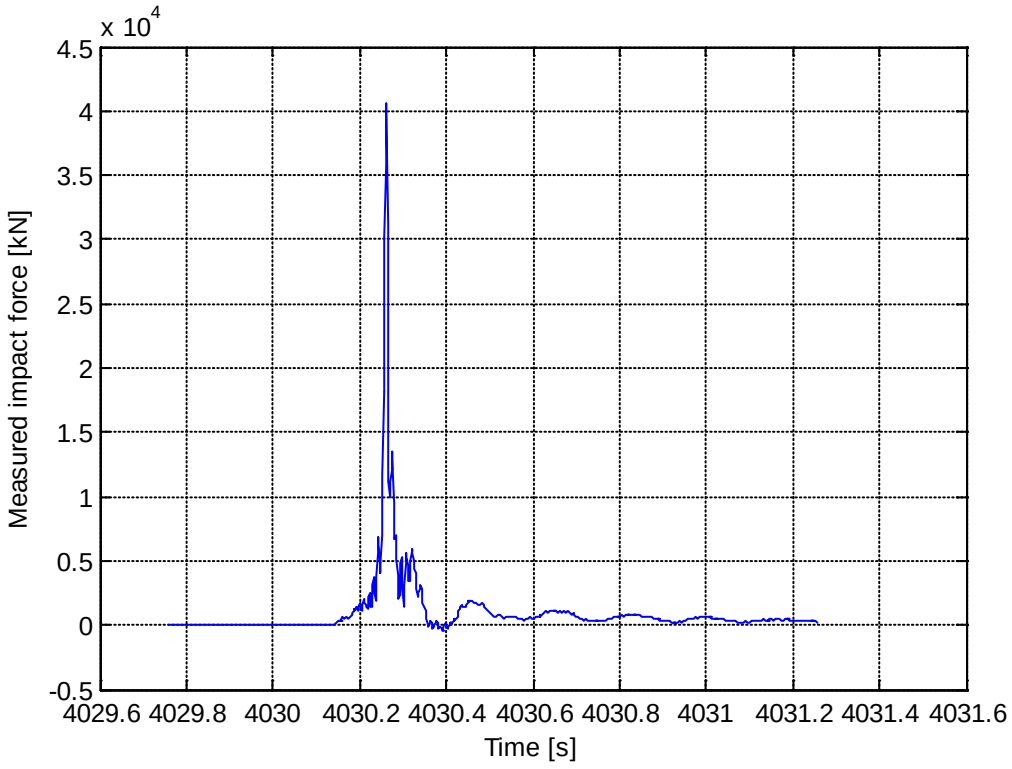

Sensor 2:

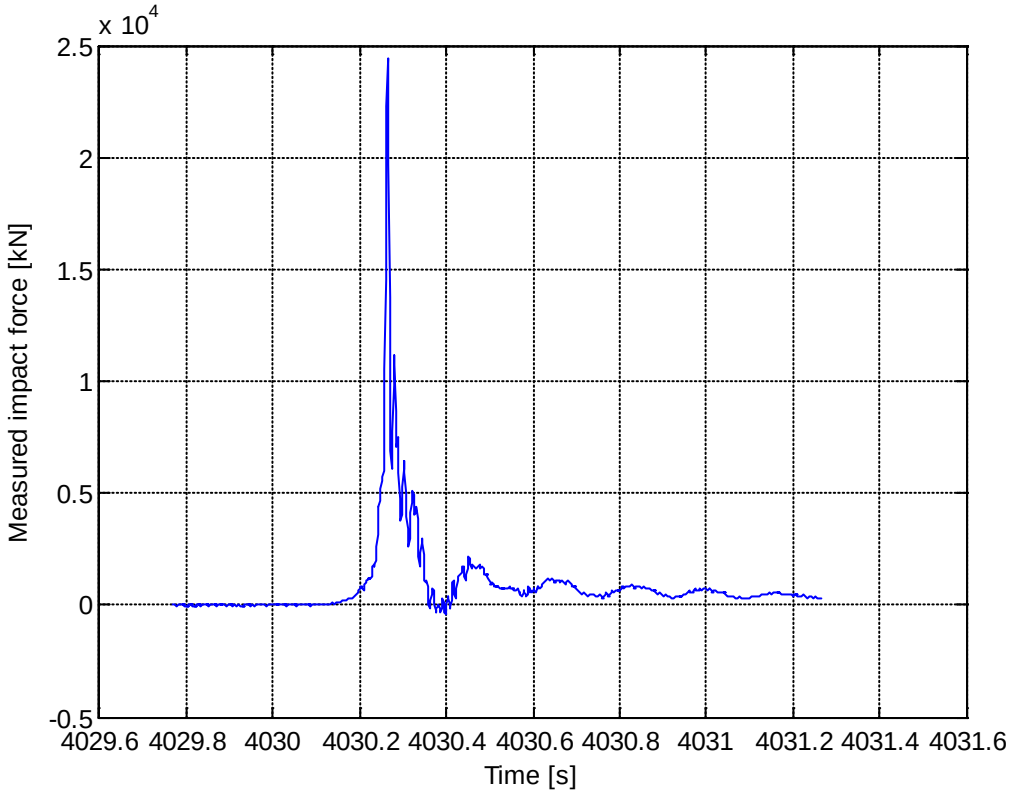

Sensor 3:

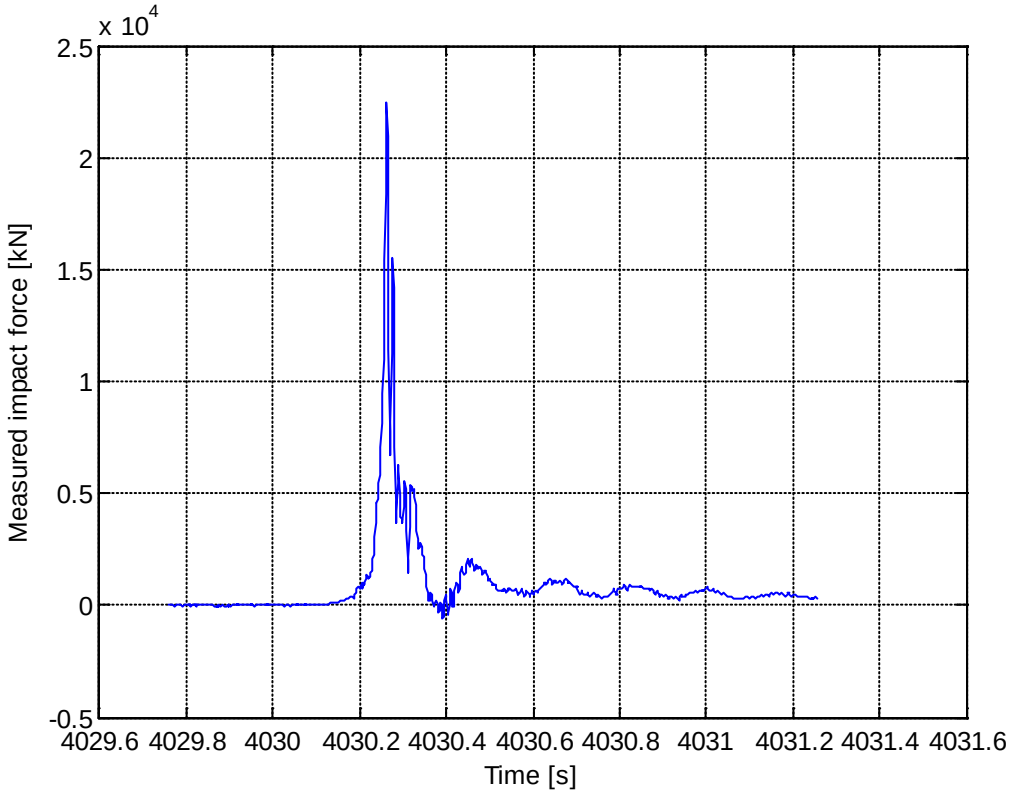

Sensor 4:

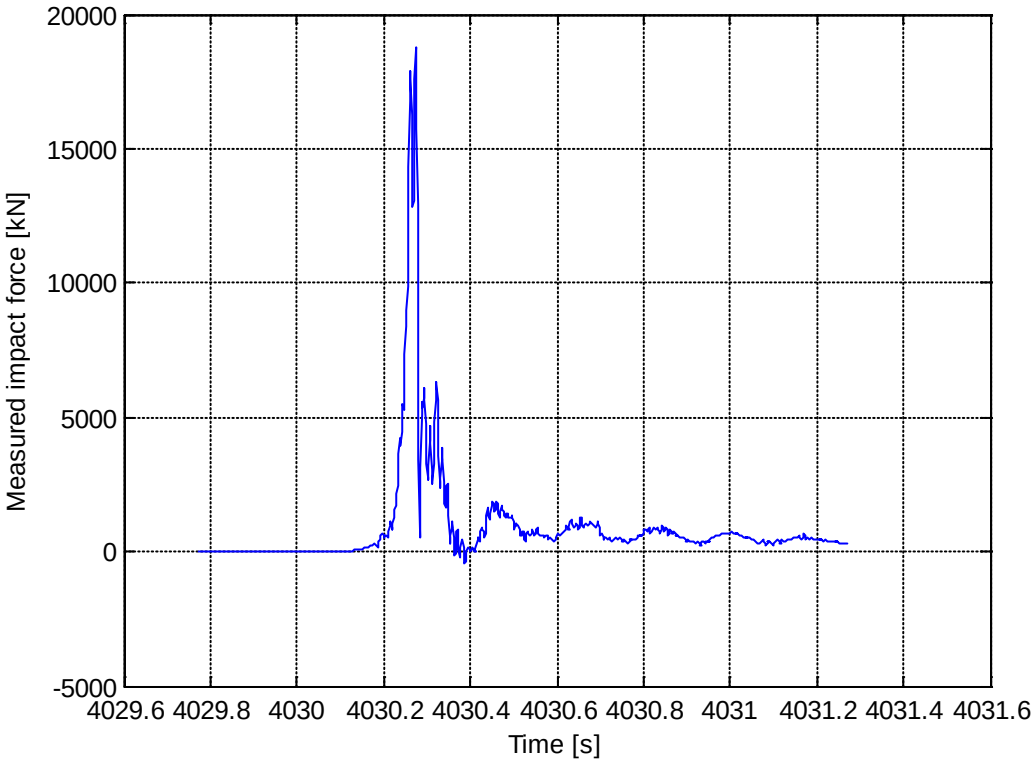

Sensor 5:

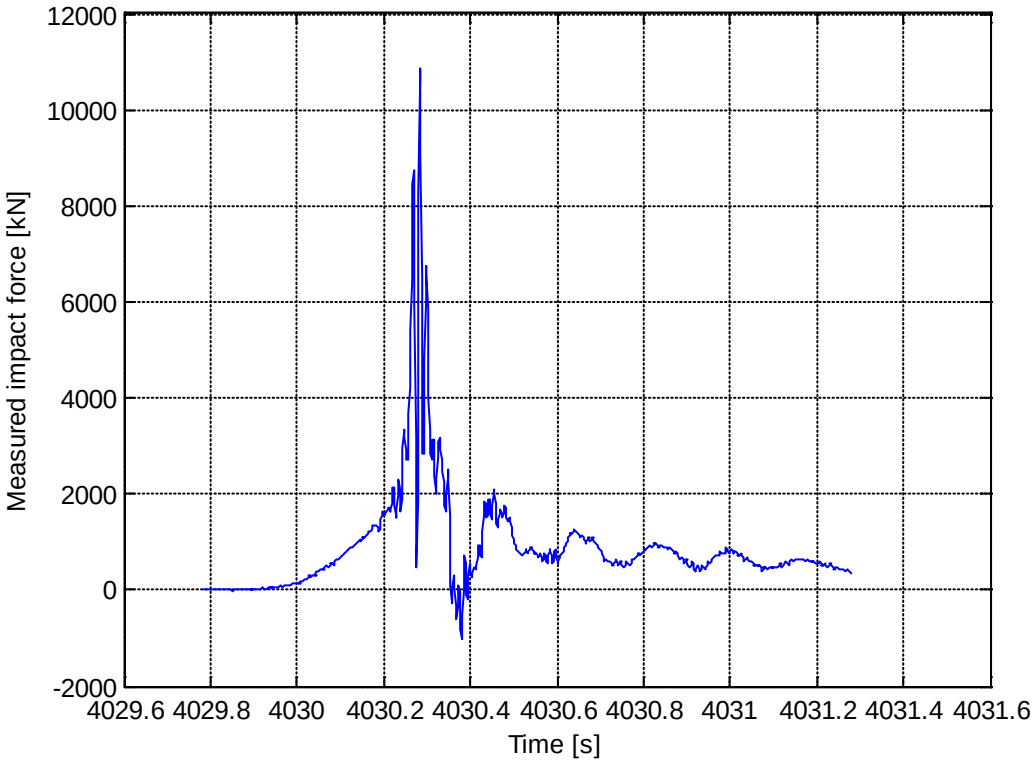

Sensor 6:

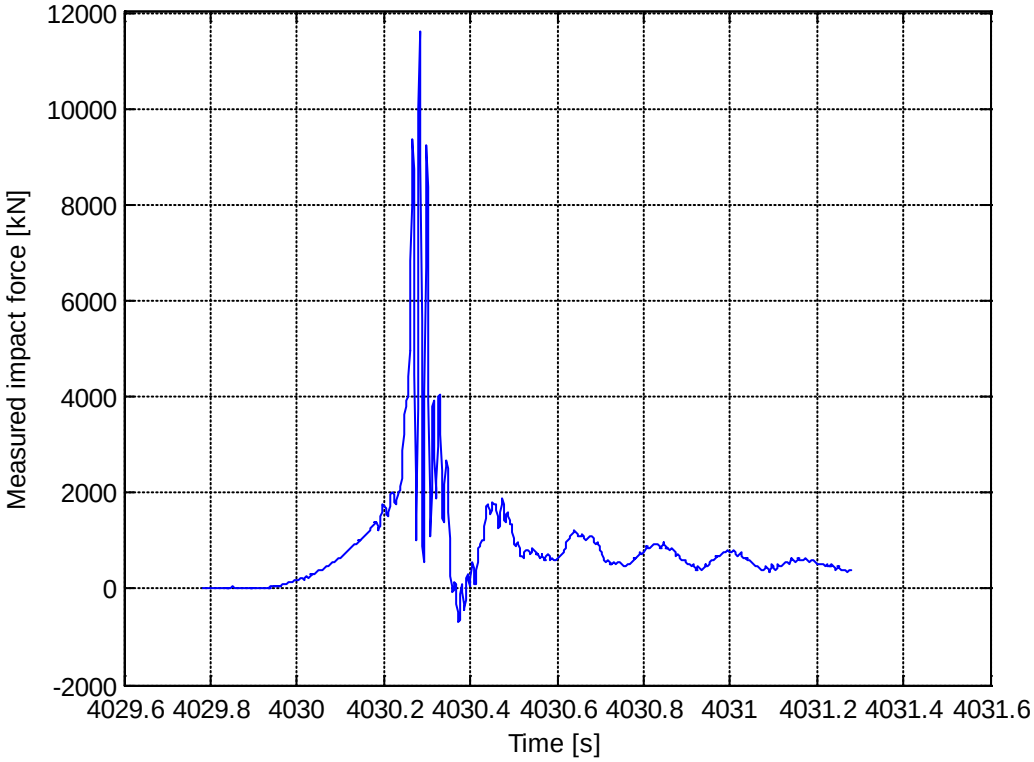

Sensor 7:

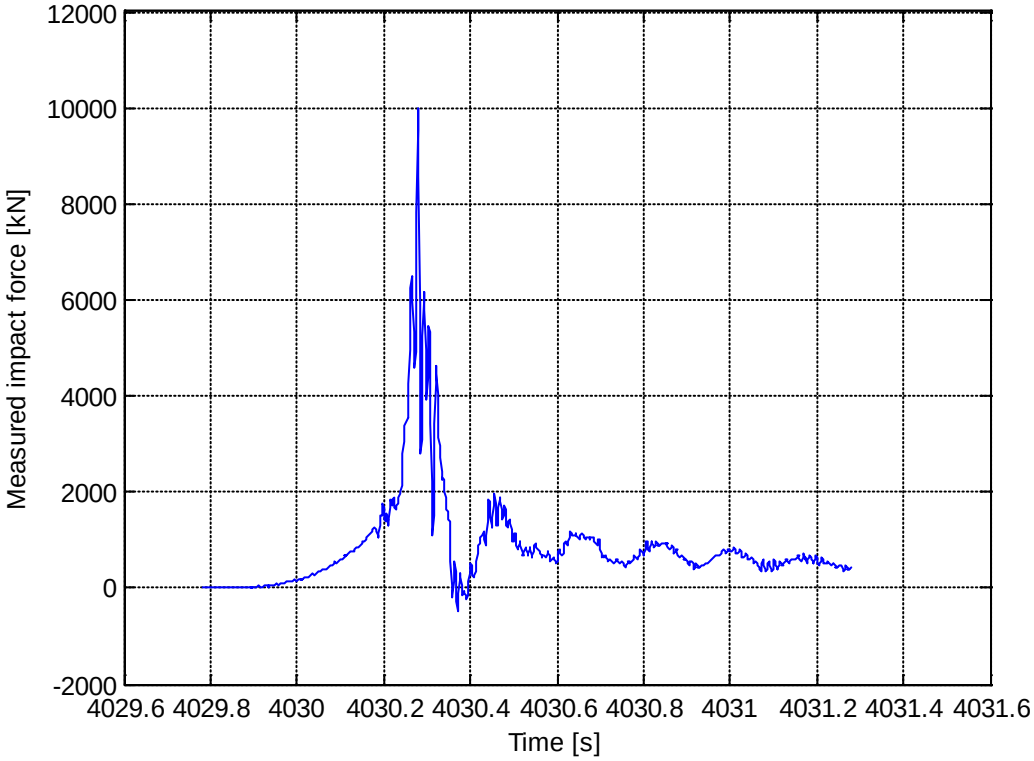

Sensor 8:

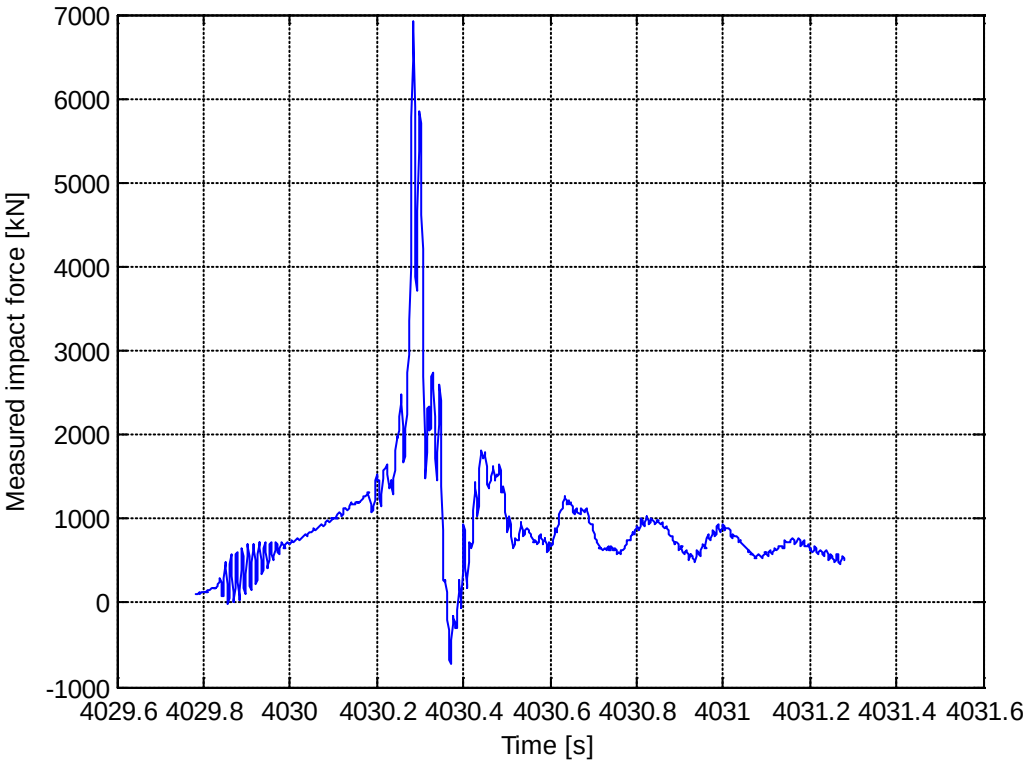
7000
6000
5000
4000
3000
2000
1000
0
-1000
Measured impact force [kN]
4029.6 4029.8 4030 4030.2 4030.4 4030.6 4030.8 4031 4031.2 4031.4 4031.6
Time [s]

Slam 3124

Sensor 1:

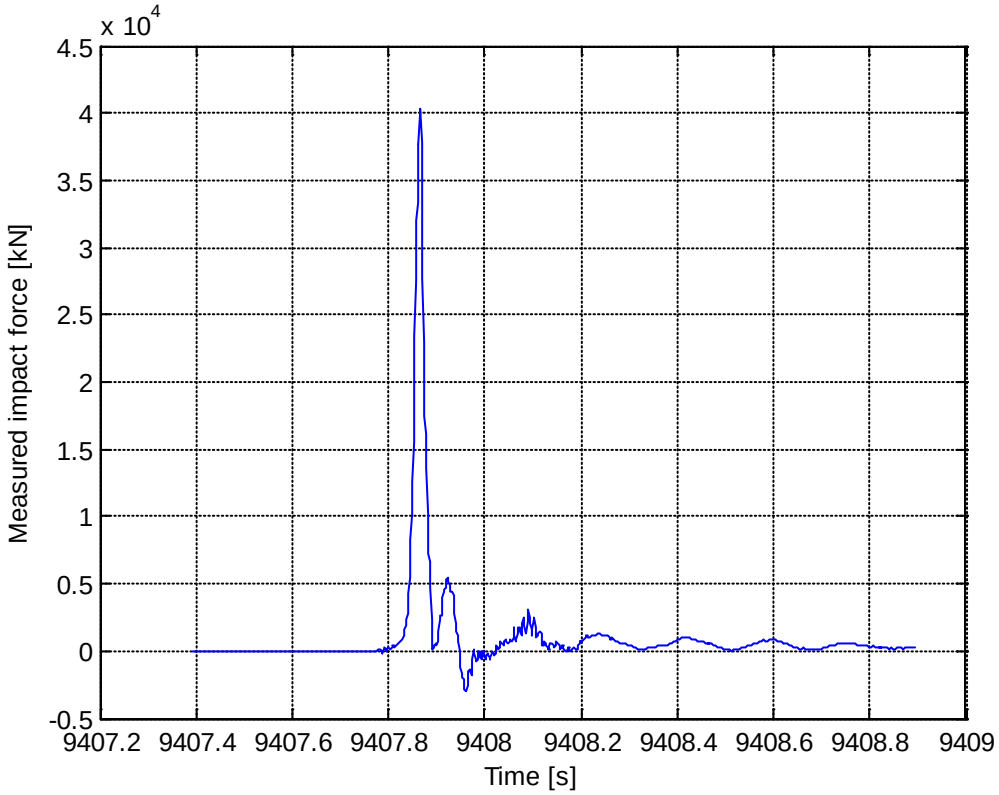

Sensor 2:

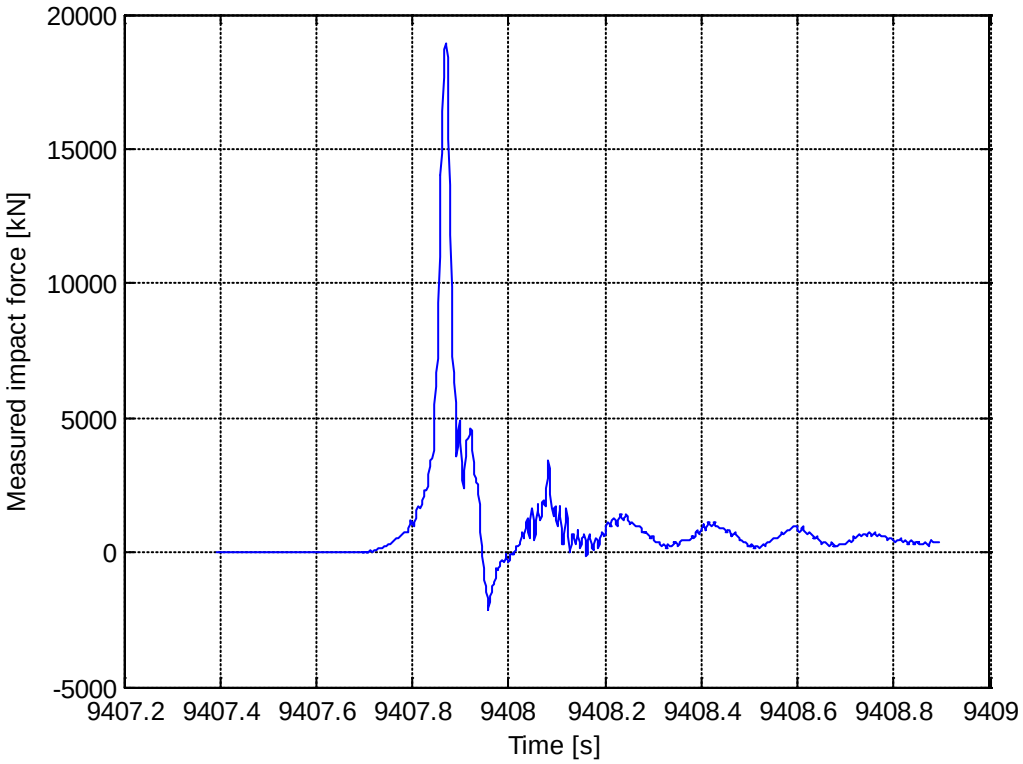

Sensor 3:

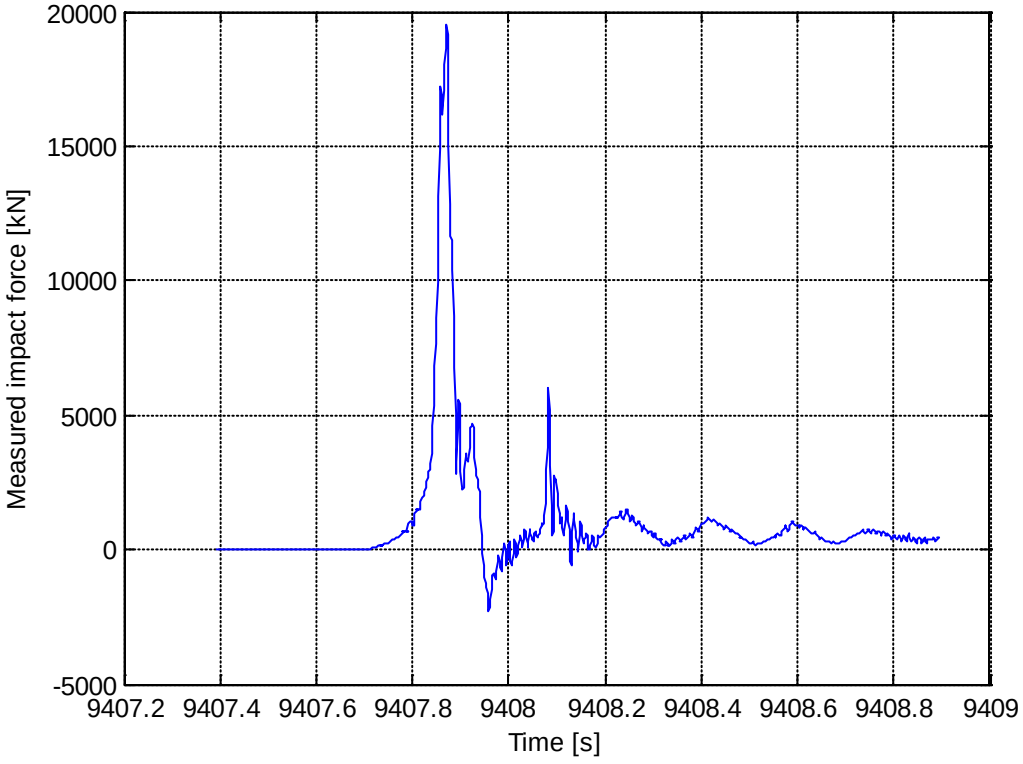

Sensor 4:

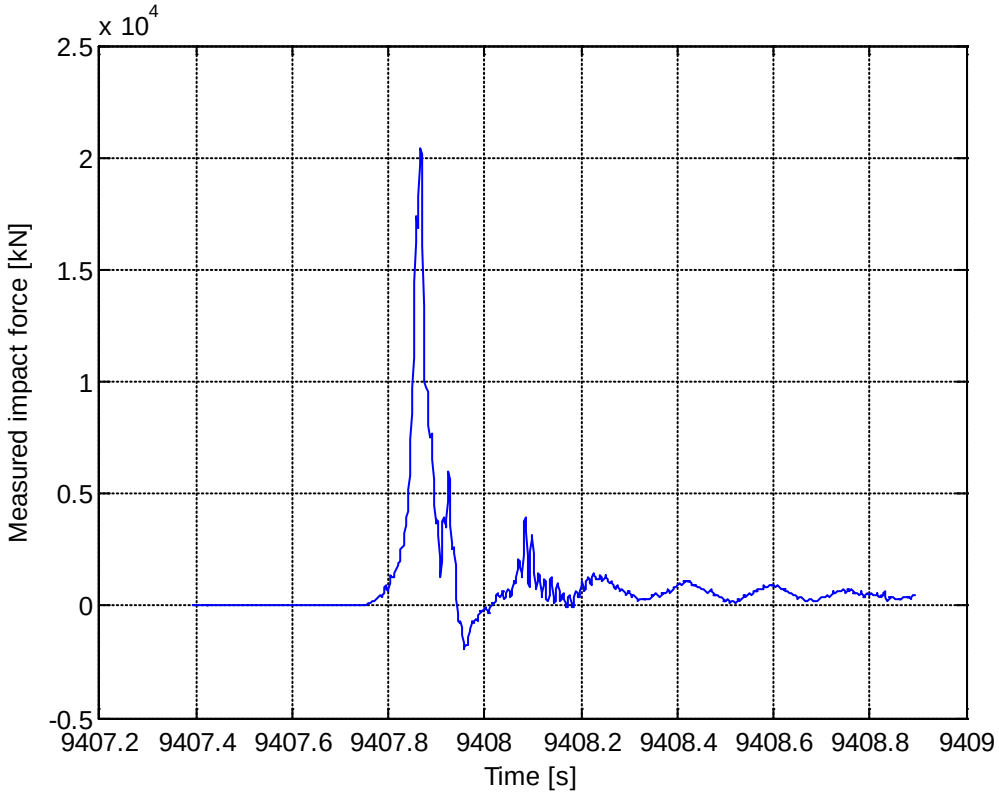

Sensor 5:

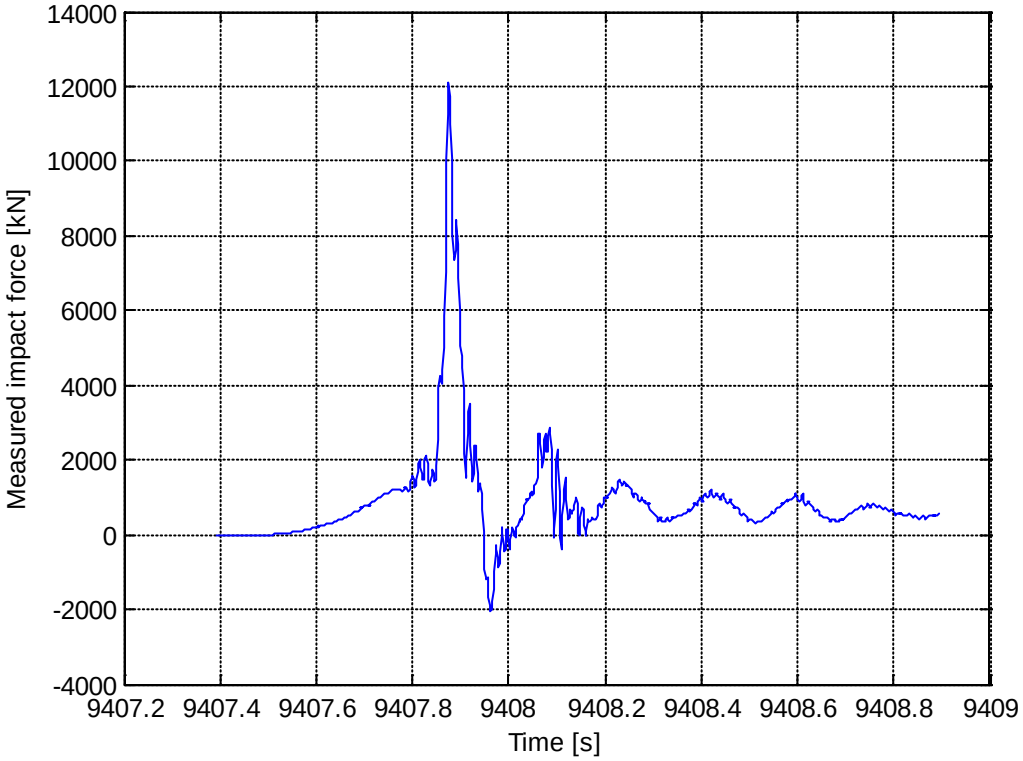

Sensor 6:

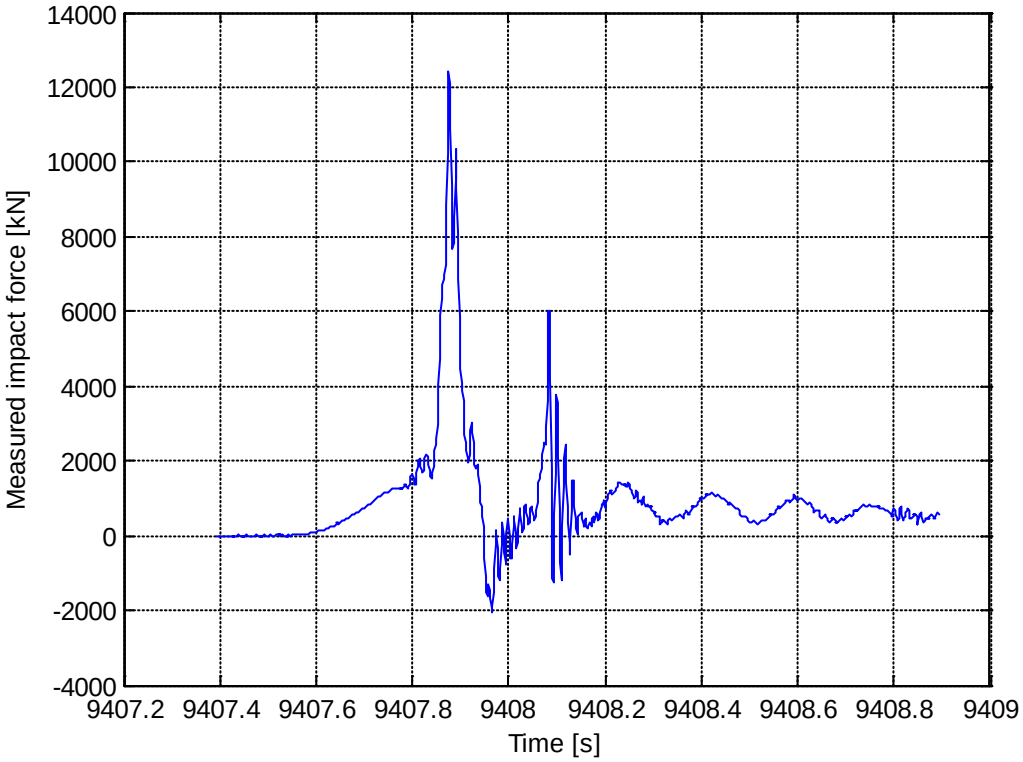

Sensor 7:

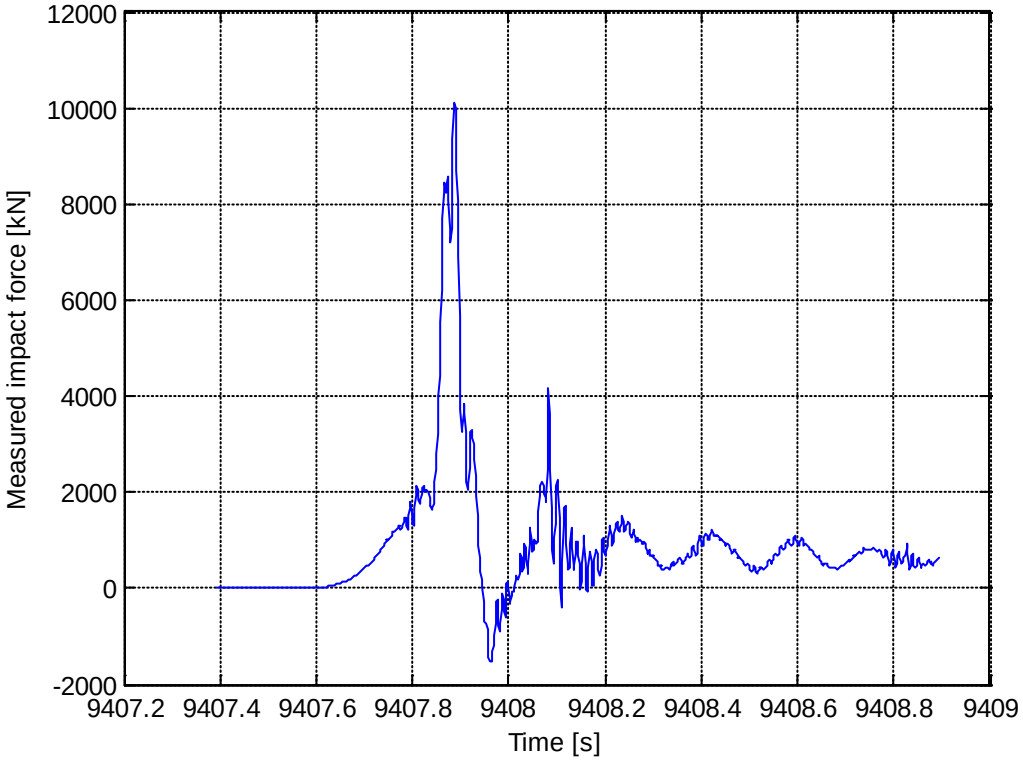

Sensor 8:

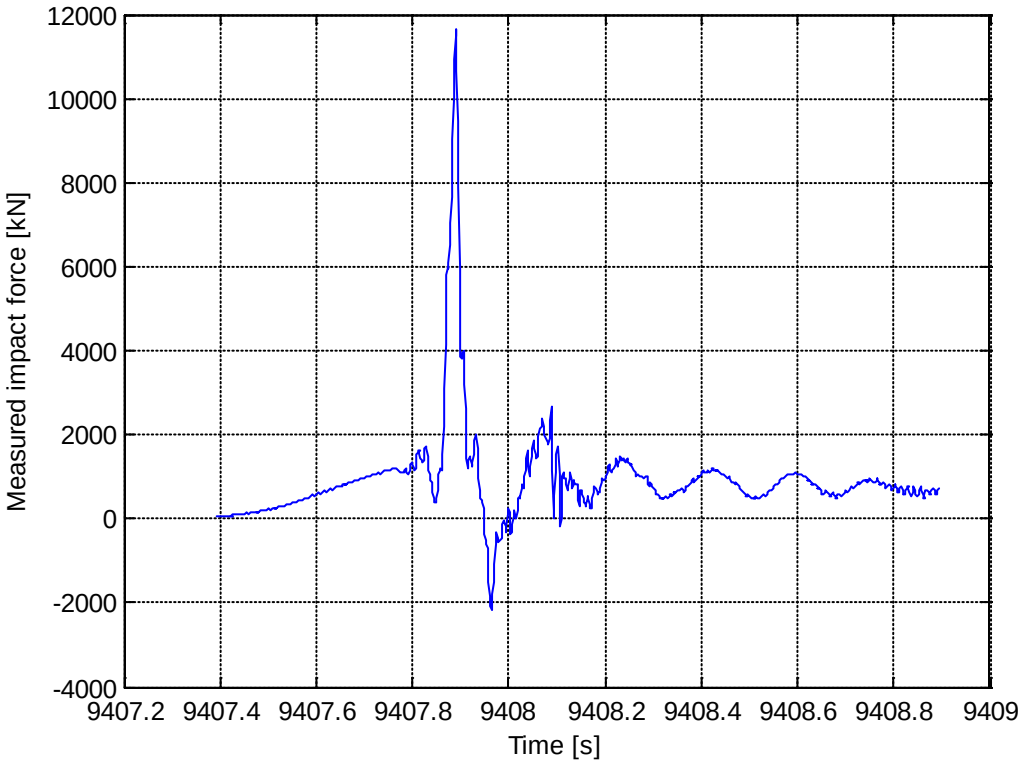
12000
10000
8000
6000
4000
2000
0
-2000
-4000
Measured impact force [kN]
9407.2
9407.4
9407.6
9407.8
9408
9408.2
9408.4
9408.6
9408.8
9409
Time [s]

Appendix B Plots of platform surge velocity

This appendix contains plots of the platform surge velocity at the same time as the largest slam in each realization occurs. The plots are also showing the measured impact force for sensor 1 during the slam.

Slam 3100:

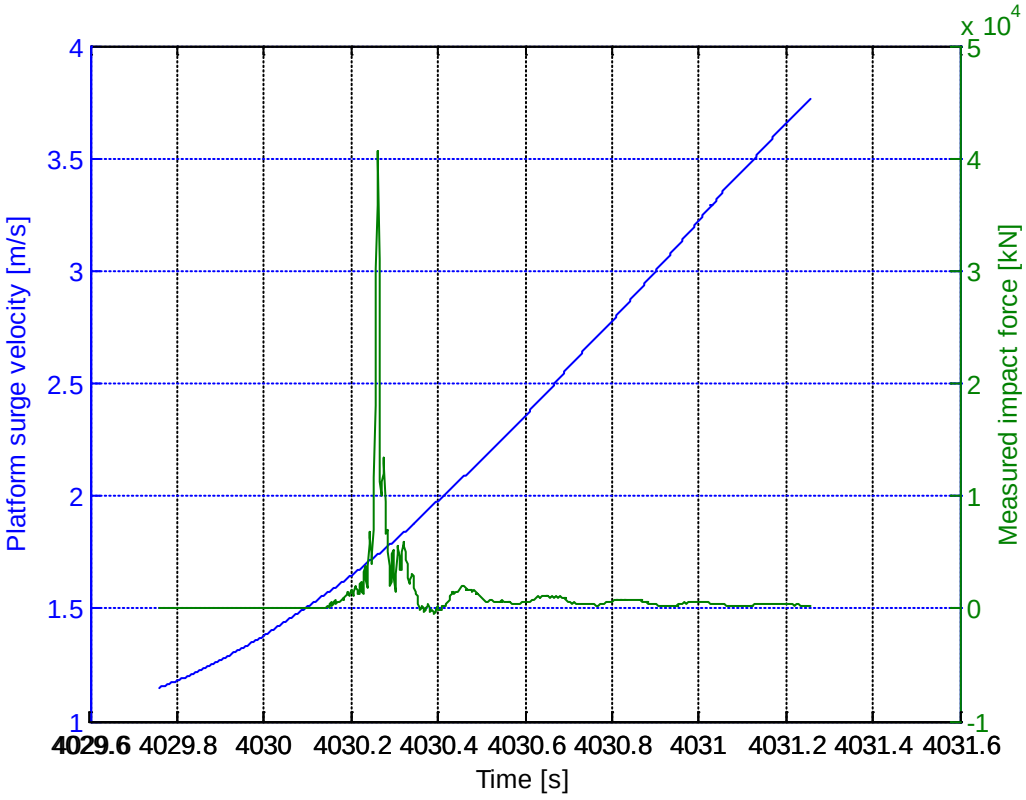

Slam 3111:

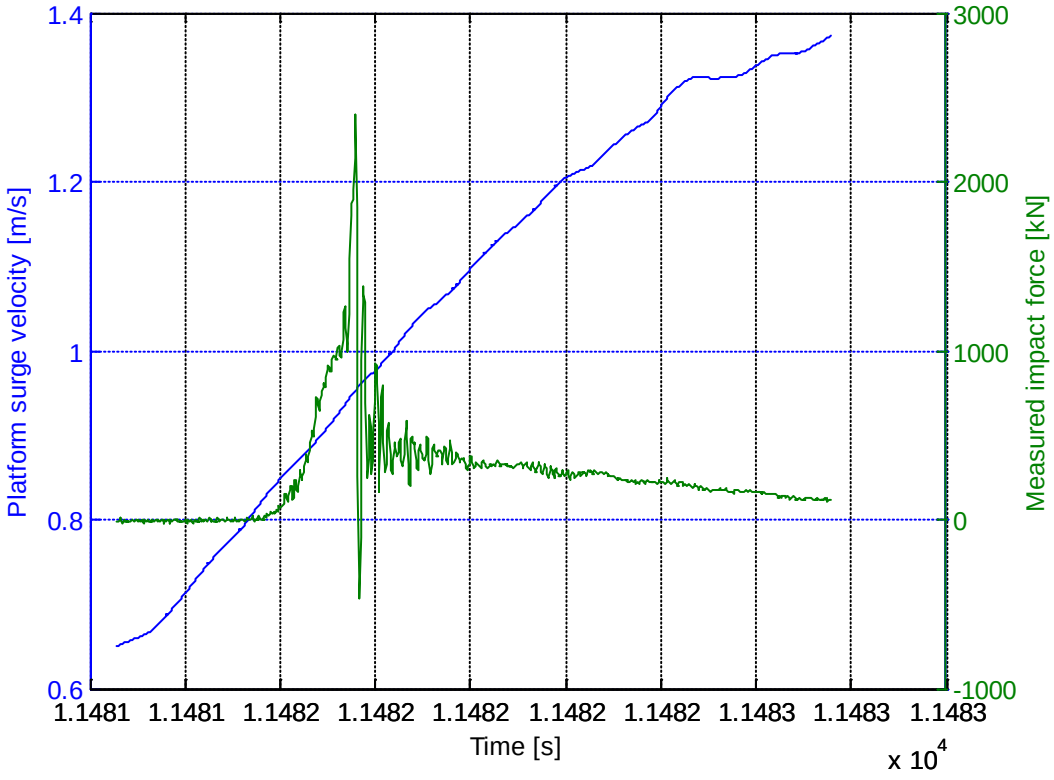

Slam 3120:

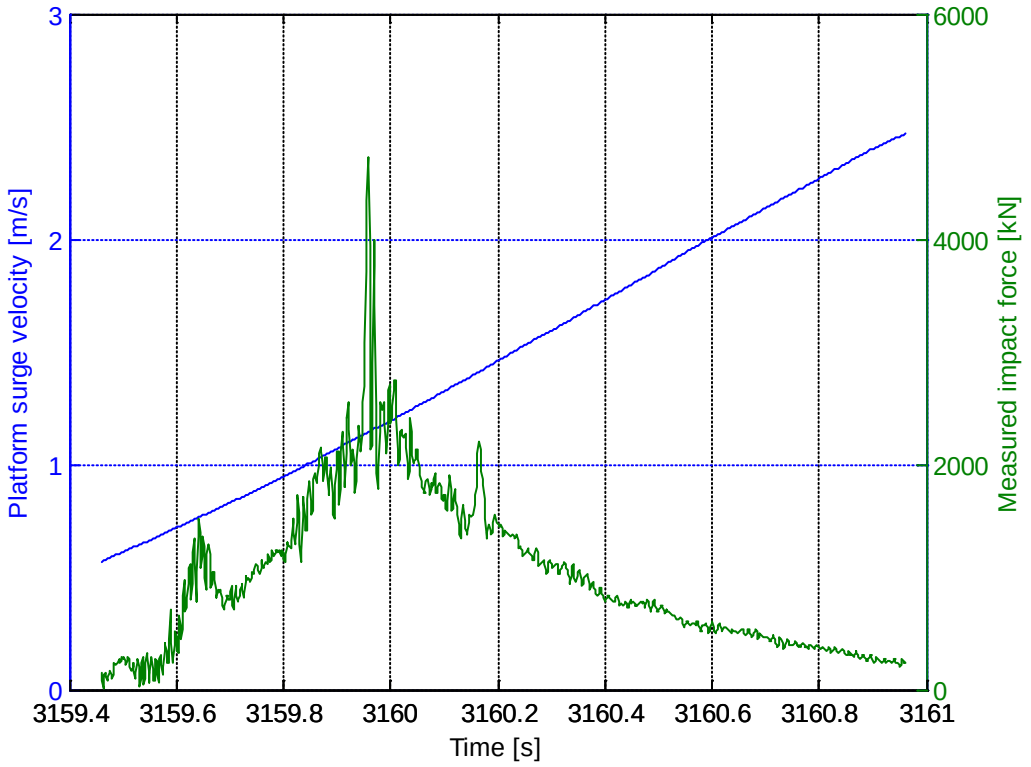

Slam 3121:

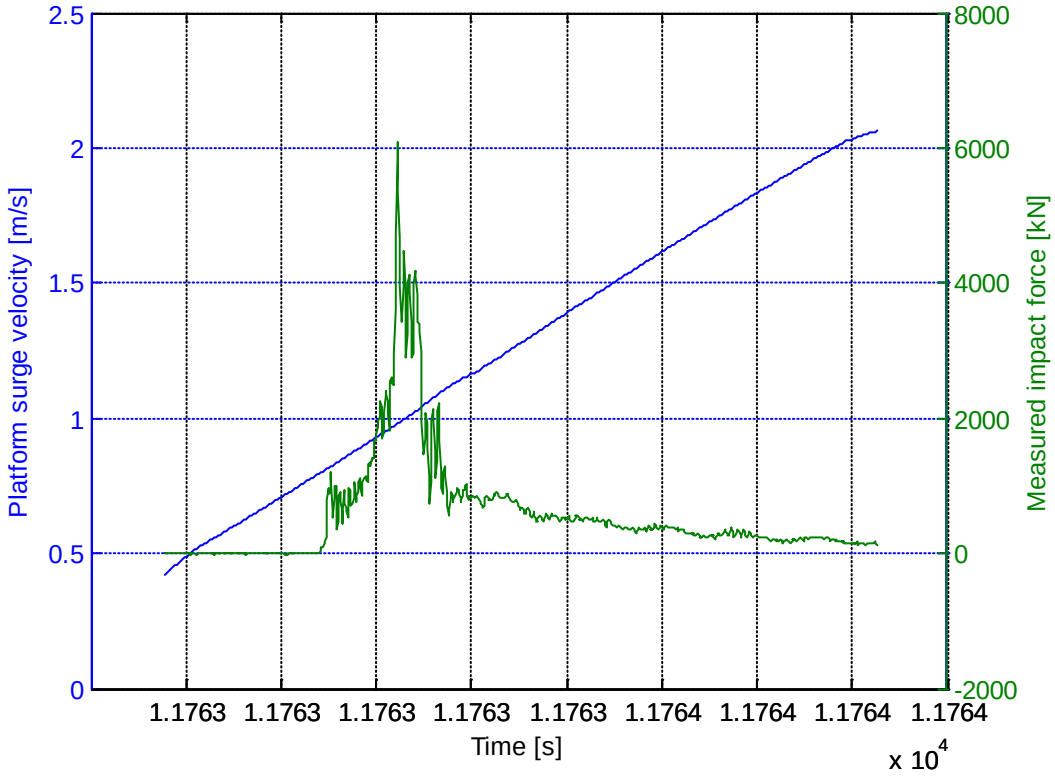

Slam 3122:

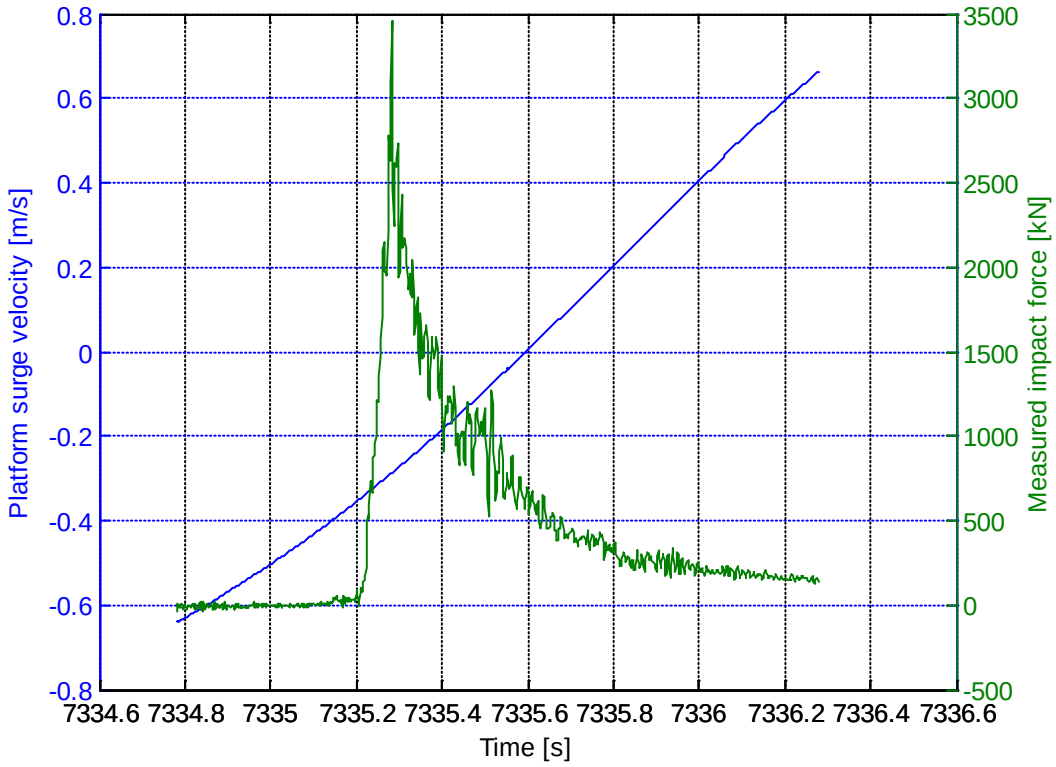

Slam 3124:

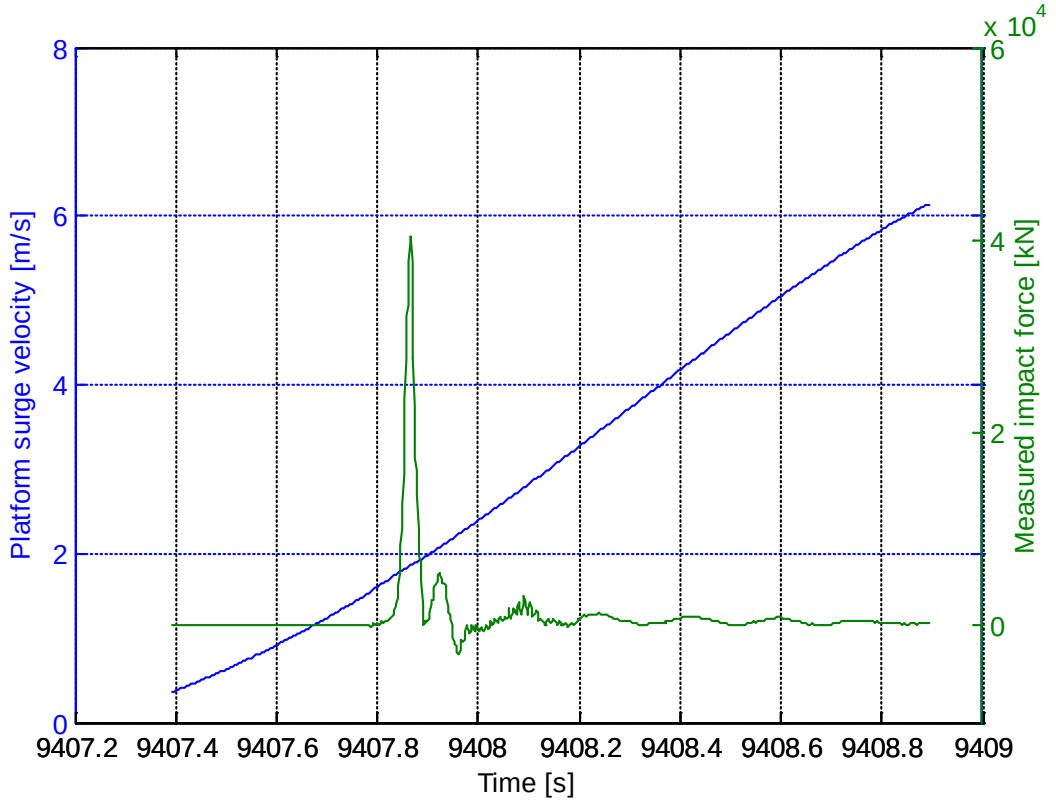

Slam 3126:

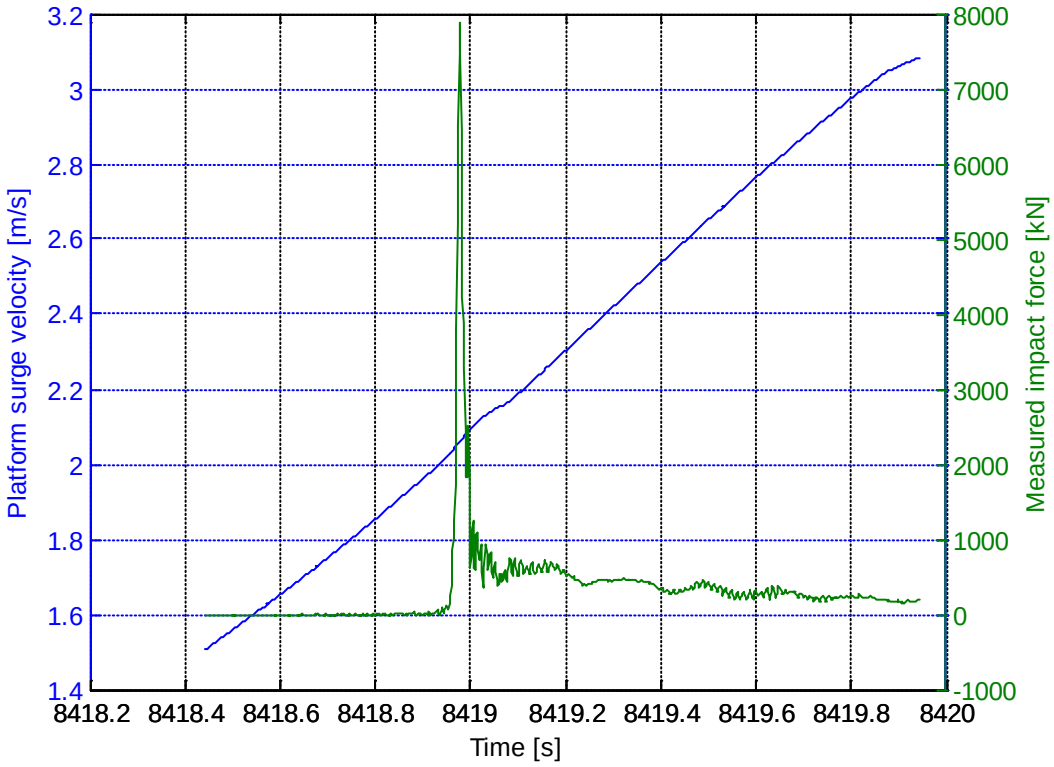

Slam 3129:

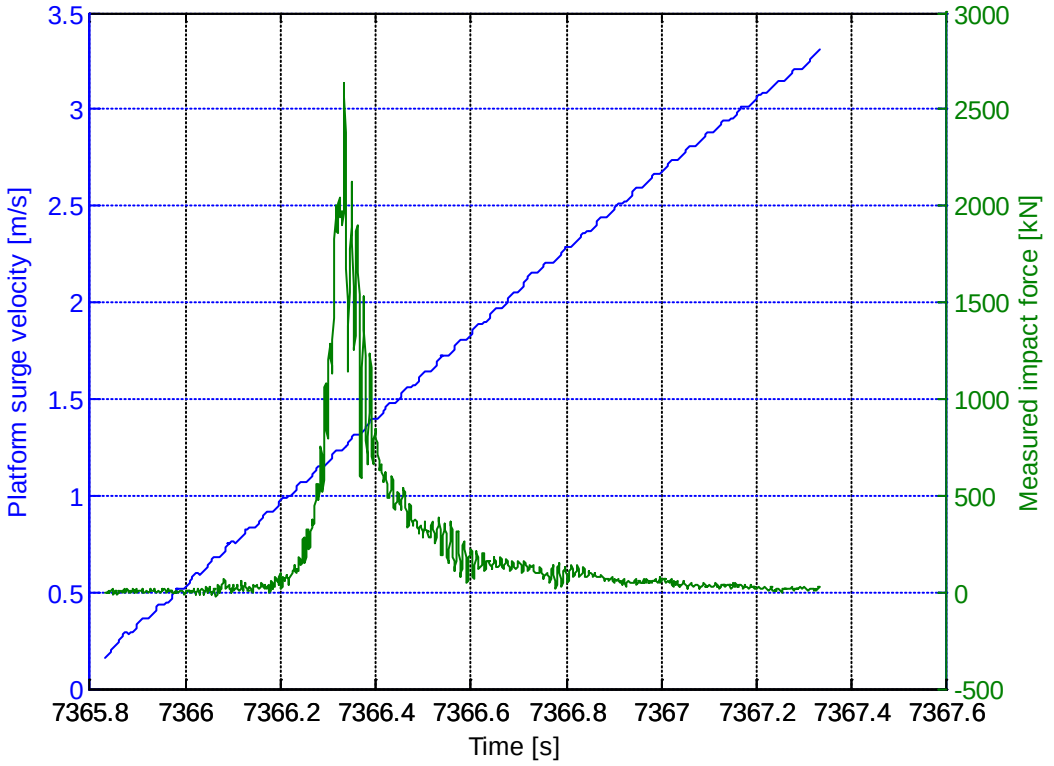

Slam 3131:

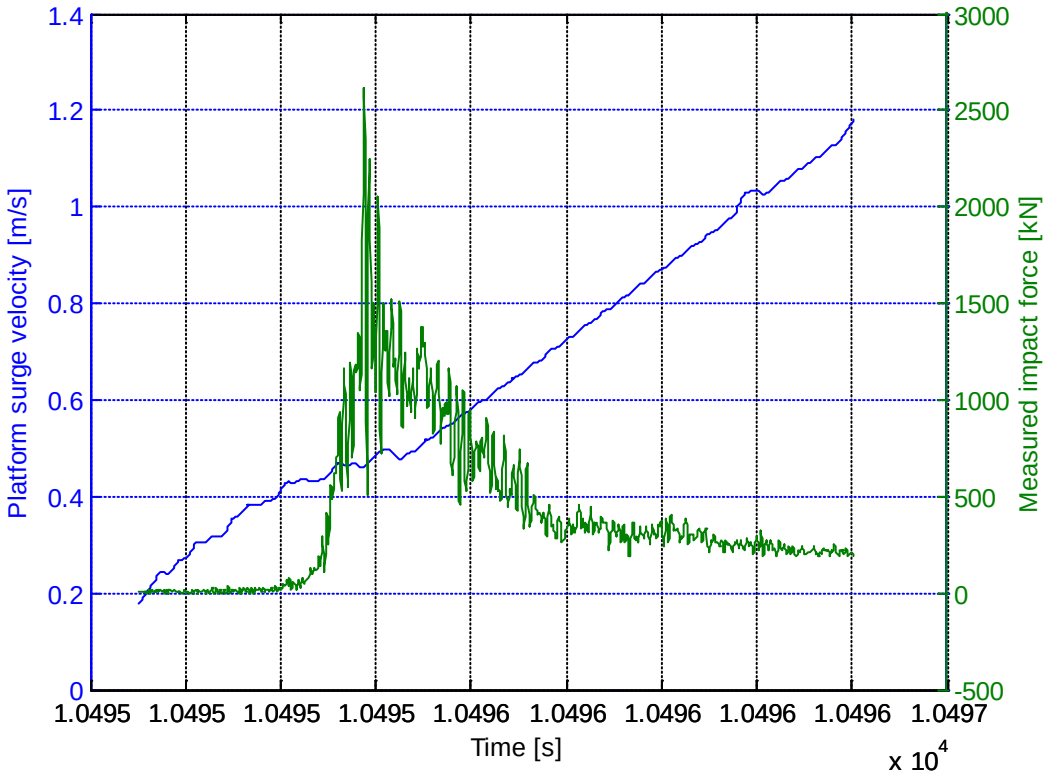

Slam 3133:

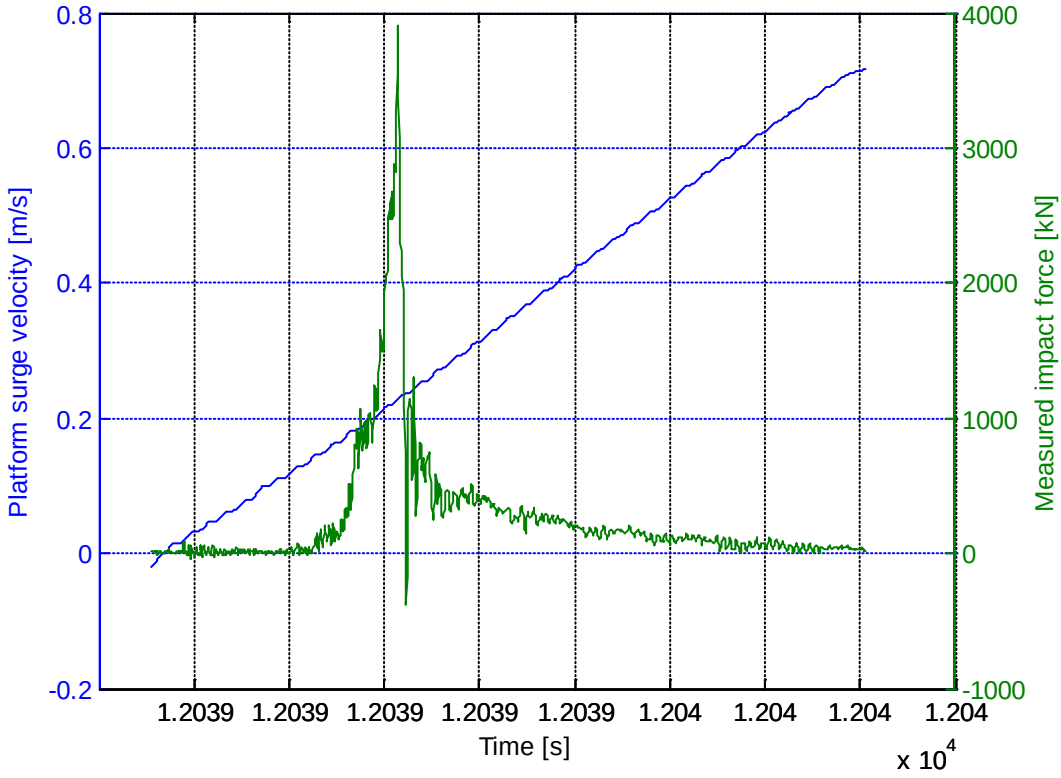

Slam 3135:

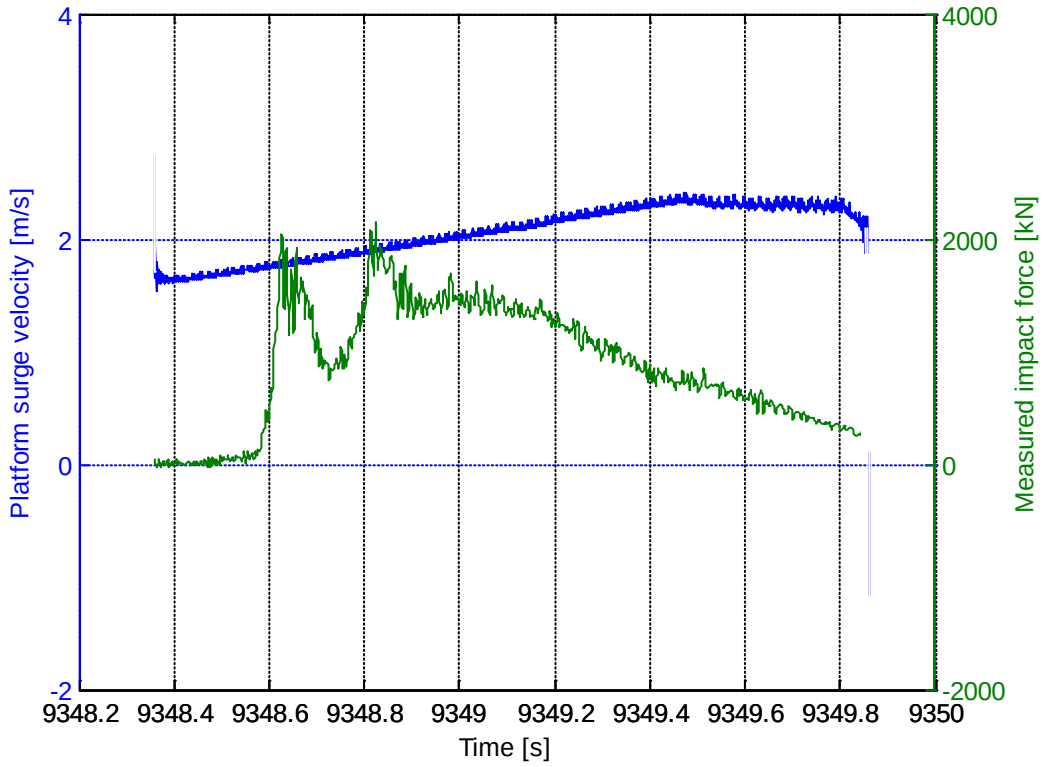

Slam 3137:

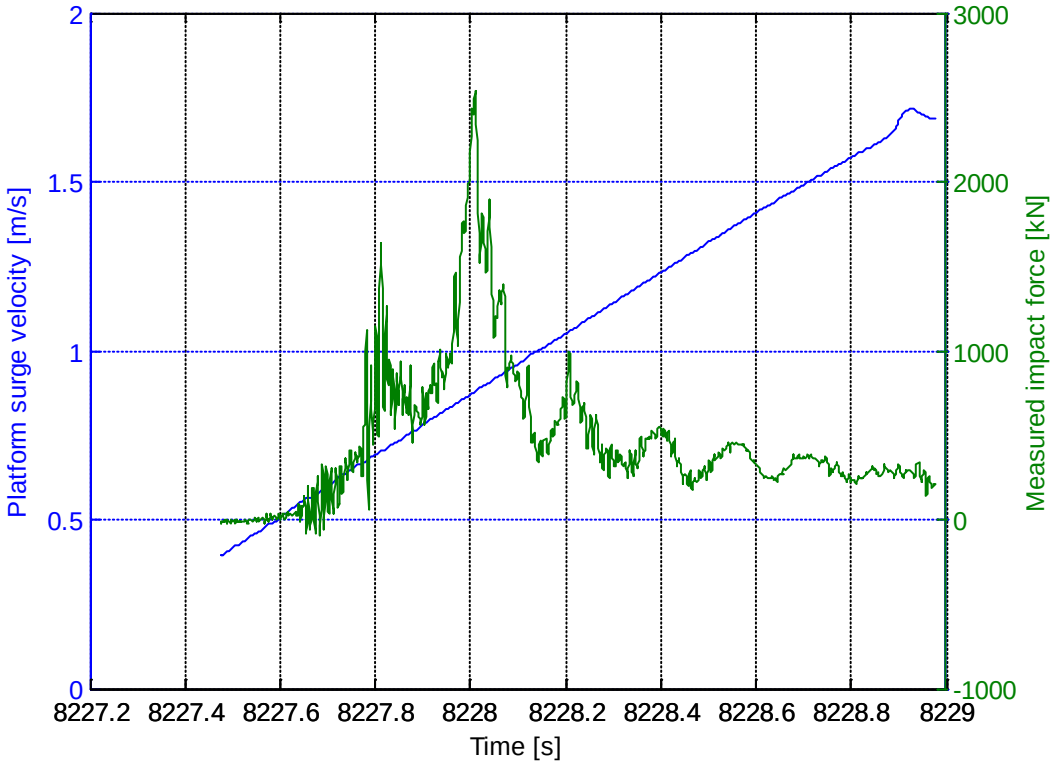

Slam 3139:

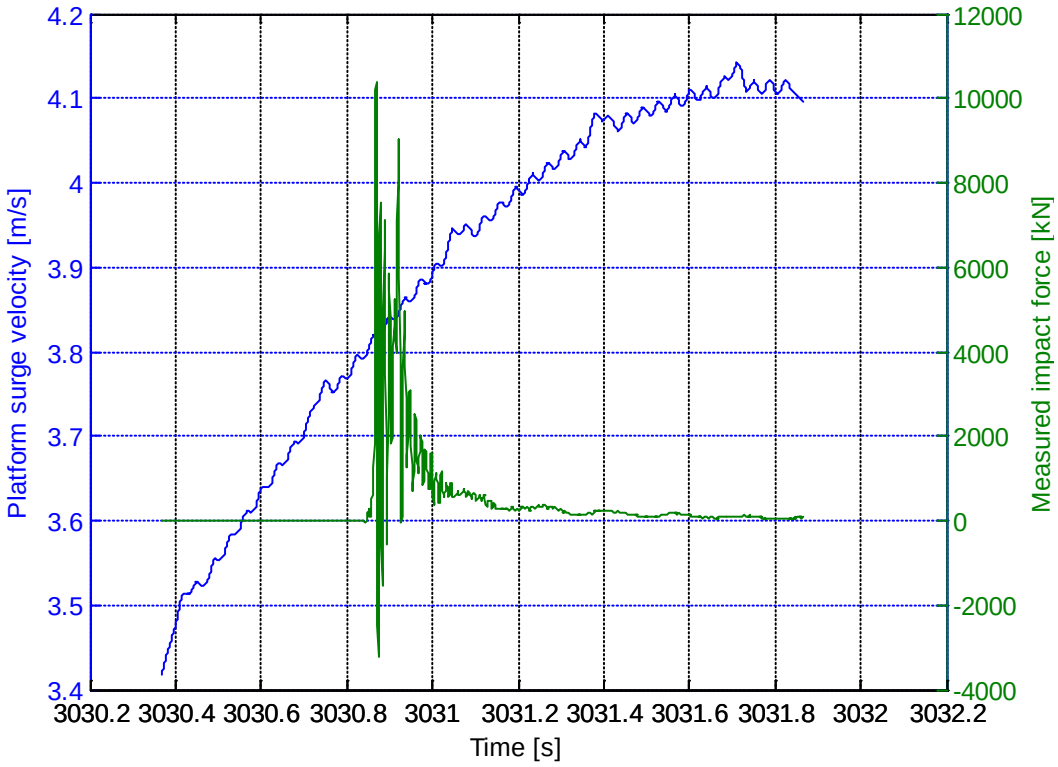

Slam 3141:

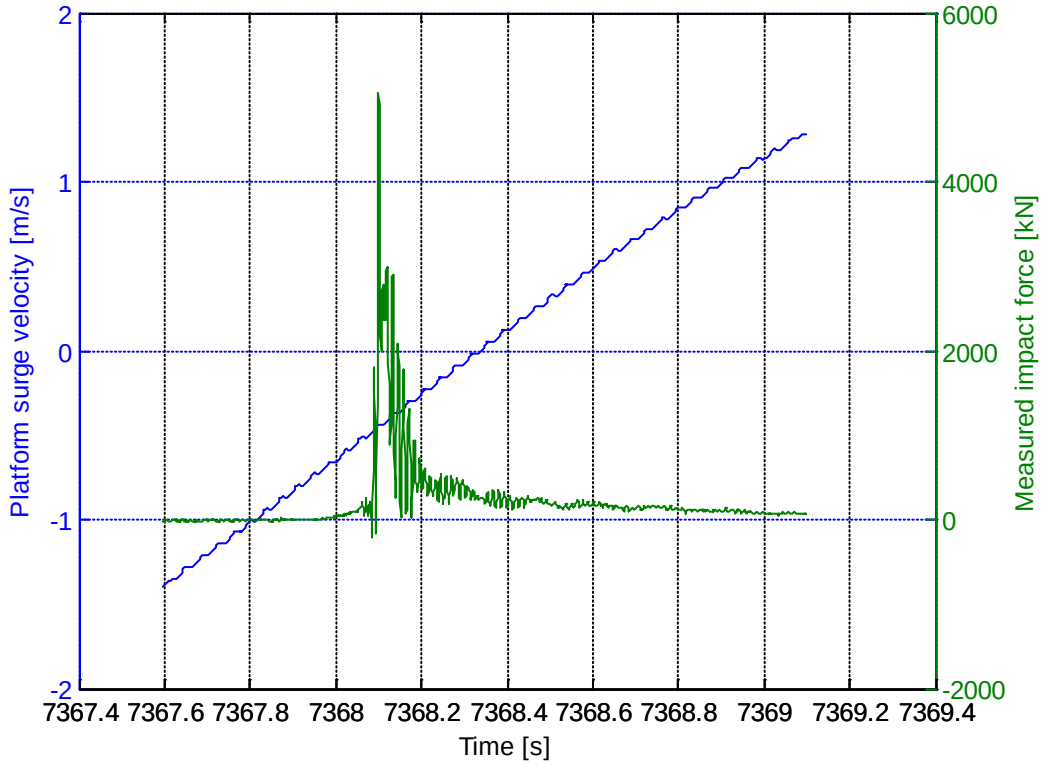

Slam 3142:

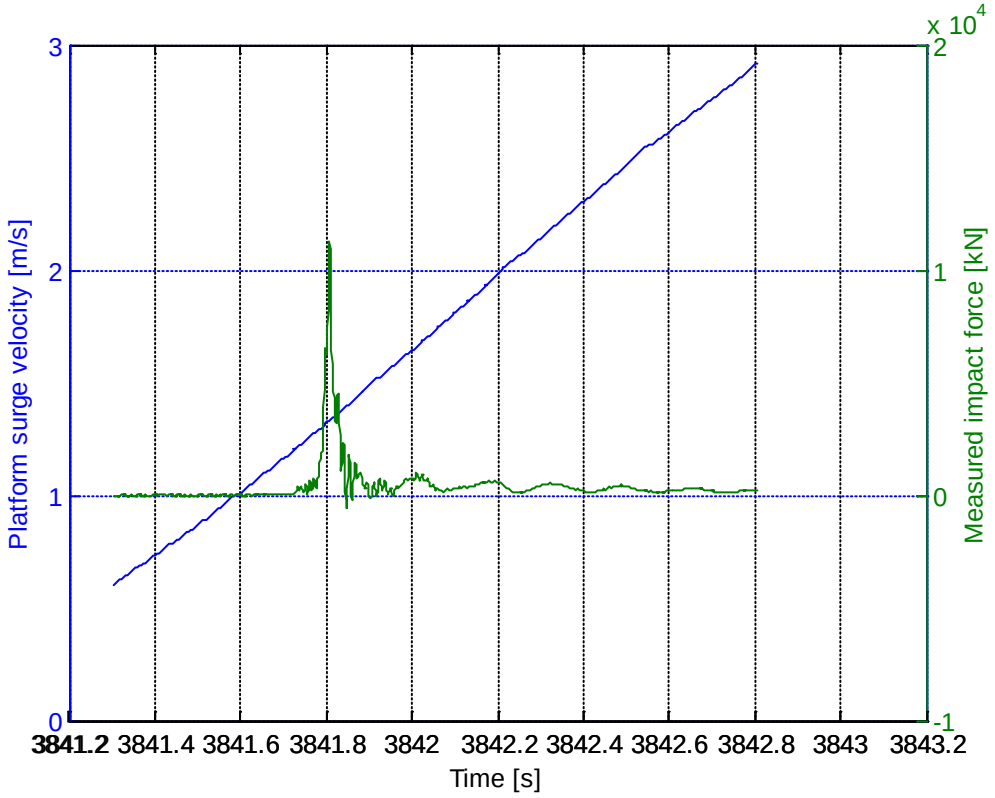

Slam 3144:

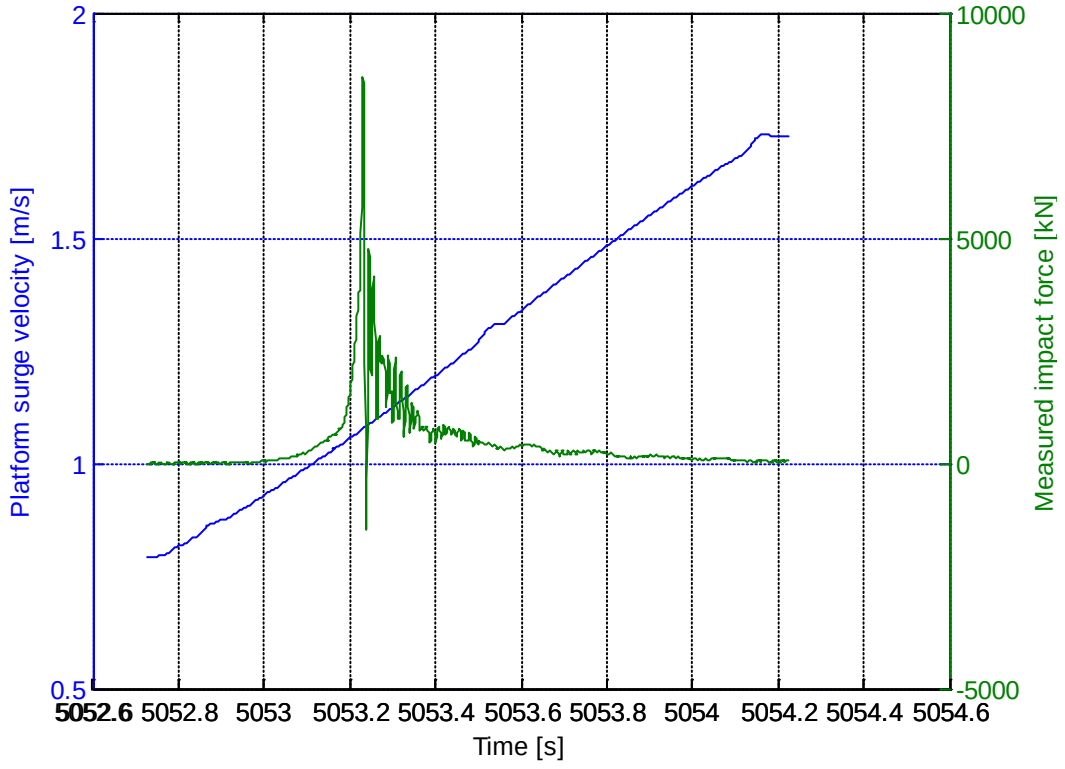

Slam 3146:

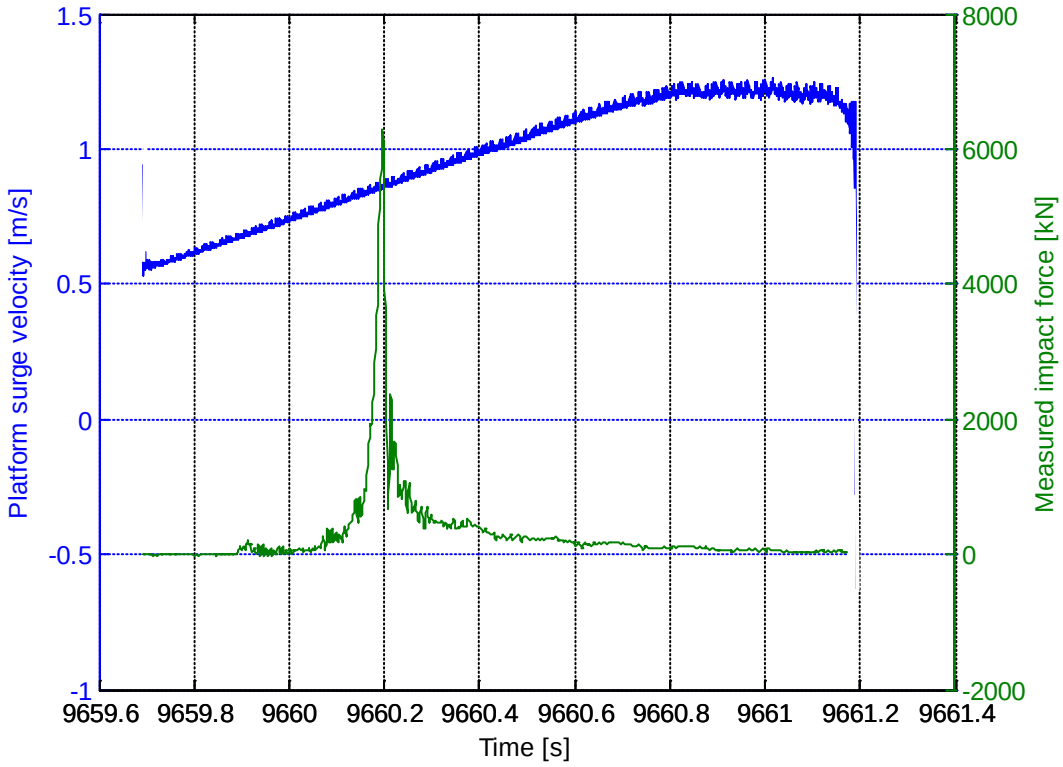

Slam 3148:

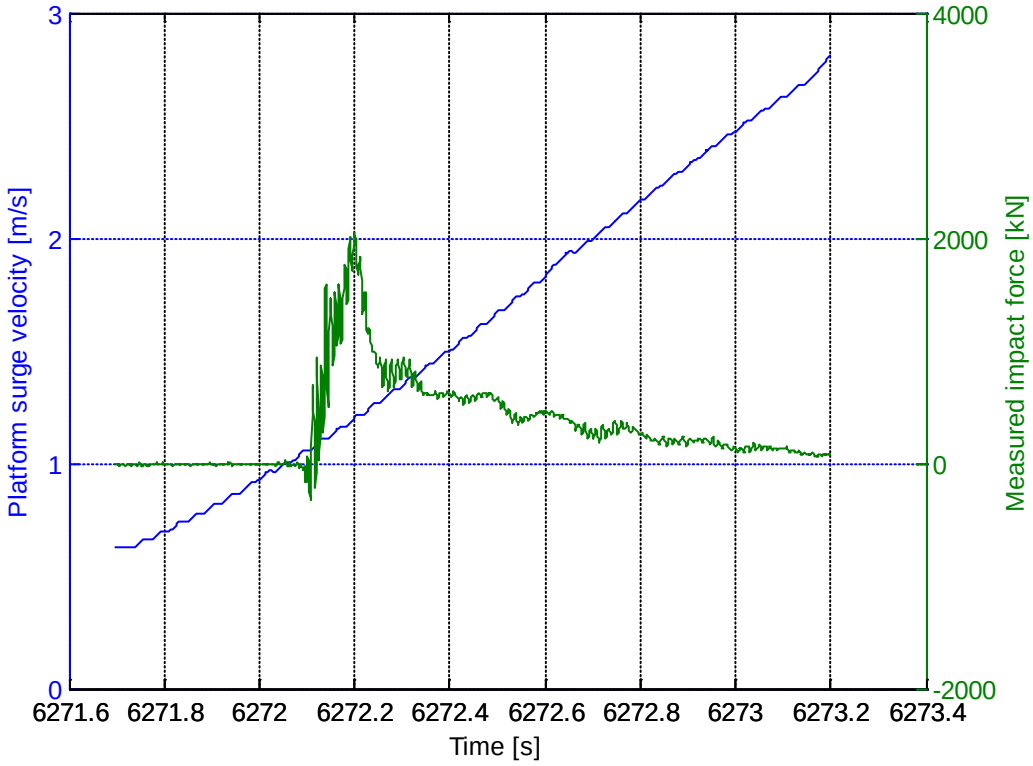

Appendix C Plots of relative wave elevation

This appendix contains plots of the relative wave elevation in front of the column at the same time as the largest slam in each realization occurs. The measurements are done by three wave probes. The distance from the column is 10m for probe 1, 6m for probe 2 and 3m for probe 3.

Slam 3100:

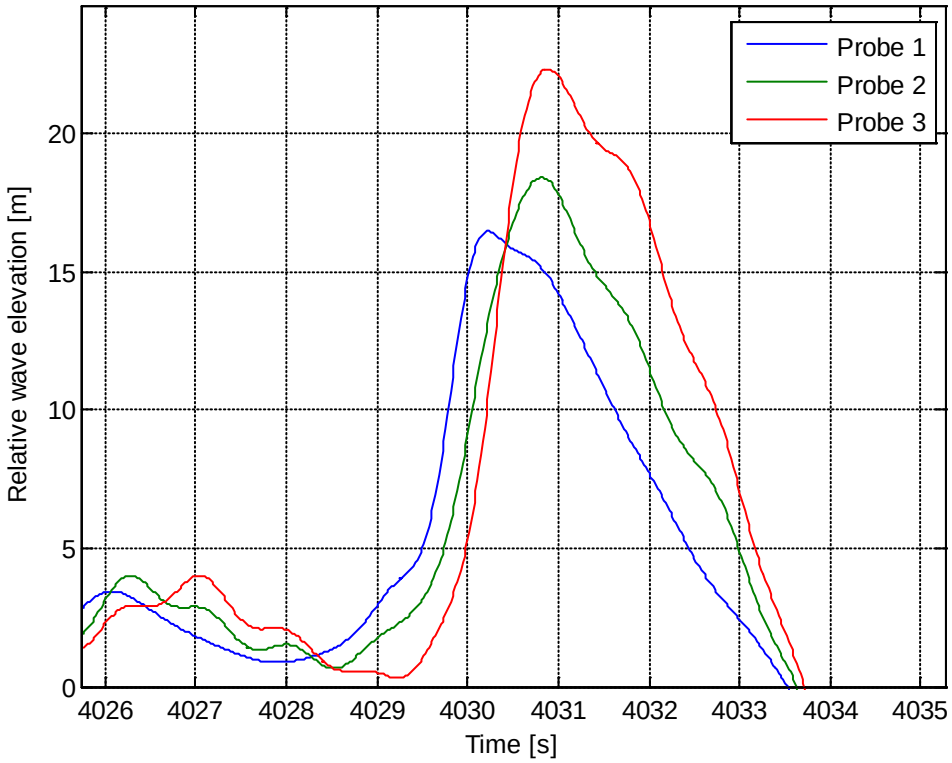

Slam 3111:

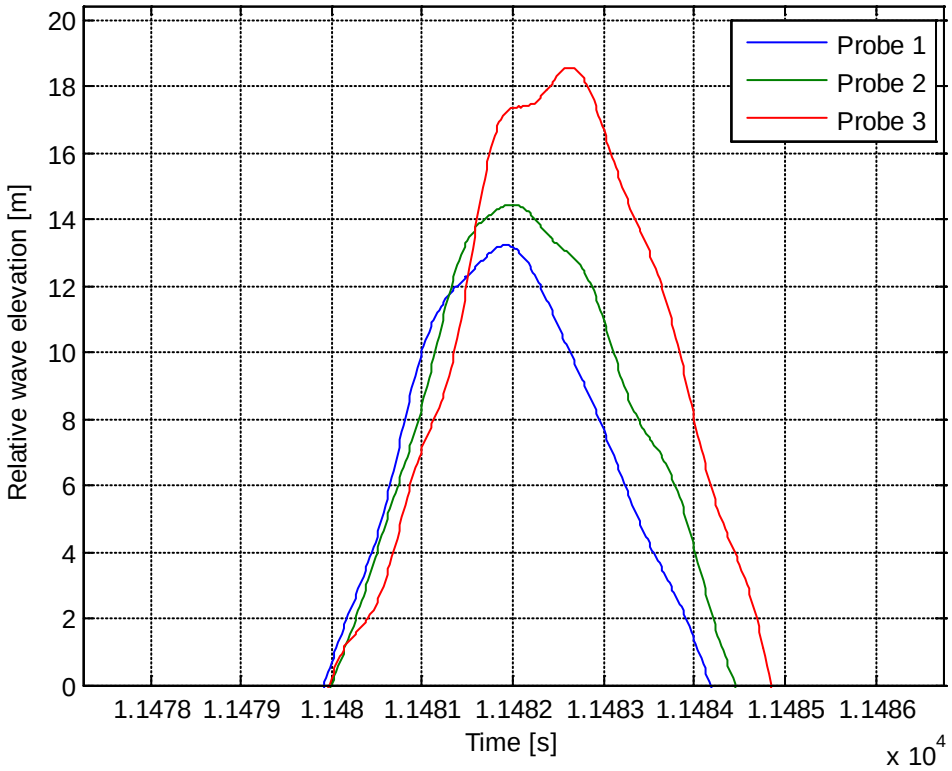

Slam 3120:

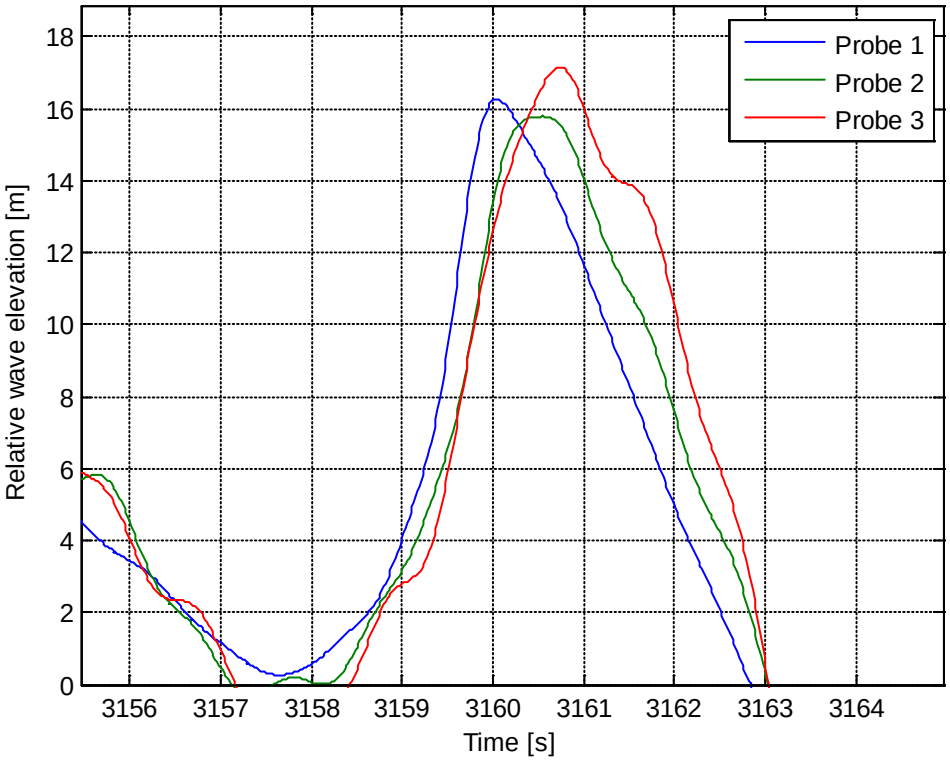

Slam 3121:

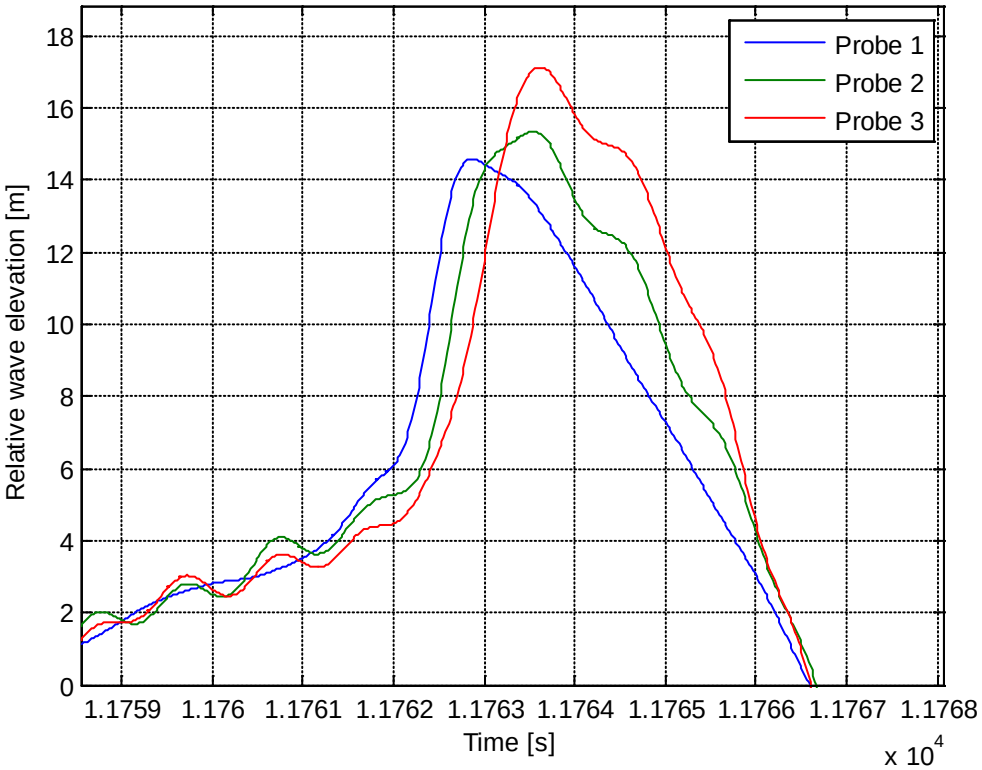

Slam 3122:

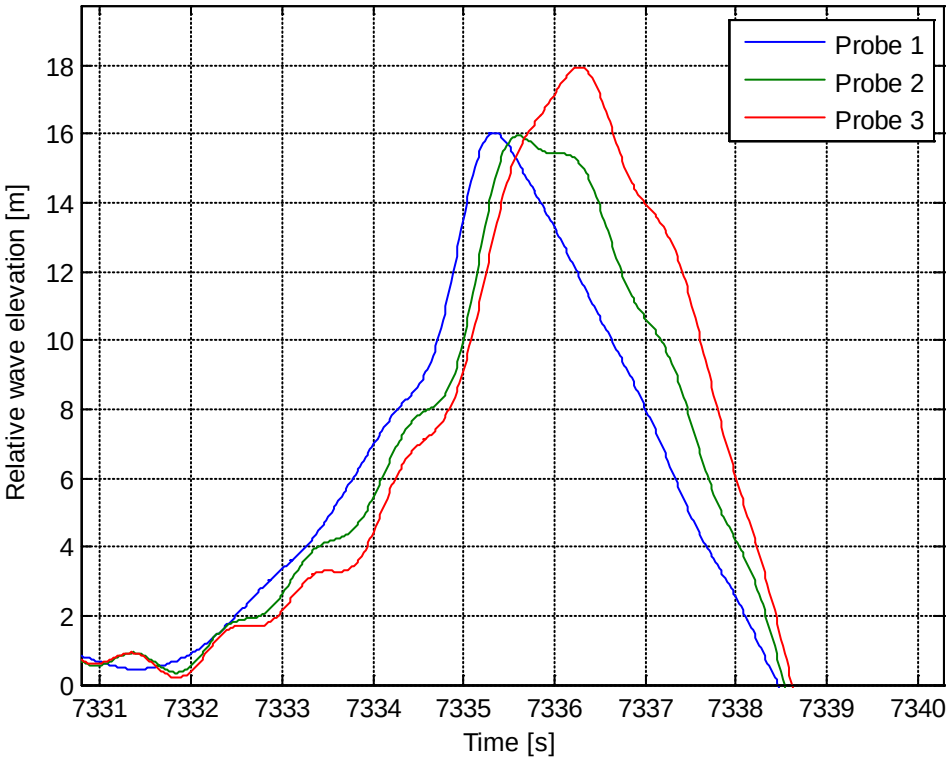

Slam 3124:

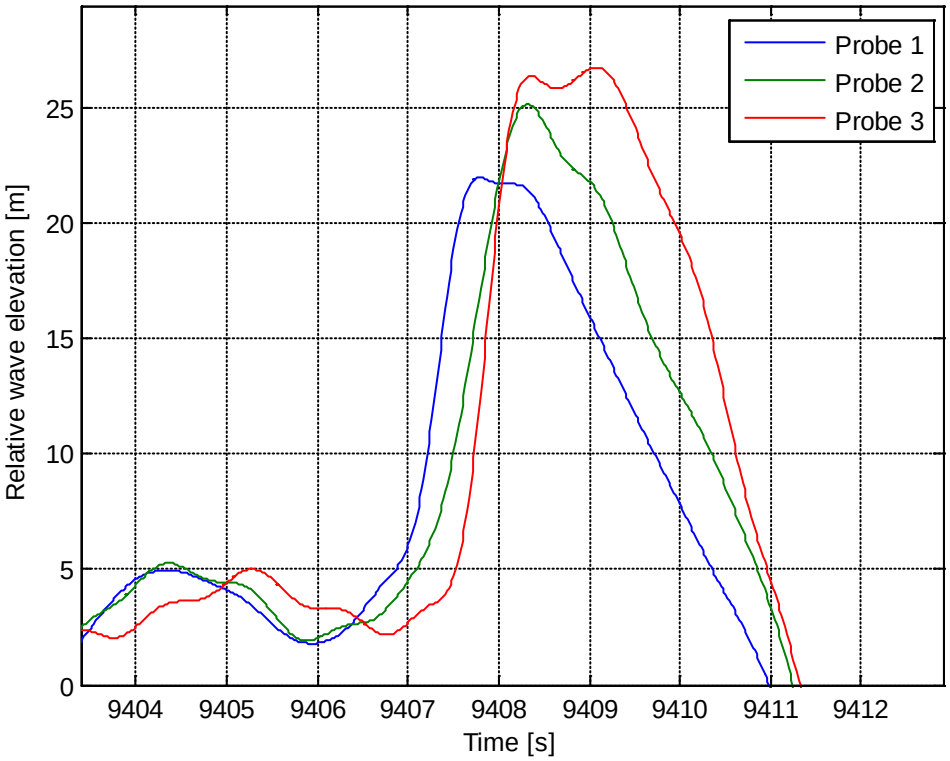

Slam 3126:

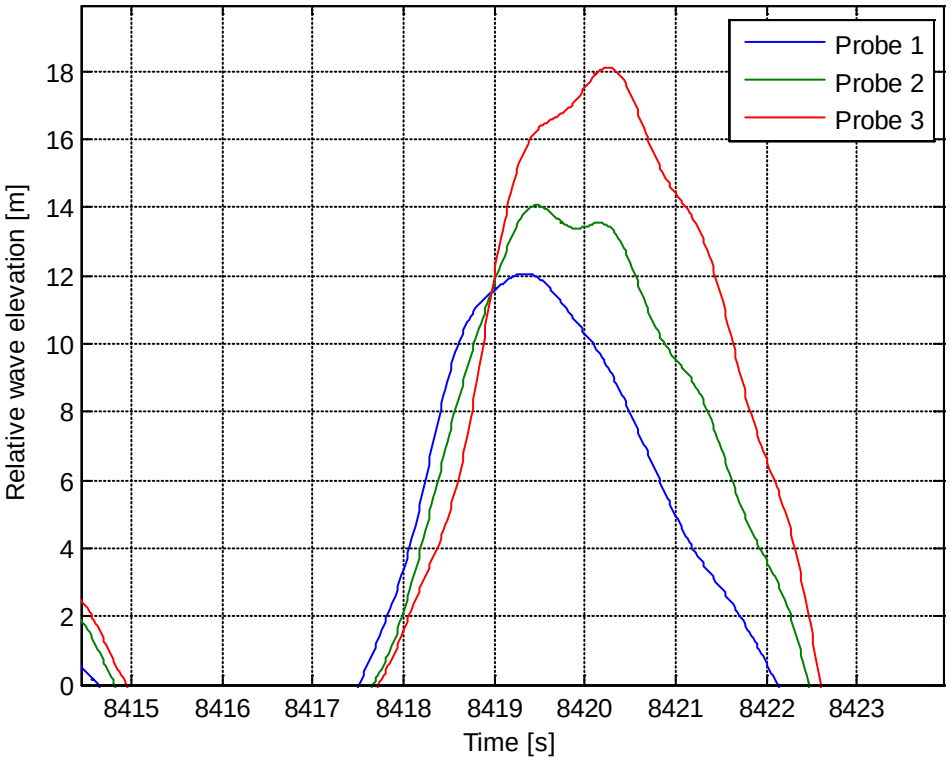

Slam 3129:

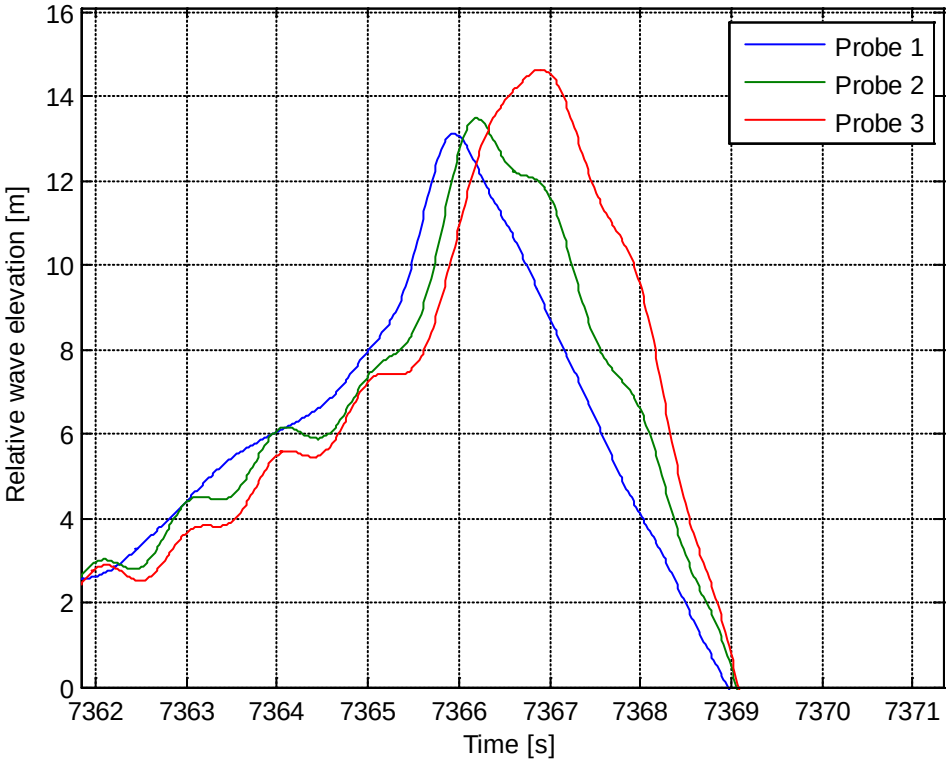

Slam 3131:

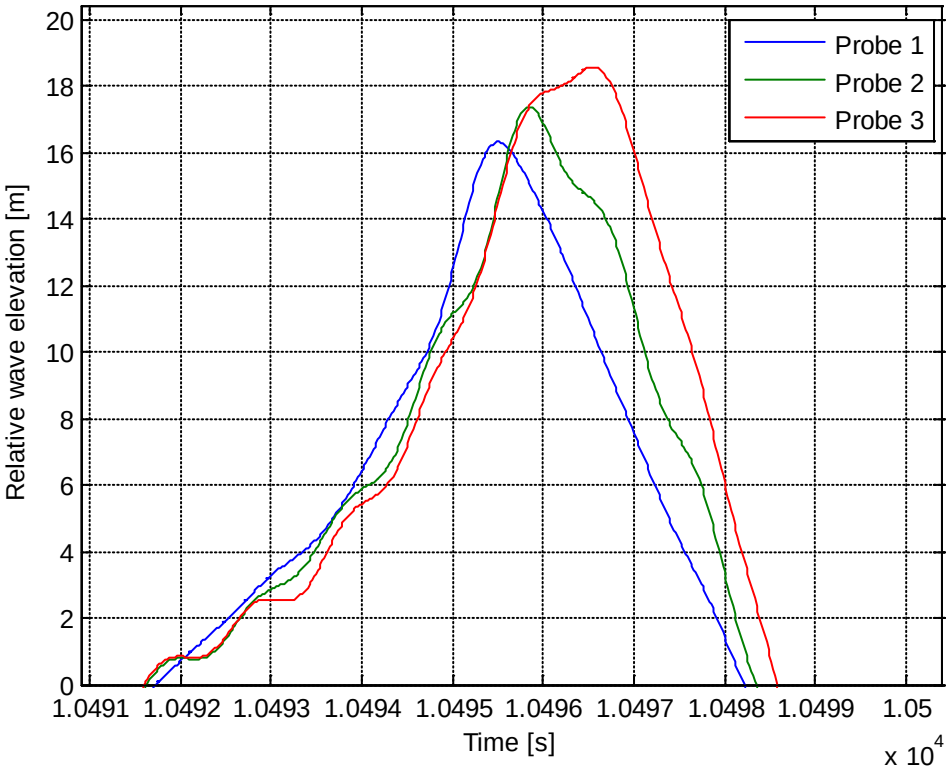

Slam 3133:

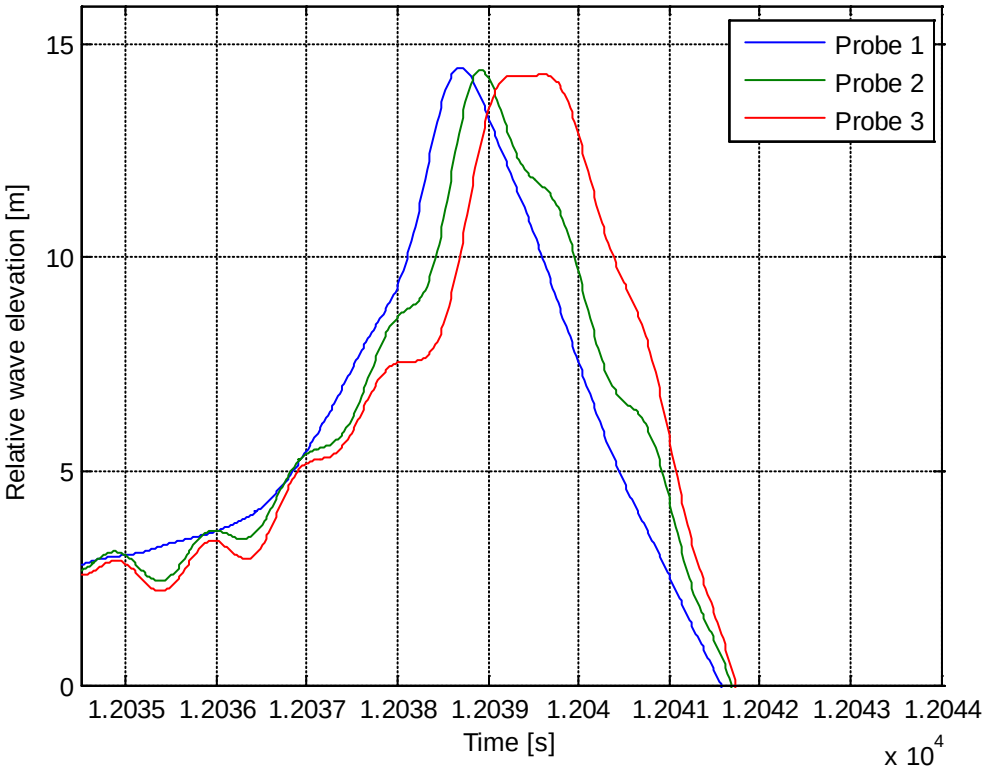

Slam 3135:

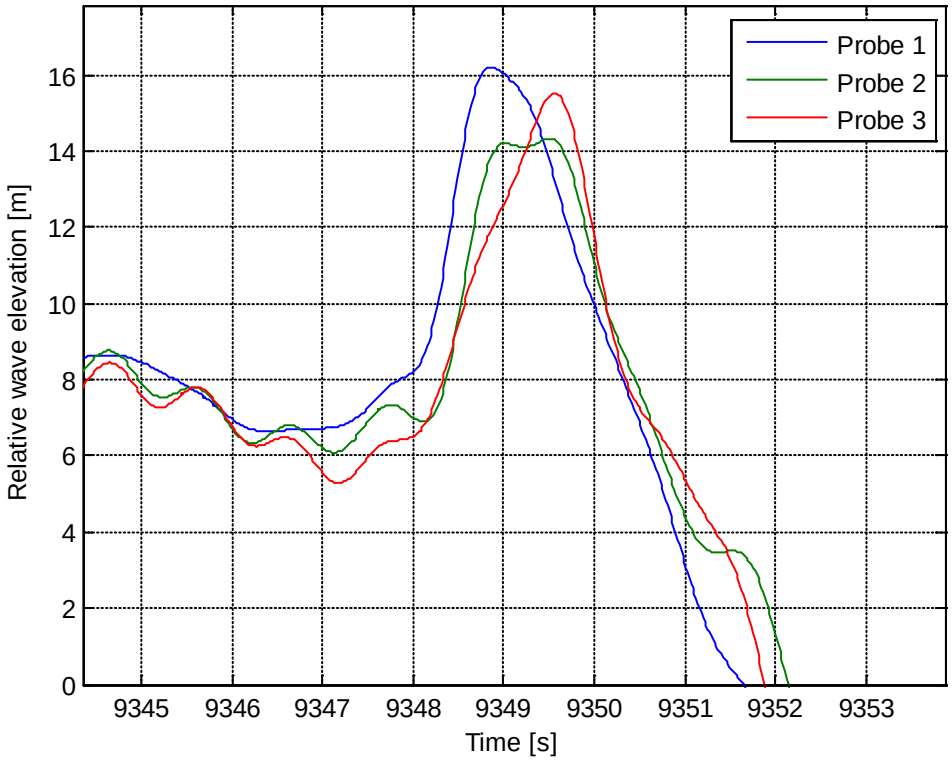

Slam 3137:

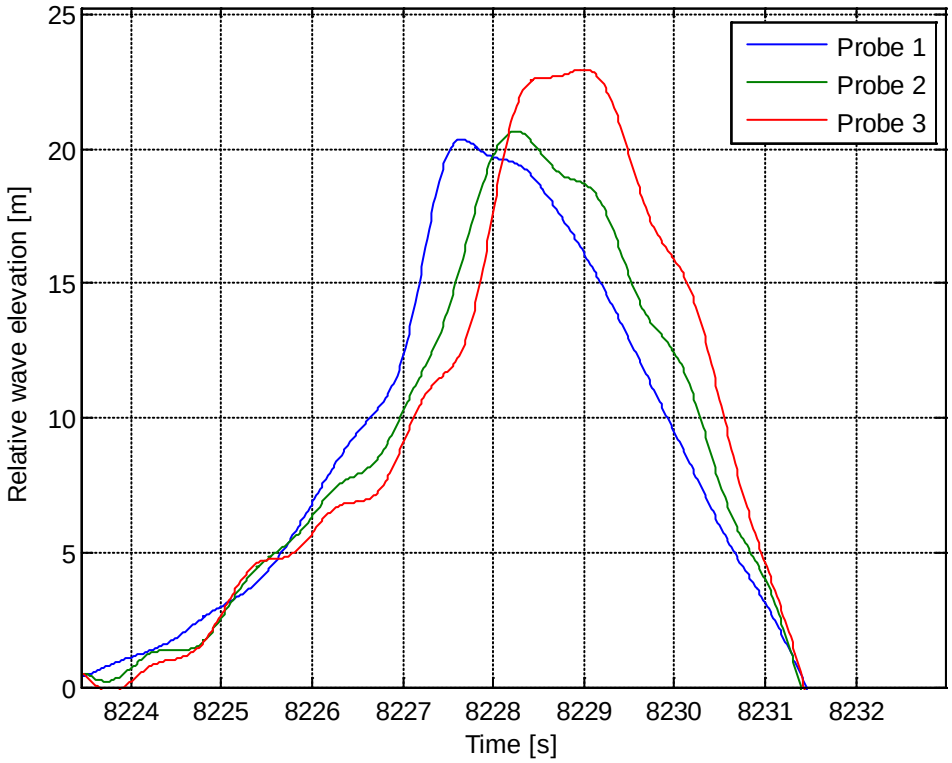

Slam 3139:

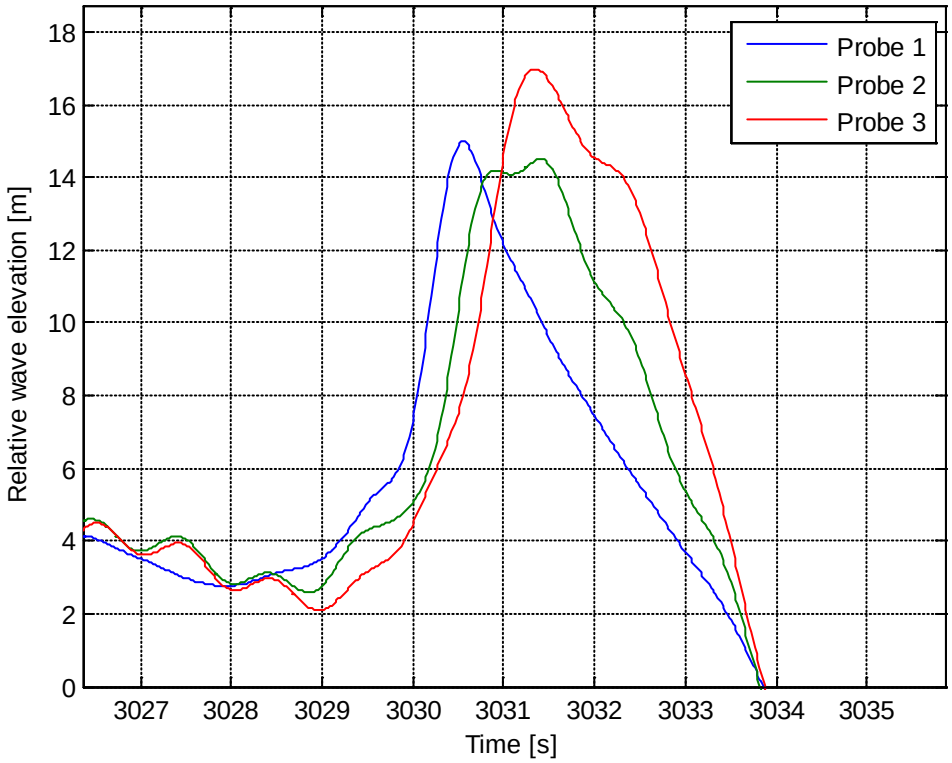

Slam 3141:

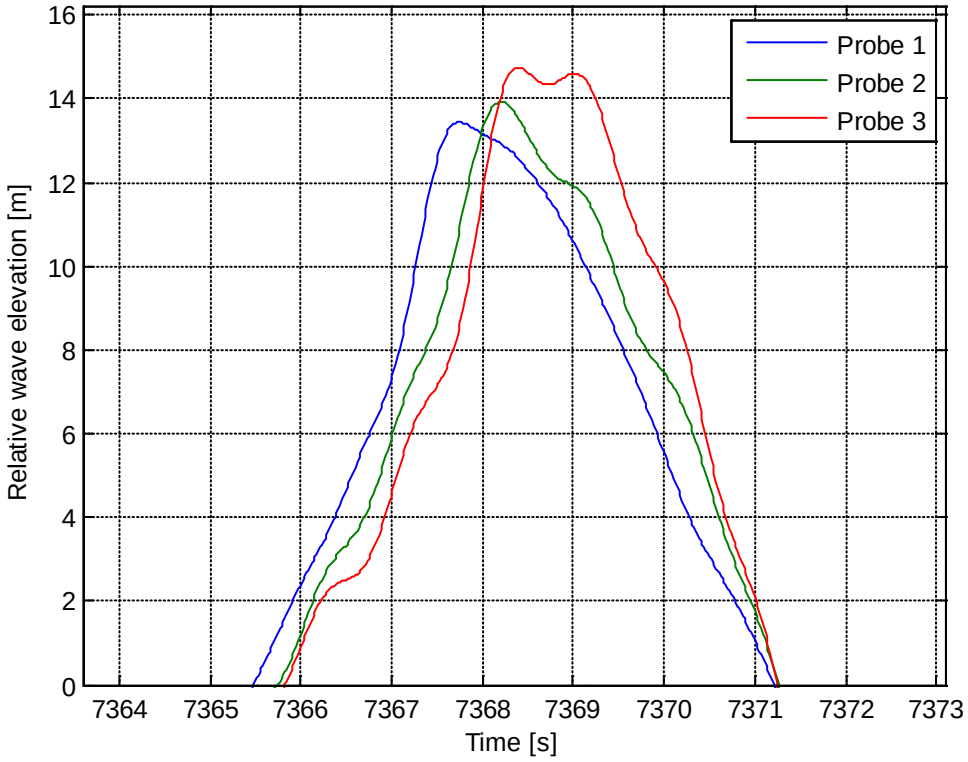

Slam 3142:

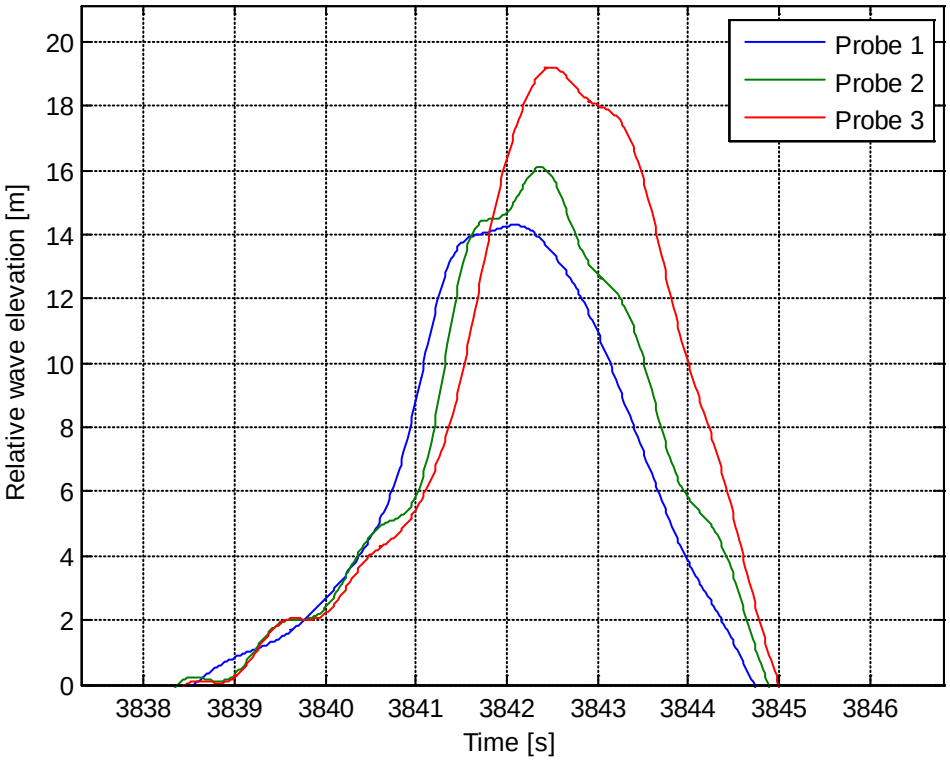

Slam 3144:

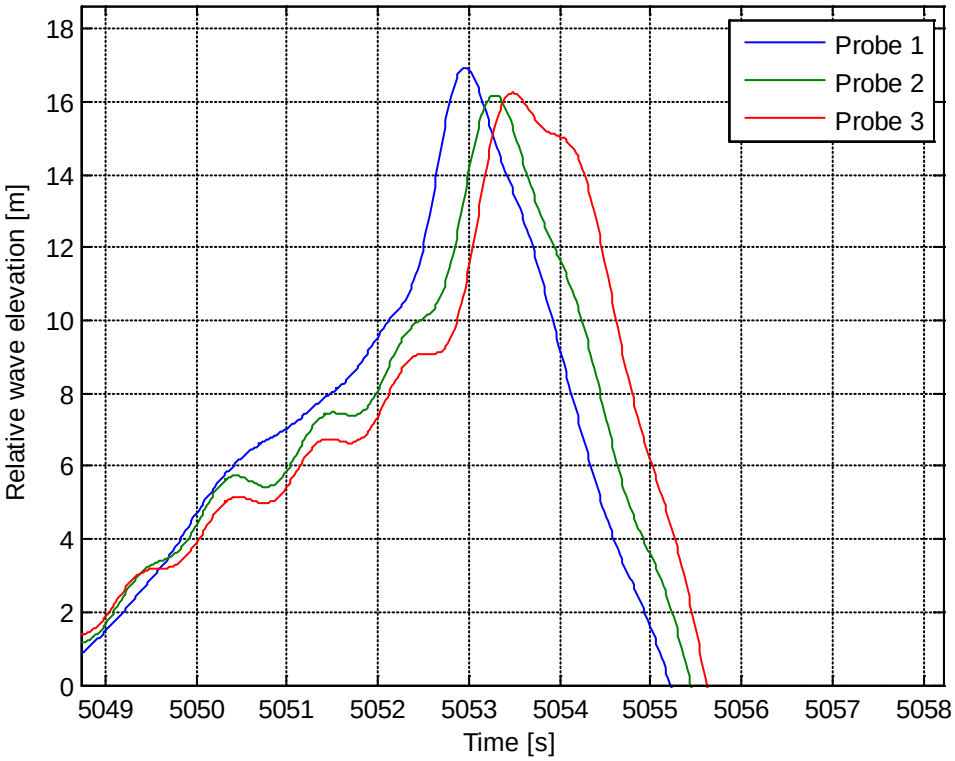

Slam 3146:

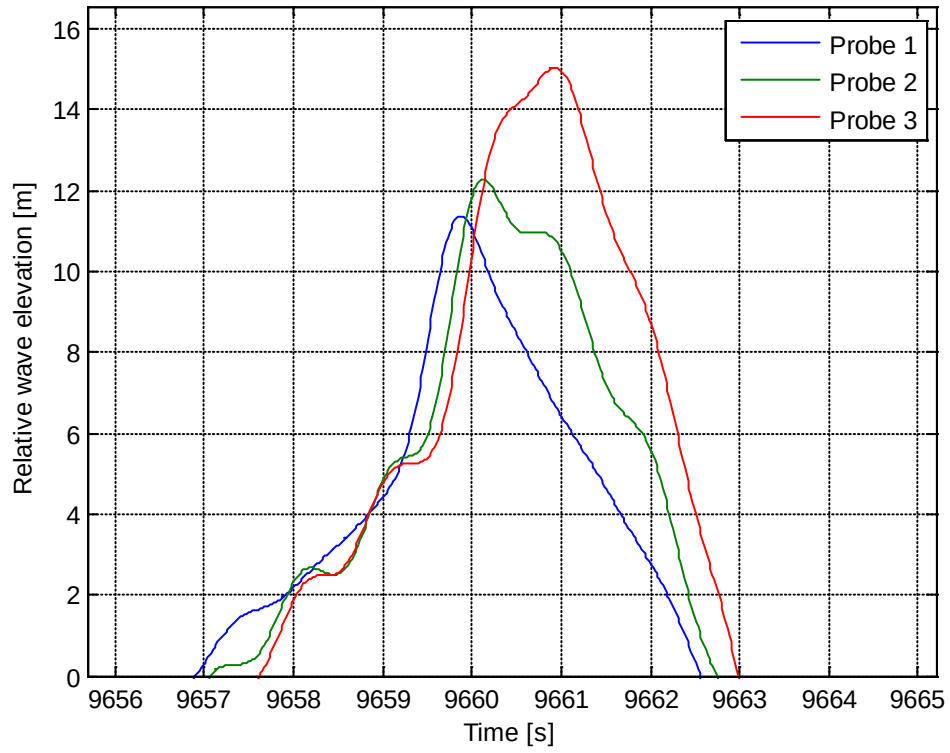

Slam 3148:

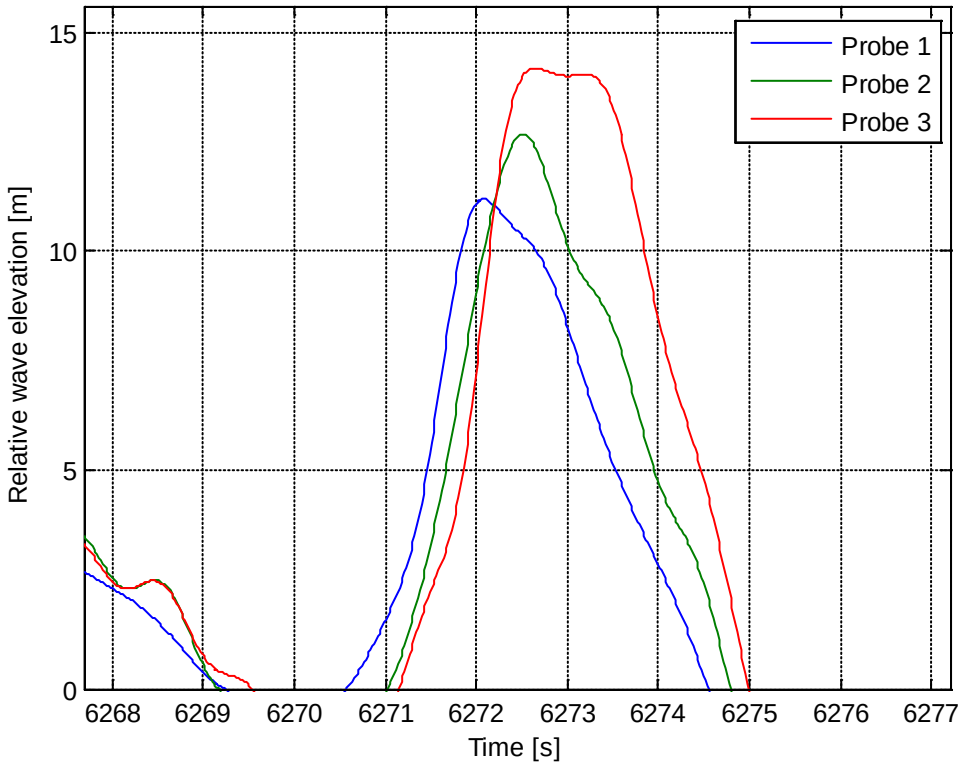

Appendix D Load models used in the structural analysis

This appendix contains plots of the load histories for each load model used in the structural analyses.

Load model 1, slam 3100:

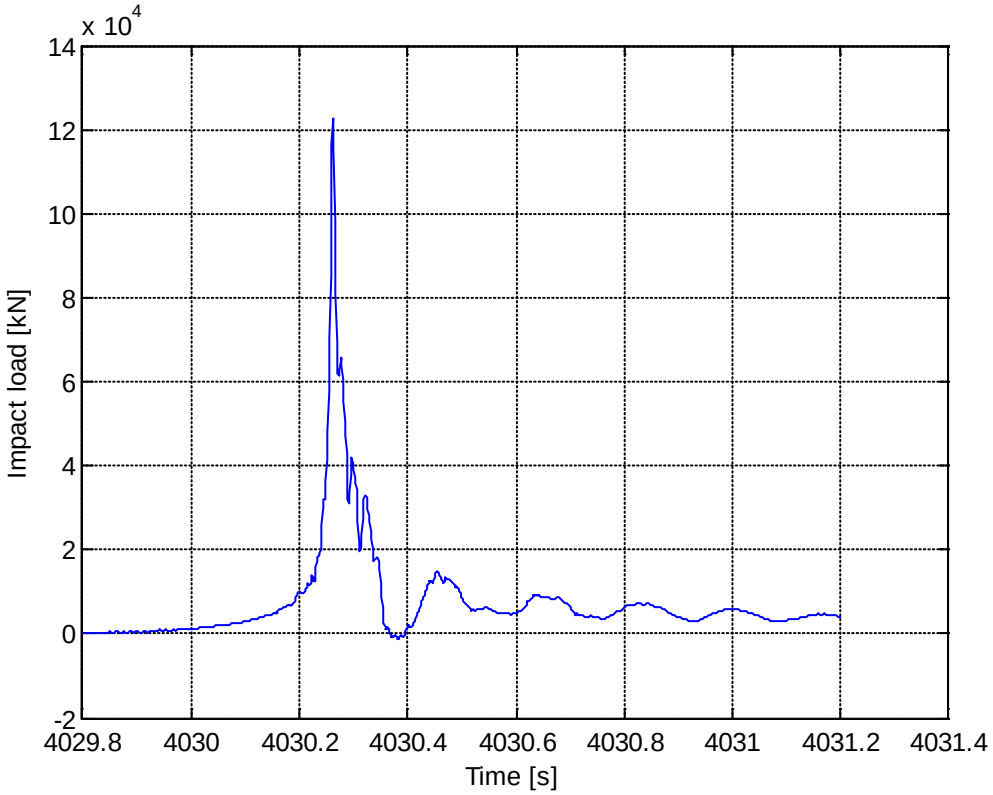

Load model 2, slam 3100:

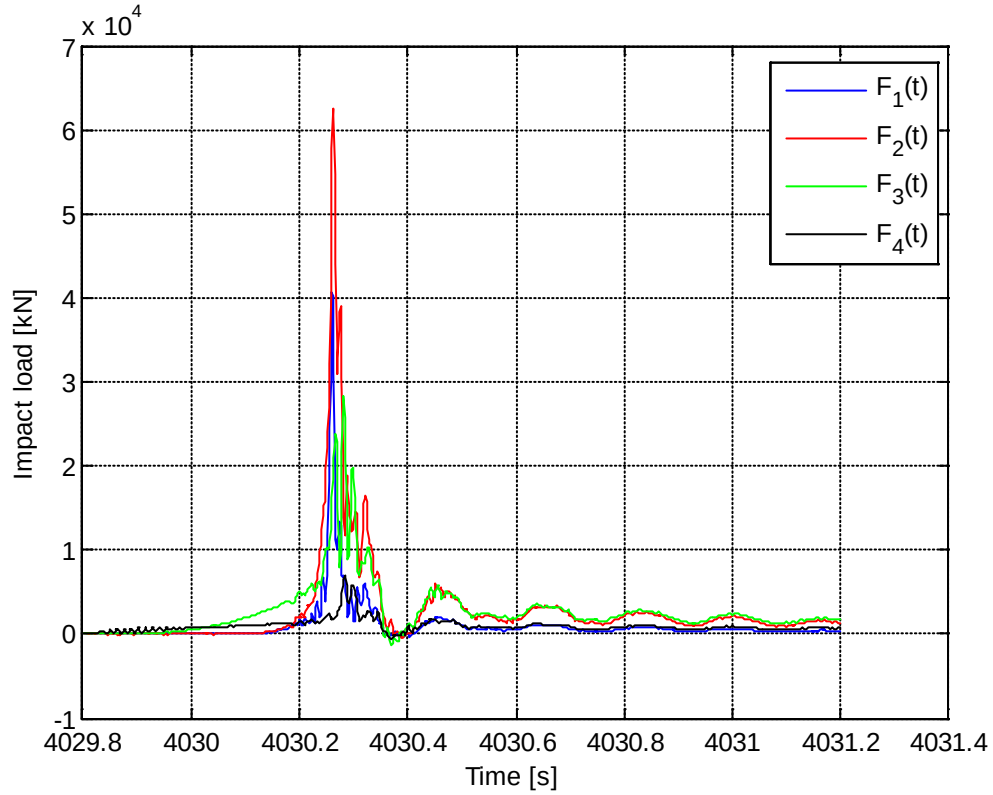

Load model 3, slam 3100:

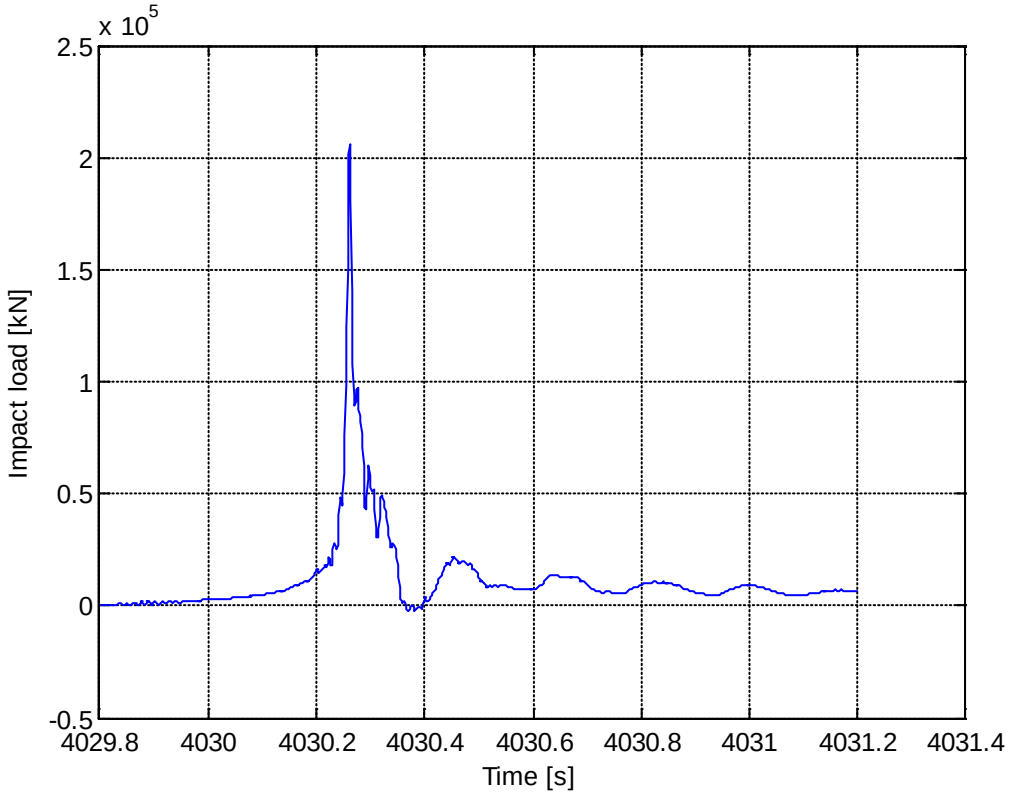

Load model 4, slam 3100:

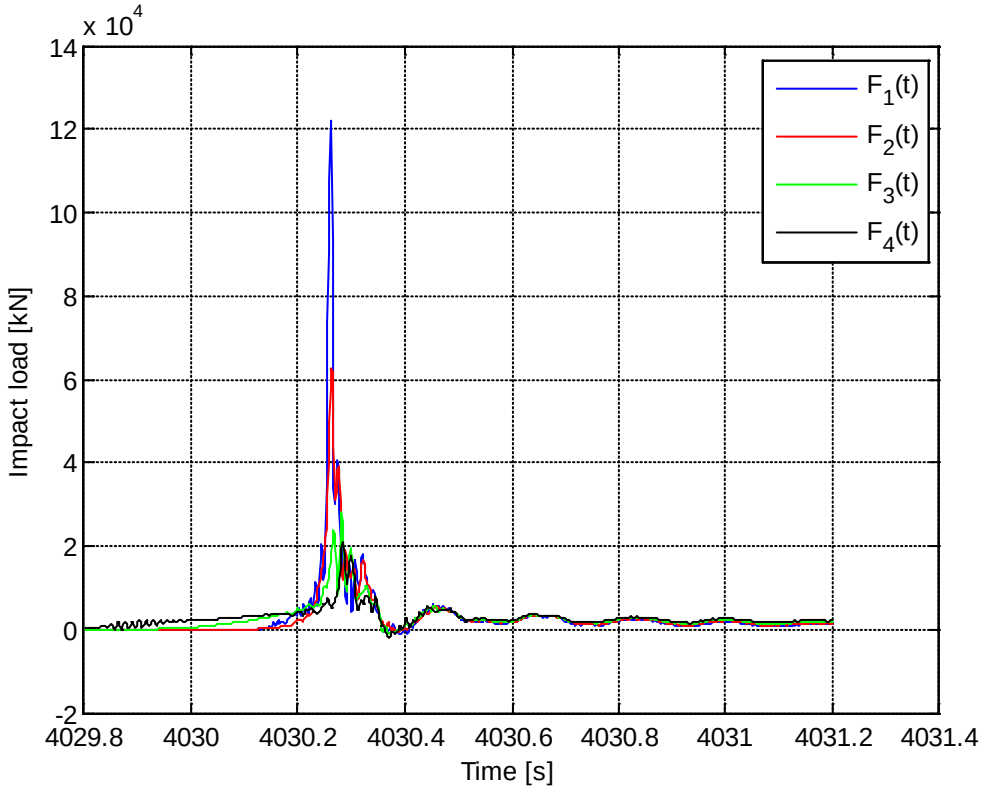

Load model 1, slam 3124:

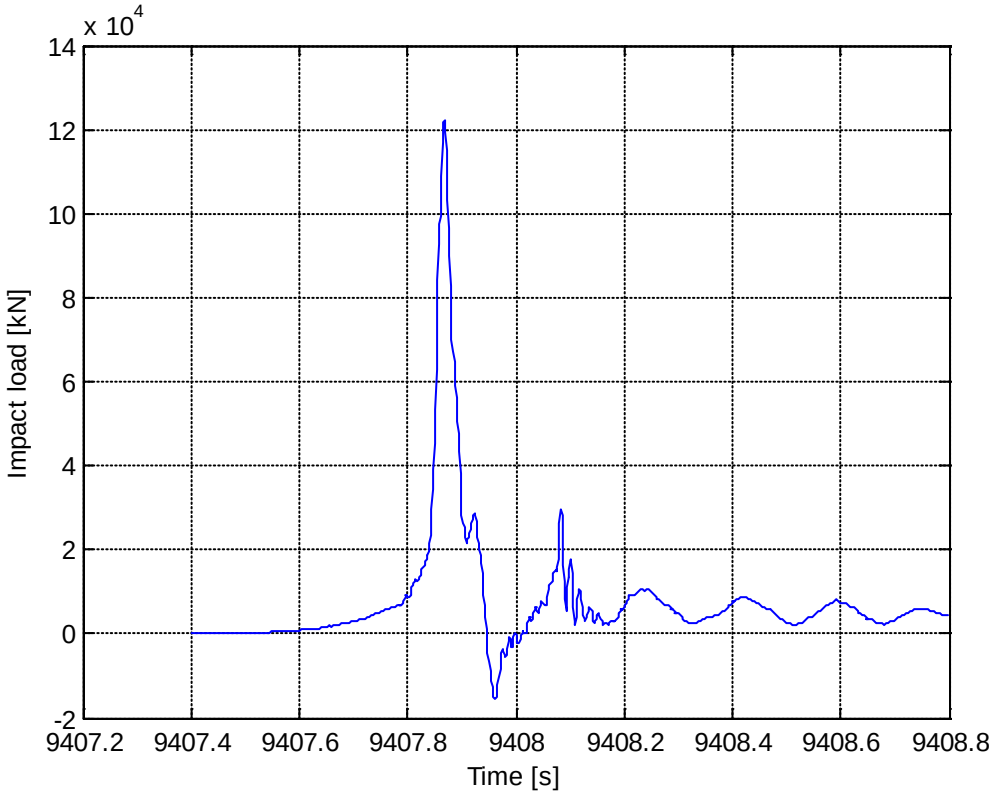

Load model 2, slam 3124:

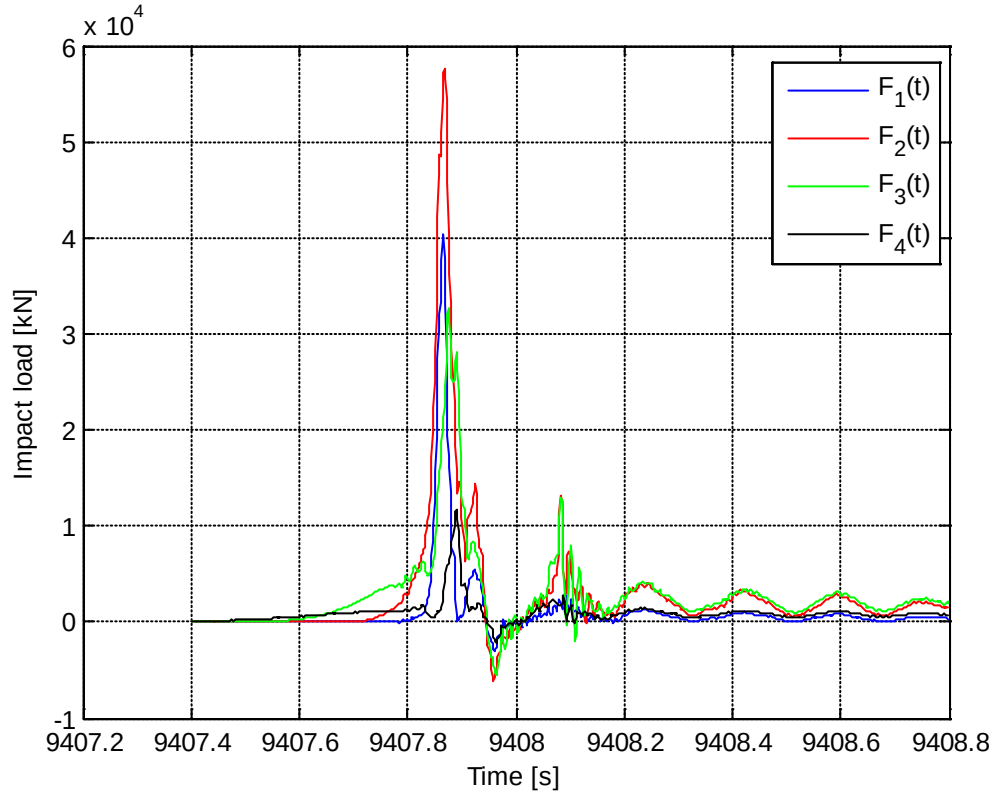

Load model 3, slam 3124:

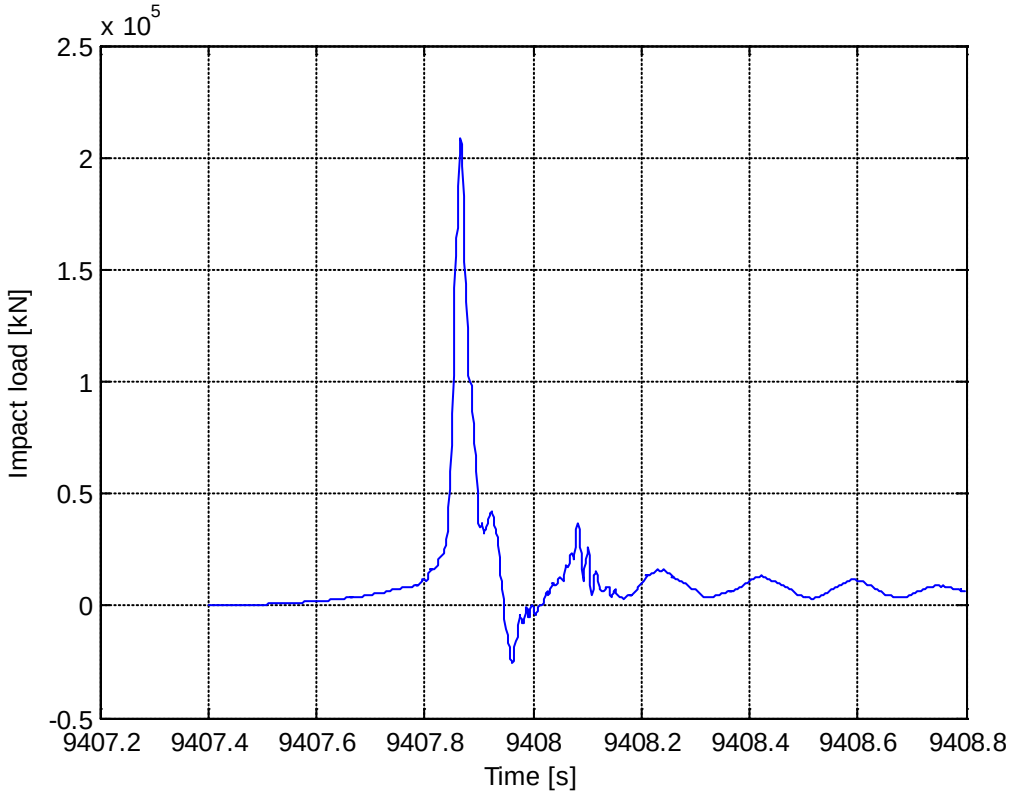

Load model 4, slam 3124:

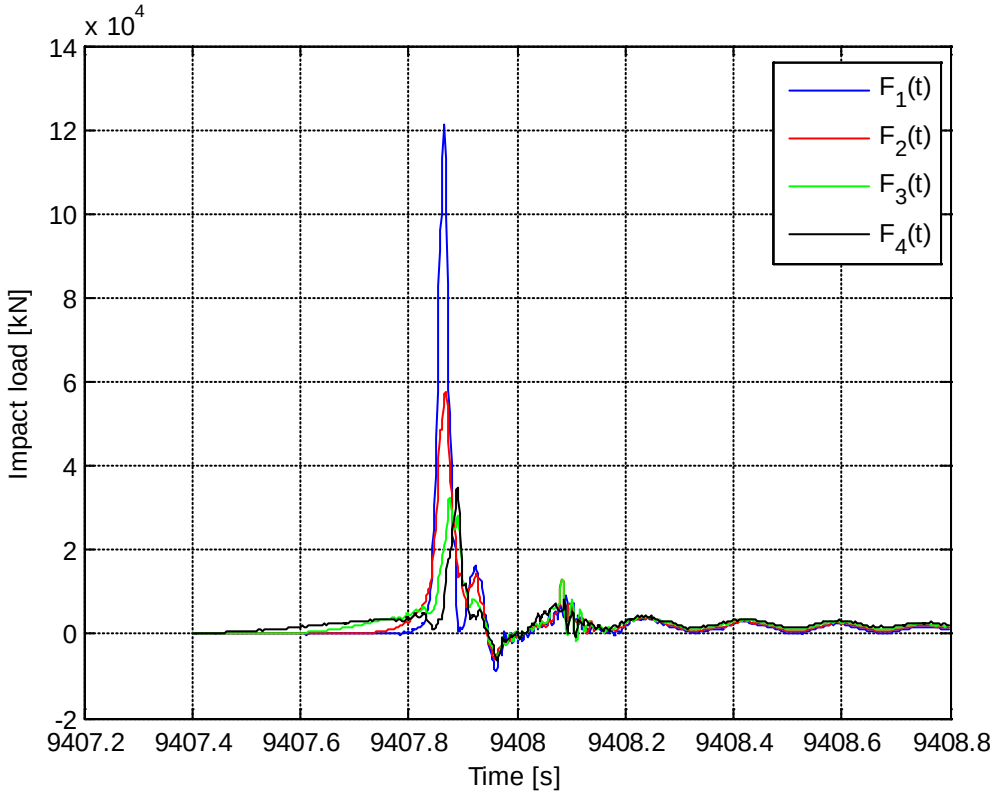

Appendix E Results from structural analyses

This appendix contains plots of the bending moments, at the top of the column, obtained from the dynamic structural analyses.

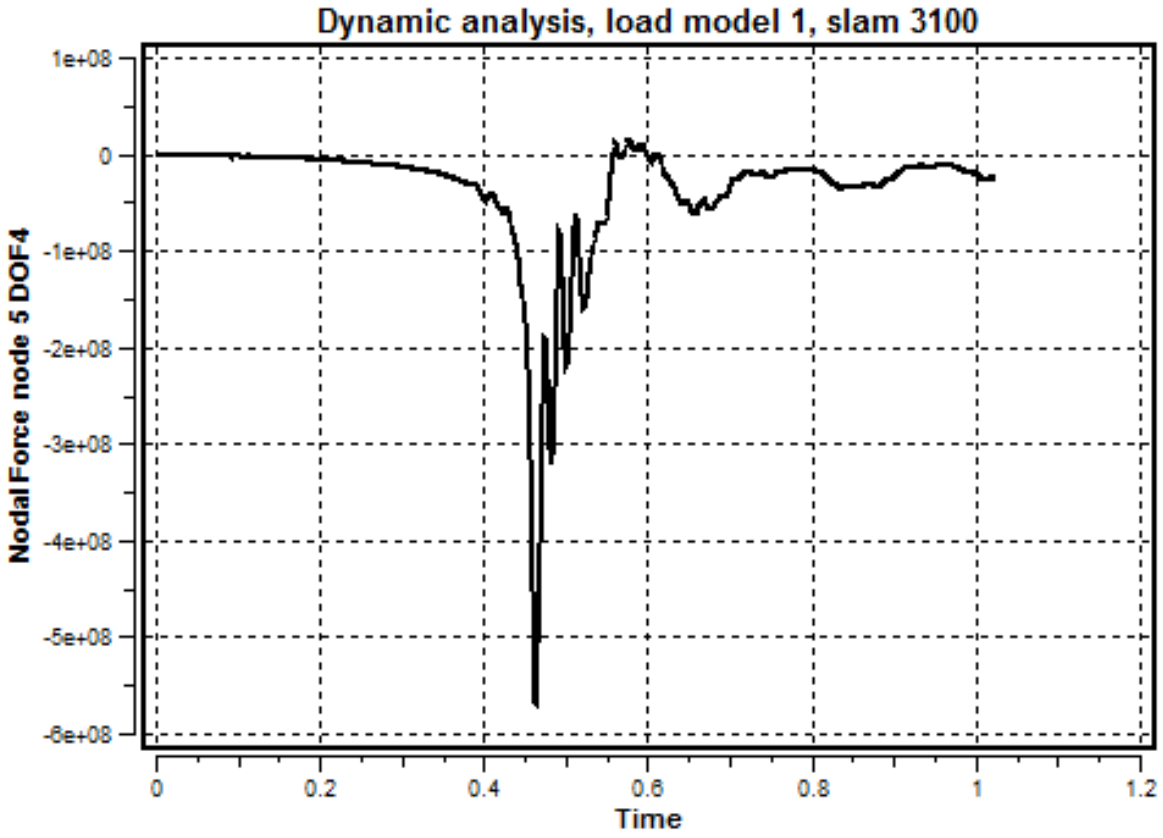
Dynamic analysis, load model 1, slam 3100
Nodal Force node 5 DOF4
1e+08
0
-1e+08
-2e+08
-3e+08
-4e+08
-5e+08
-6e+08
0
0.2
0.4
0.6
0.8
1
1.2
Time

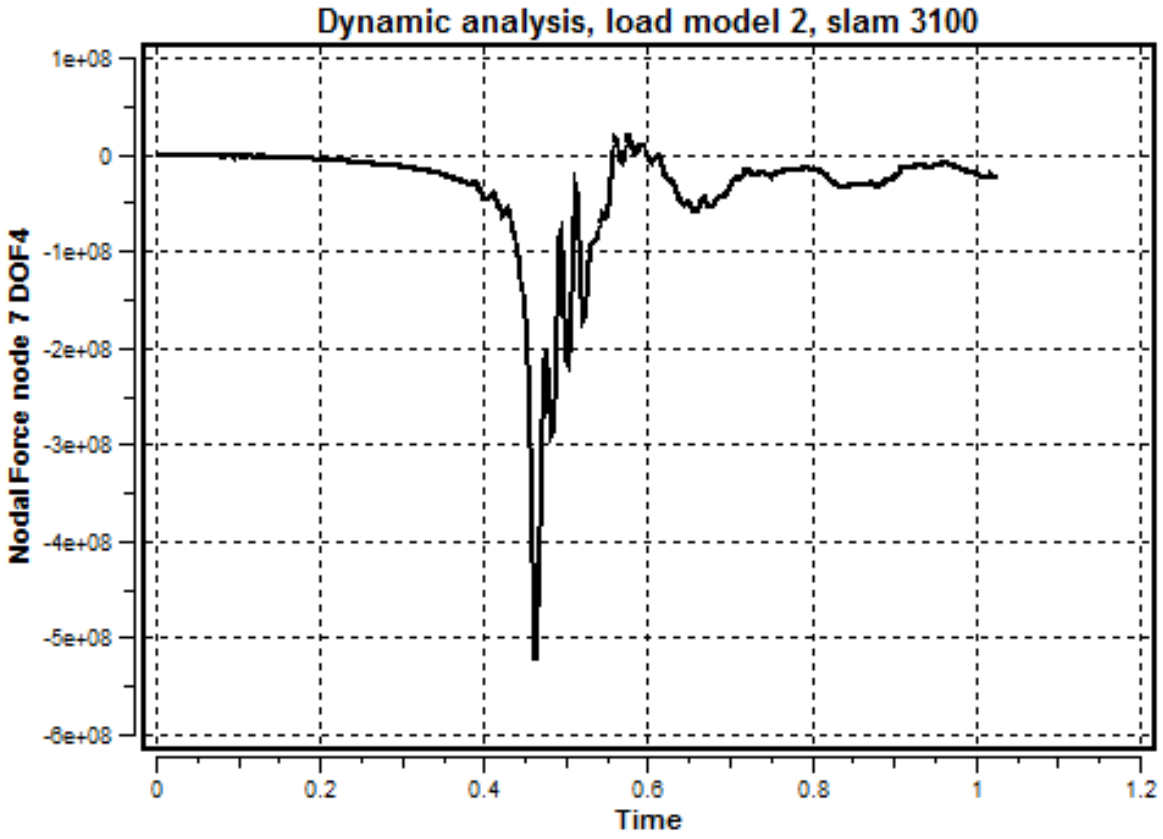
Dynamic analysis, load model 2, slam 3100
Nodal Force node 7 DOF4
1e+08
0
-1e+08
-2e+08
-3e+08
-4e+08
-5e+08
-6e+08
0
0.2
0.4
0.6
0.8
1
1.2
Time

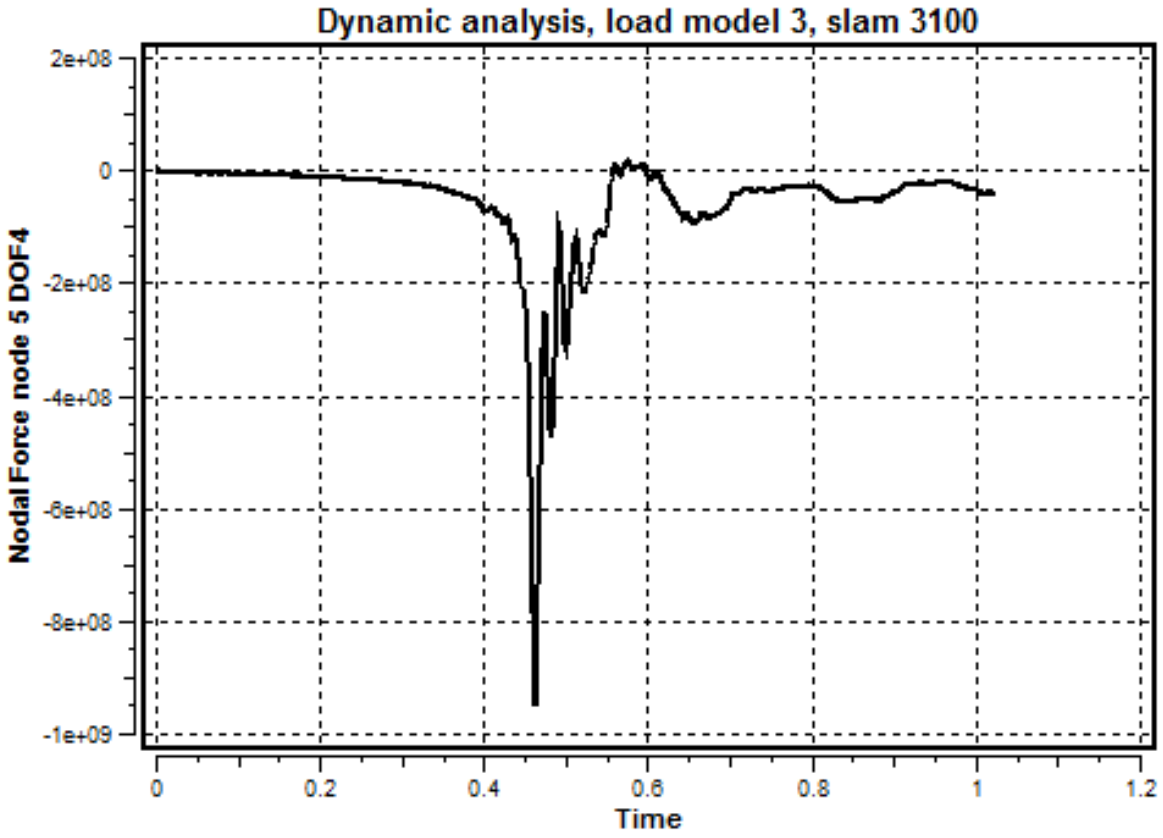
Dynamic analysis, load model 3, slam 3100
Nodal Force node 5 DOF4
2e+08
0
-2e+08
-4e+08
-6e+08
-8e+08
-1e+09
0
0.2
0.4
0.6
0.8
1
1.2
Time

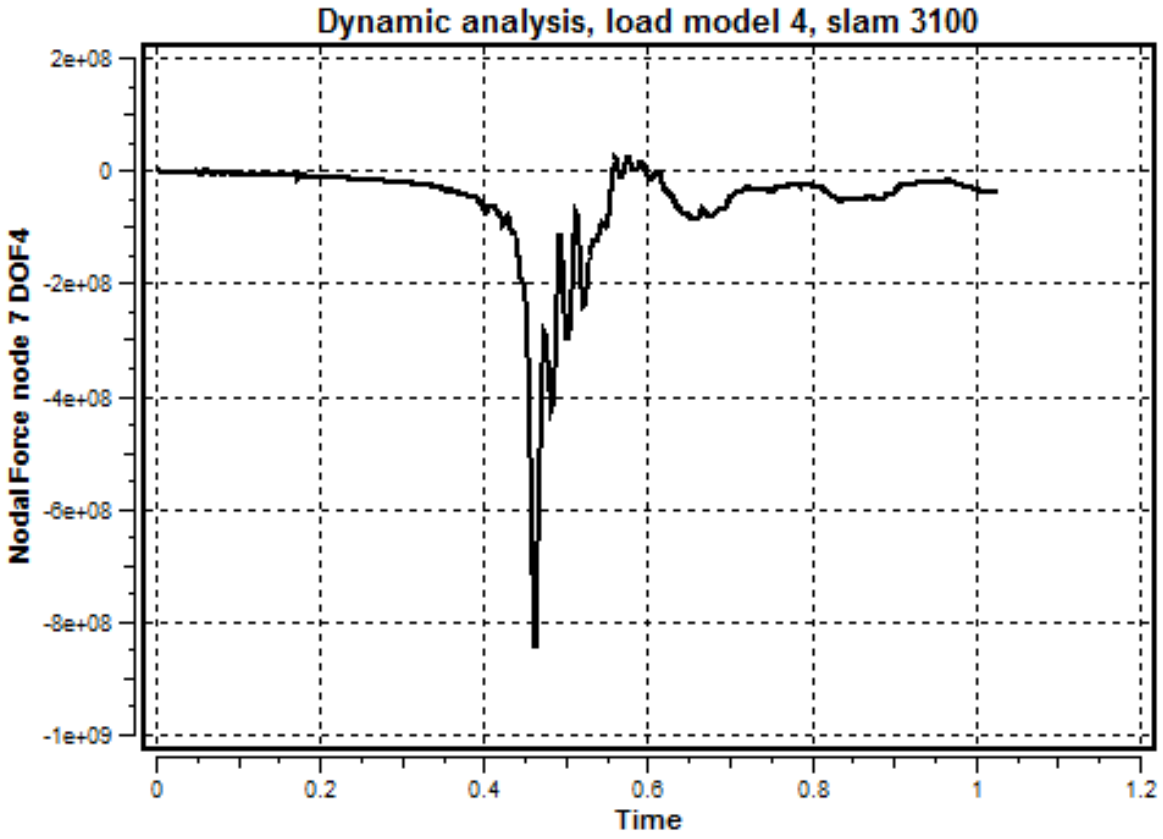
Dynamic analysis, load model 4, slam 3100
Nodal Force node 7 DOF4
2e+08
0
-2e+08
-4e+08
-6e+08
-8e+08
-1e+09
0
0.2
0.4
0.6
0.8
1
1.2
Time

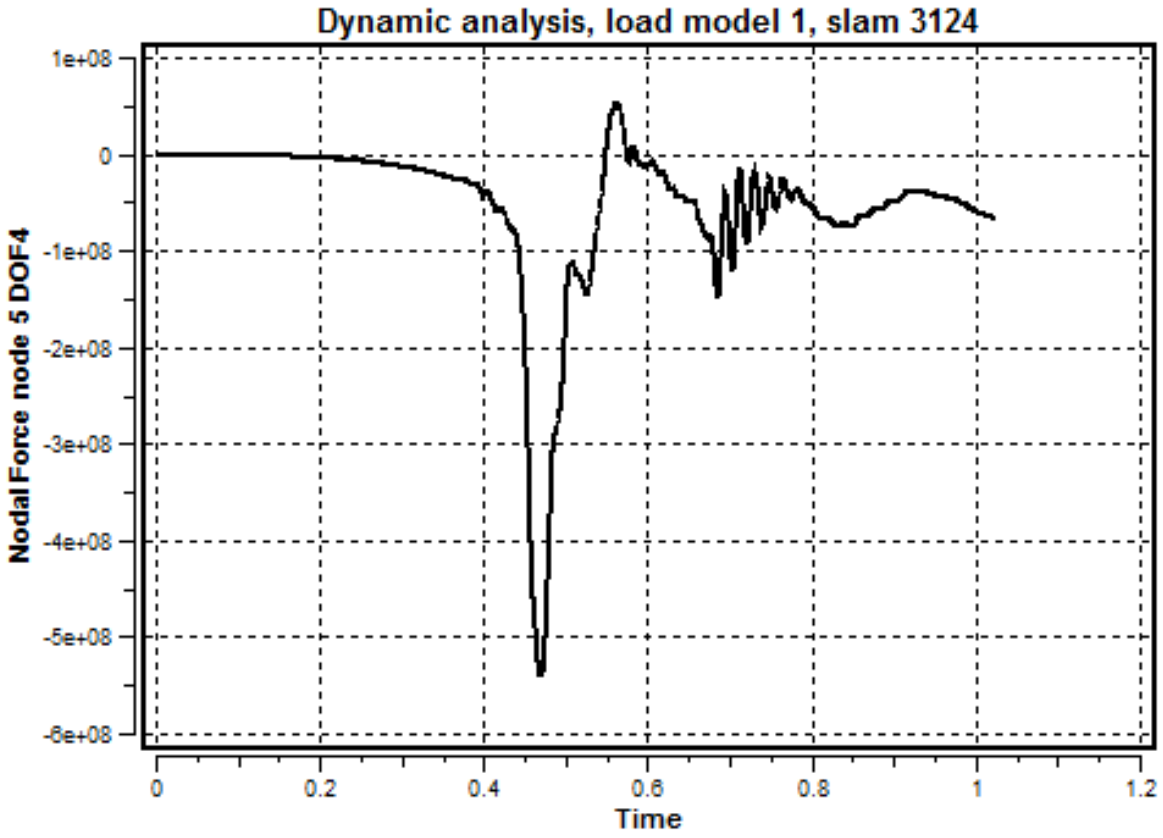
Dynamic analysis, load model 1, slam 3124
Nodal Force node 5 DOF4
1e+08
0
-1e+08
-2e+08
-3e+08
-4e+08
-5e+08
-6e+08
0
0.2
0.4
0.6
0.8
1
1.2
Time

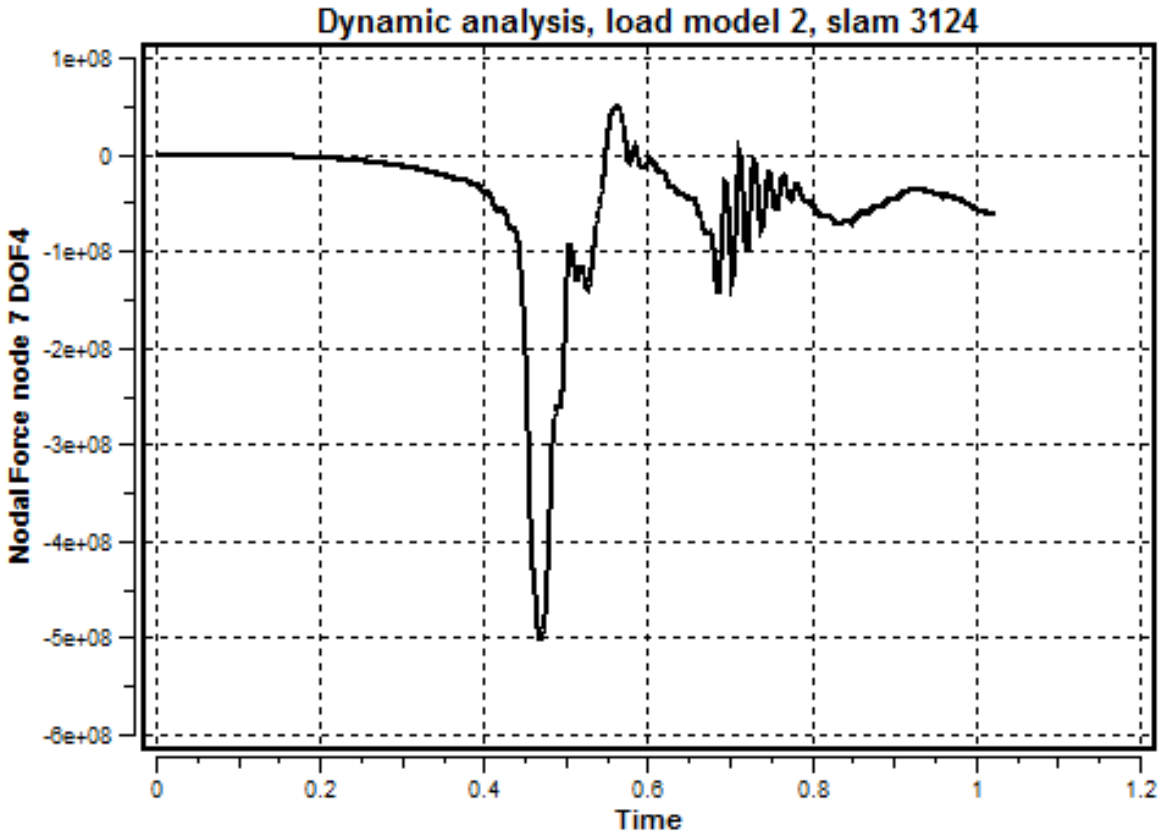
Dynamic analysis, load model 2, slam 3124
Nodal Force node 7 DOF4
1e+08
0
-1e+08
-2e+08
-3e+08
-4e+08
-5e+08
-6e+08
0
0.2
0.4
0.6
0.8
1
1.2
Time

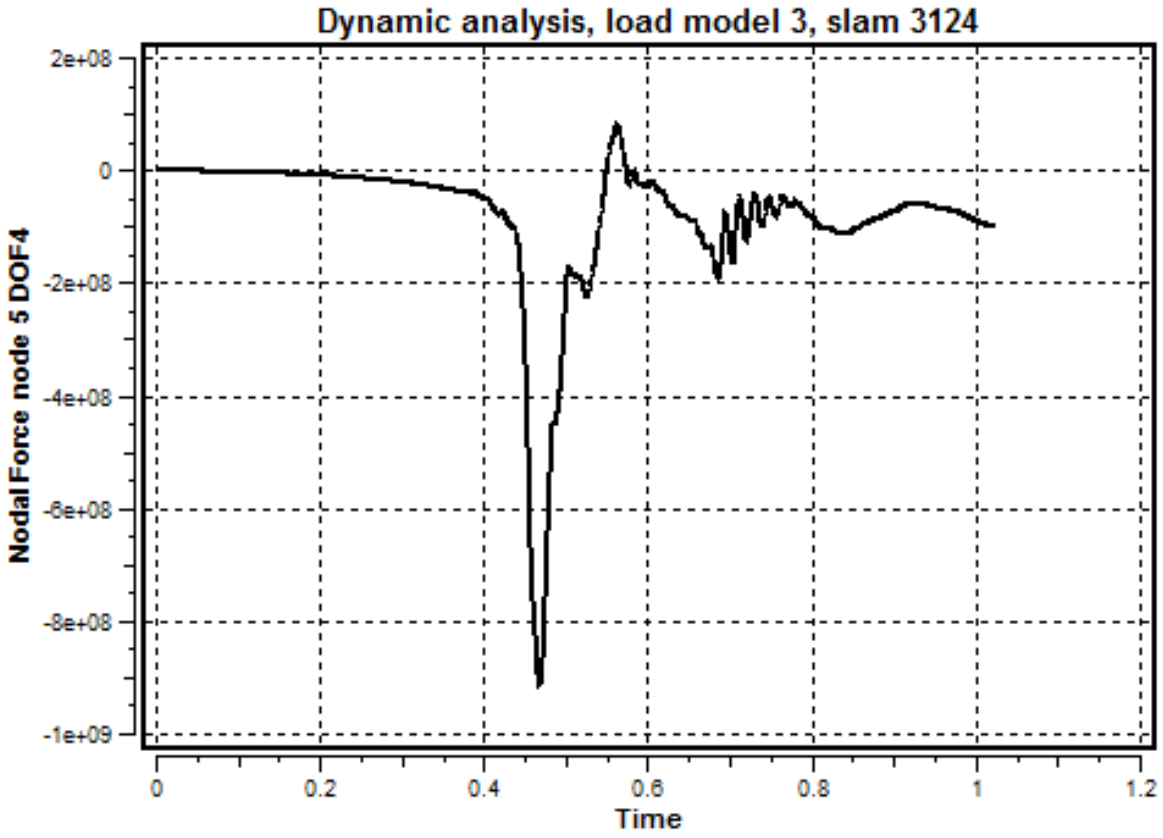
Dynamic analysis, load model 3, slam 3124
Nodal Force node 5 DOF4
2e+08
0
-2e+08
-4e+08
-6e+08
-8e+08
-1e+09
0
0.2
0.4
0.6
0.8
1
1.2
Time

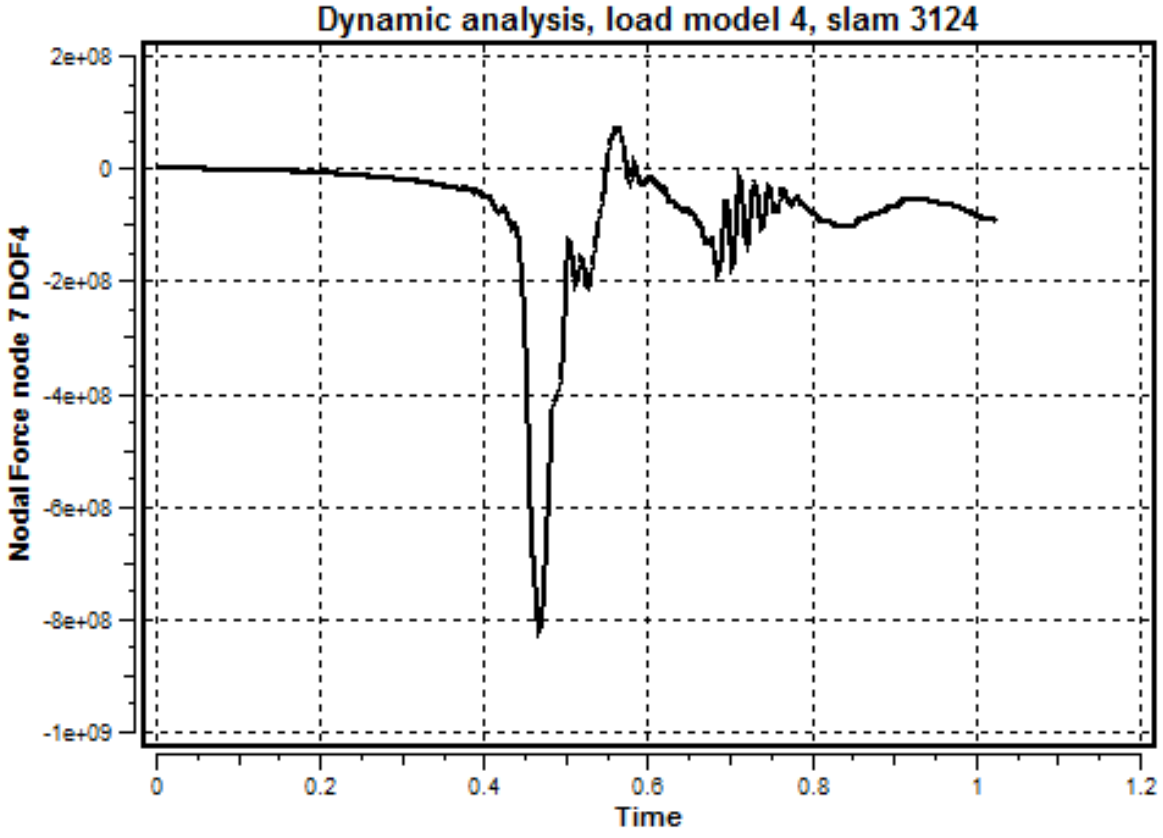
Dynamic analysis, load model 4, slam 3124
Nodal Force node 7 DOF4
2e+08
0
-2e+08
-4e+08
-6e+08
-8e+08
-1e+09
0
0.2
0.4
0.6
0.8
1
1.2
Time

Appendix F Attached DVD

The attached DVD has the following content:

- MATLAB scripts for:
  - estimating dynamics in the sensors
  - extreme value analysis
  - creating load models
  - find the surge velocity from the model tests
  - find the wave velocity from the model tests
  - estimate the surge velocity from WADAM results
  - investigation of spatial correlation
  - investigation of time variation in measured impact force
- USFOS input files for all analyses
- USFOS output files for all analyses
- Excel spreadsheet with calculations of cross section properties
- Excel spreadsheets that calculates R in the different load models

To be able to run many of the MATLAB scripts, the model test data is needed. This has to be provided from the model test results owners.